



10 CFR 52.79

February 15, 2010
NRC3-10-0012

U. S. Nuclear Regulatory Commission
Attention: Document Control Desk
Washington, DC 20555-0001

- References:
- 1) Fermi 3 Docket No. 52-033
 - 2) Letter from Ilka T. Berrios (USNRC) to Jack M. Davis (Detroit Edison),
"Request for Additional Information Letter No. 16 related to the SRP Sections
2.5.1, 2.5.2, 2.5.3, 2.5.4, and 2.5.5 for the Fermi 3 Combined License
Application" dated November 13, 2009
 - 3) Letter from Ilka T. Berrios (USNRC) to Jack M. Davis (Detroit Edison),
"Request for Additional Information Letter No. 17 related to the SRP Sections
2.5.1, 2.5.2, and 2.5.4 for the Fermi 3 Combined License Application" dated
November 24, 2009
 - 4) "Detroit Edison Company Response to NRC Request for Additional
Information Letter No. 16, Part I" dated December 23, 2009
 - 5) Letter from Ilka T. Berrios (USNRC) to Jack M. Davis (Detroit Edison),
"Request for Additional Information Letter No. 22 related to the SRP Sections
2.5.1, 2.5.2, and 2.5.4 for the Fermi 3 Combined License Application" dated
January 11, 2010
 - 6) "Detroit Edison Company Response to NRC Request for Additional
Information Letter No. 16, Part II" dated January 11, 2010
 - 7) "Detroit Edison Company Response to NRC Request for Additional
Information (RAI) Letters No. 16, 17, and 21" dated February 11, 2010

Subject: Detroit Edison Company Response to NRC Requests for Additional Information
(RAI) Letter No. 16, RAI numbers 02.05.02-1, 02.05.02-3, 02.05.02-4, 02.05.02-8,
02.05.04-27, and 02.05.04-28

In Reference 2, the NRC requested additional information to support the review of certain portions of the Fermi 3 Combined License Application (COLA). Reference 2 requested responses to specified RAIs within 45, 60, and 90 days. References 4 and 6 provided Detroit Edison's 45 and 60 day responses.

In Reference 7, Detroit Edison provided the remaining responses to Letter 16 (Reference 2), Letter 17 (Reference 3) and Letter 22 (Reference 5), with the exception of six RAIs, whose technical work had been completed but had not yet been validated. The deferred RAI numbers were: 02.05.02-1, 02.05.02-3, 02.05.02-4, 02.05.02-8, 02.05.04-27 and 02.05.04-28.

This letter provides Detroit Edison's deferred responses to the subject RIAs.

The response to RAI 02.05.02-8 contains electronic files submitted on CD as separate enclosure.

The file format and names on the enclosed CDs do not comply with the requirements for electronic submission in NRC Guidance Document, "Guidance for Electronic Submissions to the NRC," dated June 25, 2009; the files are not ".pdf" formatted. The NRC Staff requested the files be submitted in their native formats required by the software in which they are utilized to support review of the Final Safety Analysis Report.

If you have any questions, or need additional information, please contact me at (313) 235-3341.

I state under penalty of perjury that the foregoing is true and correct. Executed on the 15th day of February 2010.

Sincerely,



Peter W. Smith, Director
Nuclear Development –
Licensing and Engineering
Detroit Edison Company

- Attachments: 1) Response to RAI Letter No. 16 (Question No. 02.05.02-1)
2) Response to RAI Letter No. 16 (Question No. 02.05.02-3)
3) Response to RAI Letter No. 16 (Question No. 02.05.01-4)
4) Response to RAI Letter No. 16 (Question No. 02.05.01-8)
5) Response to RAI Letter No. 16 (Question No. 02.05.04-27)
6) Response to RAI Letter No. 16 (Question No. 02.05.04-28)

cc: Chandu Patel, NRC Fermi 3 Project Manager (w/o attachments)
Jerry Hale, NRC Fermi 3 Project Manager (w/o attachments)
Ilka T. Berrios, NRC Fermi 3 Project Manager (with CD)
Fermi 2 Resident Inspector (w/o attachments)
NRC Region III Regional Administrator (w/o attachments)
NRC Region II Regional Administrator (w/o attachments)
Supervisor, Electric Operators, Michigan Public Service Commission
(w/o attachments)
Michigan Department of Environmental Quality
Radiological Protection and Medical Waste Section (w/o attachments)

Attachment 1 to
NRC3-10-0012
Page 1

**Attachment 1
NRC3-10-0012**

**Response to RAI Letter No. 16
(eRAI Tracking No. 3918)**

RAI Question No. 02.05.02-01

RAI 02.05.02-01

FSAR Section 2.5.2.4.1.1 and FSAR Appendix 2.5BB discuss the updated characterization of large magnitude New Madrid seismic zone (NMSZ) earthquakes. Please provide the initial time (t_0) parameter used in modeling the time dependent seismic hazard model for the NMSZ. The ESBWR is designed with an operating life of 60 years and the fuel loading time is not yet certain. Please explain how you considered these factors in choosing the t_0 and Δt parameters. In addition, demonstrate the sensitivity of those parameters to the seismic hazard at the Fermi site.

Response

The assessment of the time dependent probabilities for large magnitude earthquakes in the New Madrid seismic zone (NMSZ) presented in FSAR Table 2.5.2-209 were those developed for Tennessee Valley Authority (TVA) (Reference 2.5.2-244) based on the data presented in the original Exelon Early Site Permit (ESP) submittal (Reference 2.5.2-243). The estimated parameters for the occurrence rate of large magnitude New Madrid earthquakes presented in the original Exelon ESP submittal (Reference 2.5.2-243) were based on analyses of the paleoseismic data for earthquakes in the northern portion of the New Madrid seismic zone. The computation of the time dependent probabilities presented in TVA (Reference 2.5.2-244) were based on an elapsed time since the previous event, t_0 of 191 years (early 2003, the time of the original Exelon calculations), and a nominal exposure period of 50 years, taken to be a standard plant life. Subsequent to these calculations, Exelon (References 2.5.2-253 and 2.5.2-254) presented an updated assessment of the probability of occurrence of large New Madrid earthquakes. These assessments used a t_0 of 193.83 years (October, 2005, the date of the calculations). In these calculations, Exelon (Reference 2.5.2-253 and 2.5.2-254) analyzed the paleoseismic data from the three sections of the New Madrid seismic zone (northeast, central, and southwest) and concluded that there was no statistical difference in the estimated occurrence parameters. Consequently, they used the data from all three sections to estimate the occurrence probabilities of large New Madrid events.

The process used to assess the occurrence parameters for large New Madrid earthquakes is described in detail by Exelon (Reference 2.5.2-254). The steps involve the following:

- A set of organic or cultural samples are defined that bracket the occurrence of the prehistoric New Madrid events at nominal dates of 1450 A.D. and 900 A.D.
- The age of each sample is simulated from the uncertainty distribution for the sample's age date. The resulting simulated dates are used to define a bracketed range (minimum and maximum) for the date of each event. The simulated age for the event is then sampled from a uniform distribution between the minimum and maximum ages.
- The simulated dates for the ~1450 A.D. and ~900 A.D. events along with the 1812 date are used to compute the sample of the times between earthquakes for the earthquake occurrence process (either Poisson or time dependent). This sample is used to construct an uncertainty distribution for the underlying rate parameter.

- The simulation process is repeated multiple times and the uncertainty distributions for the rate parameters are averaged over the simulations to produce the final distributions for the rate parameters.
- A discrete five-point distribution is used to represent the final distribution of the rate parameter based on models presented in Miller and Rice (Reference 1). These five point estimates were then used to compute the probability of occurrence of future large earthquake sequences at New Madrid.

The uncertainty distribution for the rate parameter for large magnitude New Madrid compound earthquakes (ruptures on the three components of the New Madrid system) is based on the sample of time intervals between compound events. These data consist of two closed intervals: the time between the ~900 A.D. and ~1450 A.D. events and the time between the ~1450 A.D. and the 1811-1812 events. In addition the data include the open interval from 1812 to the present. The likelihood function of observing the sample of time intervals between large compound earthquakes is given by:

$$L(\theta) = \left[\prod_i f(t_i) \right] \times [1 - F(t_0)] \quad (\text{Equation 1})$$

where $f(t_i)$ is the probability of observing an interval between events of t_i . The term $[1 - F(t_0)]$ is the probability that the time between events is at least as long as t_0 , the elapsed time since the most recent event. In Equation 1, parameter θ is the rate parameter of the chosen earthquake occurrence model. The maximum likelihood value of θ is obtained by maximizing Equation 1 (or, more conveniently its logarithm). An uncertainty distribution for θ is developed by computing the relative likelihood of various values of θ given the observed sample of t_i closed intervals plus the t_0 open interval and then normalizing these values to produce a probability distribution.

Two occurrence models were used to assess the probability of occurrence of future New Madrid large compound earthquakes: the Poisson model and the Brownian Passage Time (BPT) renewal model presented in Mathews et al. (Reference 2.5.2-243). For the Poisson model, the probability distribution for the time between large compound earthquakes is given by the exponential distribution:

$$f(t) = \lambda \exp(-\lambda t) \quad (\text{Equation 2})$$

and

$$F(t) = 1 - \exp(-\lambda t) \quad (\text{Equation 3})$$

where λ is the rate parameter, the average occurrence frequency of events. For a sample of n closed intervals and one open interval t_0 , the likelihood function for the sample of observed closed time intervals t_i and the open interval t_0 becomes:

$$L(\lambda) = \lambda^n \exp\left\{-\lambda \times \left[\sum_{i=1}^n t_i + t_0\right]\right\} \quad (\text{Equation 4})$$

The maximum likelihood value of the rate parameter λ is given by

$$\lambda_{\text{maximum likelihood}} = \frac{n}{\sum_{i=1}^n t_i + t_0} \quad (\text{Equation 5})$$

For the BPT model, the probability distribution for the time between large compound earthquakes is given by the inverse Gaussian distribution presented in Mathews et al. (Reference 2.5.2-243), specifically:

$$f(t) = \left(\frac{\mu}{2\pi\alpha^2 t^3}\right)^{1/2} \exp\left(-\frac{(t-\mu)^2}{2\mu\alpha^2 t}\right) \quad (\text{Equation 6})$$

and

$$F(t) = \Phi[u_1(t)] + e^{2/\alpha^2} \Phi[-u_2(t)] \quad (\text{Equation 7})$$

with

$$u_1(t) = (\sqrt{t/\mu} - \sqrt{\mu/t})/\alpha \quad (\text{Equation 8})$$

and

$$u_2(t) = (\sqrt{t/\mu} + \sqrt{\mu/t})/\alpha \quad (\text{Equation 9})$$

In Equations 6 through 9 μ is the mean inter-arrival time (repeat time), α is the aperiodicity coefficient (coefficient of variation of t), and $\Phi(\)$ is the standard normal cumulative probability function. Given a sample of n time intervals and one open interval, t_0 , the likelihood function for the observed data set is again given by Equation 4 with $f(t)$ and $F(t)$ given by Equations 6 and 7. The maximum likelihood solution for the parameters of the model must be found by numerical methods. Because of the very limited data set, the estimate of the aperiodicity coefficient, α , is highly uncertain. Therefore, the value of α was constrained to values reported from examination of larger data sets. Based on examination of a number of data sets, the Working Group (Reference 2) developed an uncertainty distribution for the aperiodicity coefficient for the BTP model consisting of three weighted values of 0.3 (weight 0.2), 0.5 (weight 0.5), and 0.7 (weight 0.3). The Working Group (Reference 2) distribution was adopted to constrain α . Uncertainty distributions for μ were developed for each value of α using the relative likelihood process described above.

Given values of μ and α , the probability of occurrence of a large New Madrid compound earthquake (rupture of the three components) is given by the expression:

$$P_{renewal}(\text{event in time } t_0 \text{ to } t_0 + \Delta t) = \frac{F(t_0 + \Delta t) - F(t_0)}{1 - F(t_0)} \quad (\text{Equation 10})$$

where $F(t)$ is given by Equation 7. The value of $P_{renewal}$ (event in time t_0 to $t_0 + \Delta t$) is then converted into an equivalent Poisson rate to be added to the hazard from the remaining sources using the expression:

$$\lambda_{renewal} = \frac{-\ln[1 - P_{renewal}(\text{event in time } t_0 \text{ to } t_0 + \Delta t)]}{\Delta t} \quad (\text{Equation 11})$$

The sensitivity of the computed occurrence frequencies of large New Madrid earthquakes to the selection of t_0 and Δt is summarized in Table 1. Three cases are shown. The first case corresponds to the values presented in the Fermi 3 FSAR Table 2.5.2-209 using the original values from the Exelon (Reference 2.5.2-243) simulation of earthquake dates for the northeastern portion of the New Madrid zone. For the Poisson model, the value of equivalent annual frequency given in the last column is the mean of the derived likelihood distribution for the Poisson rate parameter λ . For the BPT renewal model, the value of equivalent annual frequency given in the last column is the mean of the equivalent Poisson rates (Equation 11) computed using the weighted average of the derived likelihood distributions for μ averaged for each value of α .

The second case presented in Table 1 represents the effect of using the updated values from the Exelon (Reference 2.5.2-254) simulation of earthquake dates for all three portions of the New Madrid zone. These values produce slightly lower mean occurrence frequencies (a reduction in the average rate of two percent).

The third case presented in Table 1 corresponds to the current planned exposure of Fermi 3. This case is computed using the updated Exelon (Reference 2.5.2-253 and 2.5.2-254) earthquake date simulations. At this time, the Combined License (COL) is expected to be issued for Fermi 3 in the third quarter of 2012. Therefore, for computing the frequency of occurrence of large magnitude New Madrid earthquakes for the Fermi 3 site, it is assumed that no large earthquake occurs in the New Madrid zone before 2013, giving a t_0 value of 201 years. The value of Δt is set to 60 years, including the maximum of 20 years for construction after issuing the Combined License plus 40 years of operation. The results for this case show a slight reduction in the Poisson rates due to an overall longer period of elapsed time since the first earthquake considered in the data set (the ~900 A.D. earthquake), as indicated by the effect of increasing

$\sum_{i=1}^n t_i + t_0$ on the maximum likelihood Poisson rate computed using Equation 5. The revised values of t_0 and Δt produce a slight increase in the BPT equivalent rates. The effective difference in the weighted average is about a 0.7 percent increase in the mean annual frequency

of New Madrid earthquakes compared to the values used in the PSHA calculation for the Fermi 3 site presented in FSAR Section 2.5.2.4. Because the total hazard at the Fermi site includes the contributions of other earthquake sources, the net effect of the change in the occurrence rate of large New Madrid earthquakes would be a 0.7 percent or less increase in the total mean hazard. This translates into less than 0.5 percent increase in the GMRS ground motion levels. This is a negligible difference and no adjustment to the Fermi 3 PSHA model is considered to be warranted.

Table 1 Computed Frequency of Occurrence of Large Magnitude New Madrid Earthquakes		
Case	Model	Equivalent Annual Frequency
Revision 1 of Fermi 3 FSAR $t_0 = 191$ (2003 – 1812) $\Delta t = 50$	Poisson	0.00276
	BPT	0.00124
	Weighted Average	0.00200
Updated Exelon FSAR Earthquake Date Simulations $t_0 = 191$ (2003 – 1812) $\Delta t = 50$	Poisson	0.00274
	BPT	0.00117
	Weighted Average	0.00196
Current Exposure of Fermi 3 Using Updated Exelon Earthquake Date Simulations $t_0 = 201$ (2013 – 1812) $\Delta t = 60$	Poisson	0.00272
	BPT	0.00131
	Weighted Average	0.00201

References

1. Allen C. Miller, III and Thomas R. Rice, 1983, "Discrete Approximations of Probability Distributions," Management Science, Vol. 29, No. 3, pp. 352-362.
2. Working Group on California Earthquake Probabilities (Working Group). "Earthquake Probabilities in the San Francisco Bay Region: 2002-2031." U.S. Geological Survey Open-File Report 03-214. 2003.

Proposed COLA Revision

None

**Attachment 2
NRC3-10-0012**

**Response to RAI Letter No. 16
(eRAI Tracking No. 3918)**

RAI Question No. 02.05.02-03

RAI 02.05.02-03

*FSAR Sections 2.5.1.1.4.4 and 2.5.2.4.1 discuss significant seismic sources at distances greater than 320 km from the Fermi site, including the New Madrid and Wabash Valley seismic zones. The FSAR does not discuss the Western Quebec seismic zone (WQSZ) in Canada even though it is a similar distance from the Fermi site as the New Madrid seismic zone (NMSZ). Previous research has provided paleoseismic evidence for two $M > 7$ earthquakes in the past 7000 years in the Ottawa River Valley (Aylsworth and Lawrence 2000, *Geology*, v28, no 10, p 903-906). Please include a discussion of the WQSZ, including the significance of this paleoseismic evidence to the seismic zone's characterization and its consequent impact on seismic hazard at the Fermi site.*

Response

Large prehistoric landslides in the Ottawa River valley that may have been earthquake-induced were investigated by Aylsworth et al. (Reference 1). The landslides were mapped in marine clayey silt, commonly known as the Leda clay, which was deposited in an inland sea that occupied these valleys at the end of the last ice age. Age dating of many of the large landslides indicates that the majority occurred within a relatively short period of time. Aylsworth et al (Reference 1) believe that a strong case can be made that the landslides were the result of a large earthquake and resulting liquefaction ca. 7060 years B.P. Also, these investigators report that another large earthquake occurred in ca. 4550 years B.P. and caused multiple landslides spatially distributed within different paleovalleys. They believe the only action capable of inducing the observed widespread, concurrent slope movement is related to one large earthquake or several earthquakes, closely spaced in time. The investigators state that landslides of the magnitude described would need to be associated with a significant ($M > 6$) earthquake in the immediate area, or a very large ($M > 7$) earthquake nearby, which would be essentially equivalent to the 1663 Charlevoix earthquake. Therefore, Aylsworth et al. (Reference 1) believe that these large earthquakes should be included in seismic hazard estimates.

The text that follows indicates what seismic sources the Electric Power Research Institute and Seismic Owners Group (EPRI-SOG) teams defined for the Western Quebec Seismic Zone. These sources are shown on attached Figures 1 through 6. Also shown on each of these figures is the location of landslide and disturbed terrain area studied by Aylsworth et al. (Reference 1).

Bechtel (Figure 1)

Bonnechere Graben (Source BEC-07). This source zone is based on the Ottawa-Bonnechere Graben faults.

West Quebec Seismic Zone (Source BEC-C). This source zone represents a seismicity-based source encompassing the western Quebec seismicity.

Dames & Moore (Figure 2)

Western Quebec Seismic Zone (Source DAM-01). This source zone was drawn primarily on the basis of an intense zone of seismicity that trends west-northwest from northern New York State through the Timiskaming region in eastern Ontario. The zone encompasses portions of the failed rift area of the St. Lawrence Rift as well as the Ottawa-Bonnechere Graben. Dames and Moore also defined a default zone that has the same geometry as Source DAM-01.

Law Engineering (Figure 3)

Ottawa-Bonnechere Graben (Source LAW-11). A Mesozoic rift that is a reactivated Paleozoic aulacogen and part of the St. Lawrence Rift System.

Rondout Associates (Figure 4)

Tremblant (Source RND-35). This area has frequent earthquake activity but no readily apparent structures that are causing these earthquakes. The zone includes the Ottawa-Bonnechere Graben, which is described as an Ordovician graben with many en echelon high angle faults with stepovers. Although the graben is not expressed in gravity data, wide-angle reflection data indicate a highly disturbed zone in the Moho beneath the graben.

Weston Geophysical (Figure 5)

Western Quebec Zone (Source WGC-05). The region of this source zone is geologically complex and incorporates elements that could be treated as separate tectonic features. It is considered a single seismotectonic region by the WGC team, however, because it is a distant contributor to hazard for the majority of EUS sites and a finer resolution of the region into sub-sources is not expected to appreciably alter hazard at these sites. This source is adjacent to the St. Lawrence Rift zone (Source WGC-04), which has distinctively lower observed seismicity.

Woodward-Clyde Consultants (Figure 6)

Three source zones are defined for the Western Quebec region.

Greater Western Quebec Seismic Zone (Source WCC-15). This source zone is based on an observed concentration of seismicity.

Western Quebec Seismic Zone (Source WCC-16). A more restricted interpretation of the Greater Western Quebec Seismic Zone (Source WCC-15) is the basis for this source zone.

Western Quebec Crustal Block (Source WCC-19). The crustal block that defines this zone was identified from Bouguer gravity gradient data. The block is coincident with the observed extent of western Quebec seismicity, which includes moderate-to-large and small magnitude earthquakes.

Woodward-Clyde Consultants also defined a default zone that encompasses the same region as their Source WCC-15. They are treated as a single source with the combined P^* in the PSHA.

Potential Impact of Paleoseismic Data on Characterization of Western Quebec Seismic Zone

As shown on Figures 1 through 6, each of the EPRI-SOG expert teams defined seismic sources that encompass the area of landslide and disturbed terrain studied by Aylsworth et al. (Reference 1). Table 1 summarizes the teams' assessments in terms of the probability of activity (P^*) and maximum magnitude distribution for each source zone. In general, the teams gave a high combined probability of there being at least one active source that encompasses the area of the inferred paleoseismic activity, with the lowest value being 0.71 for the Law Engineering team. If the Aylsworth et al. (Reference 1) interpretations are correct, then it is expected that the probability of an active source (capable of producing an earthquake of m_b 5 or larger) in the area should be increased to 1.0. As a sensitivity analysis, the probability of activity of the alternative sources defined by each team was increased such that the team's aggregate probability of activity for the Western Quebec Seismic Zone is 1.0. These values are listed in the fifth column of Table 1. Where a team defined alternative sources, the probability assigned to each was set to maintain the relative probability of activity defined in the EPRI-SOG study.

The maximum magnitude distributions assigned by the EPRI-SOG teams for the western Quebec sources are listed in the fourth column of Table 1. The distributions for the various sources have mean values of maximum magnitude in the range of m_b 6.2 to 6.8. Based on the three m_b to M conversions used in the Fermi 3 PSHA, this range in m_b translates into a range of M from 5.8 to 7.1.

Aylsworth et al. (Reference 1) suggest two options for the size of the inferred paleoearthquake. They indicate that it may have been as large as the 1663 Charlevoix earthquake, but also indicate that an event the size of the 1988 Saguenay earthquake could have been capable of producing the observed effects. The size of the 1663 earthquake is based on maximum intensity and felt effects. The maximum intensity is listed as MMI IX in the NCEER-91 catalog (FSAR Reference 2.5.2-241) and MMI X in USGS list of historic earthquakes. The magnitude estimates include m_b 7.0 in the NCEER91 catalog (FSAR Reference 2.5.2-205) and USGS National Seismic Hazard Mapping Project catalogs (FSAR Reference 2.5.2-207), and moment magnitude M 7.1 to 7.5 (Reference 2). The size of the 1988 Saguenay earthquake is m_{bLg} 6.5, M 5.8. For the purposes of the sensitivity analysis, two options are considered for the size of the largest observed event in the Western Quebec Seismic Zone, m_b 6.5 [weight 1/3] and 7.0 [weight 2/3]. The value of m_b 7.0 is preferred given the extent of the observed effects. These values were then used to develop maximum magnitude distributions for the Western Quebec Seismic Zone using the approaches outlined by the six EPRI-SOG expert teams. These maximum magnitude distributions are listed in the sixth column of Table 1. Figure 7 shows mean earthquake occurrence frequencies computed for each of the

EPRI-SOG expert teams for their set of Western Quebec Seismic Zone seismic sources with the modified maximum magnitude distributions. Also shown on Figure 7 is the combined mean earthquake occurrence relationship computed as the average of the individual team mean results.

Impact on Hazard at the Fermi 3 Site.

A sensitivity calculation was performed to assess the potential impact of including the Western Quebec Seismic Zone sources on the Fermi 3 site hazard. Using the seismicity parameters defined in EPRI (FSAR Reference 2.5.2-202) along with the updated P* and updated maximum magnitude distributions listed in Table 1 the mean hazard from the Western Quebec Seismic Zone sources was computed. Figure 8 shows the resulting mean hazard curves (mean annual frequency of exceedance) for the Western Quebec Seismic Zone sources compared to the mean hazard for hard rock conditions from all of the sources used in the updated PSHA reported in the Fermi 3 FSAR Tables 2.5.2-211 through 2.5.2-217. At the 10 Hz spectral acceleration level where the total mean hazard computed for the Fermi 3 site equals 10^{-4} the mean hazard from the Western Quebec Seismic Zone sources is less than 10^{-6} , or less than 1 percent of the total hazard from all other sources. Similarly at 10^{-5} total mean hazard, the mean hazard from the Western Quebec Seismic Zone sources is less than 10^{-7} . For 1 Hz spectral acceleration, the contribution from the Western Quebec Seismic Zone sources is somewhat larger. At the ground motion level where the total mean hazard computed for the Fermi 3 site equals 10^{-4} the mean hazard for the Western Quebec Seismic Zone sources equals about 2×10^{-6} , or 2 percent of the total, and at the ground motion level where the total mean hazard equals 10^{-5} the mean hazard for the Western Quebec Seismic Zone sources equals about 10^{-7} , or 1 percent of the total. If these sources as modified were added to the model, the differences in mean frequency of exceedance would correspond to about a 1 percent change in the GMRS at low spectral frequencies, with smaller differences at higher spectral frequencies. This is a negligible difference and no adjustment to the Fermi 3 PSHA model is considered to be warranted.

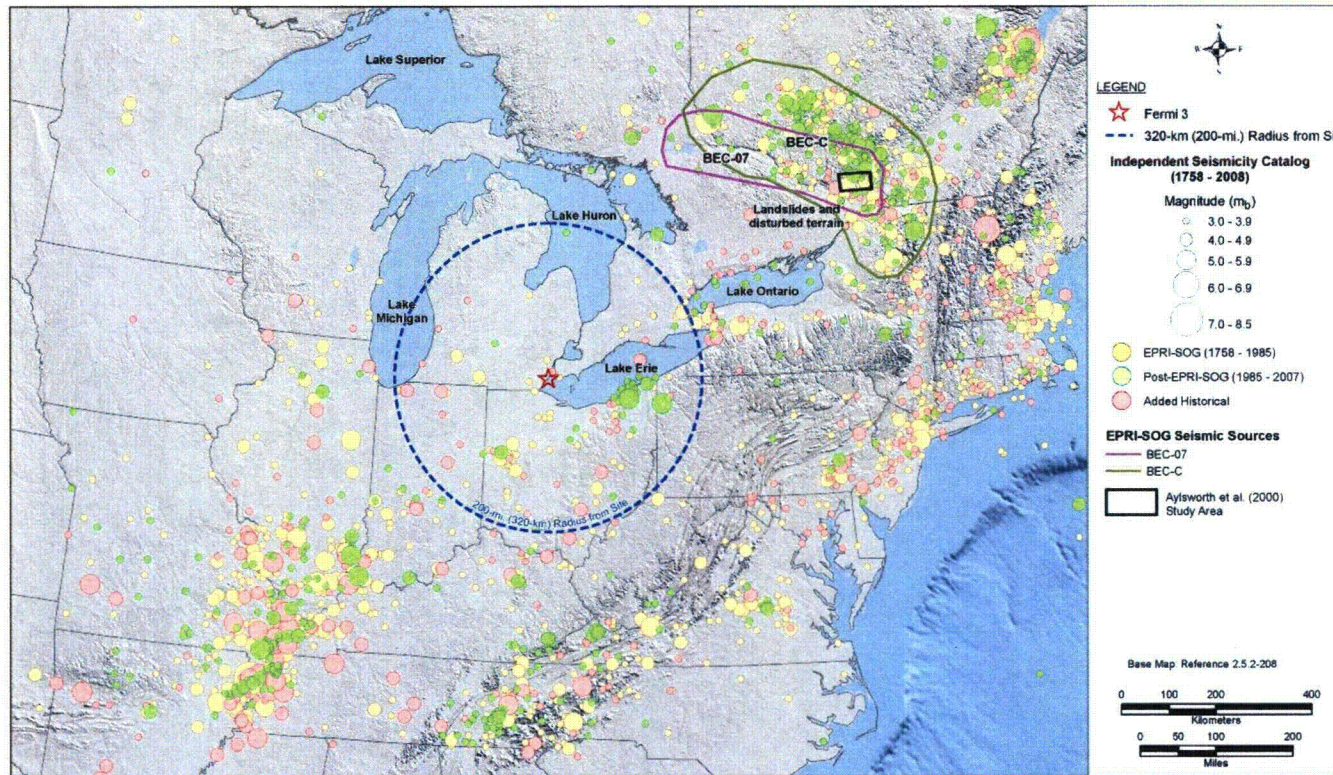
References

1. Aylsworth, J.M., Lawrence, D.E., and Guertin, J., 2000, Did two massive earthquakes in the Holocene induce widespread landsliding and near-surface deformation in part of the Ottawa Valley, Canada, *Geology*, v. 28; no. 10; p. 903–906.
2. Ebel, J.E., 2009, On the magnitude of the 1663 Charlevoix earthquake (abs.), *Seismological Research Letters*, v. 89, n, 2, p. 343.

Table 1
Summary of Seismic Source Parameters for Western Quebec Seismic Zone

EPRI-SOG Team	Seismic Source	Probability of Activity (P*) Assigned in EPRI-SOG (1988)	Maximum Magnitude Distribution (m _b) Assigned in EPRI-SOG (1988) *	Probability of Activity (P*) Used in Sensitivity Analysis	Maximum Magnitude Distribution (m _b) Used in Sensitivity Analysis*
Bechtel	Source BEC-07	0.45	6.0 [0.1] 6.3 [0.4] 6.6 [0.5]	0.563	6.5 [0.033] 6.6 [0.033] 6.8 [0.133] 7.0 [0.134] 7.1 [0.133] 7.3 [0.267] 7.6 [0.267]
	Source BEC-C	0.35	6.0 [0.1] 6.3 [0.4] 6.6 [0.5]	0.437	6.5 [0.033] 6.6 [0.033] 6.8 [0.133] 7.0 [0.134] 7.1 [0.133] 7.3 [0.267] 7.6 [0.267]
Dames & Moore	Source DAM-01	0.61	6.6 [0.75] 7.2 [0.25]	1.0	6.5 [0.25] 7.0 [0.5] 7.2 [0.25]
	Default for Source DAM-01	0.39	6.6 [0.8] 7.2 [0.2]	Not needed as P* of DAM-01 is now 1.0	
Law Engineering	Source LAW-11	0.71	6.0 [0.5] 6.8 [0.5]	1.0	6.5 [0.167] 6.8 [0.167] 7.0 [0.667]
Rondout Associates	Source RND-35	1.0	6.6 [0.3] 6.8 [0.6] 7.0 [0.1]	1.0	6.6 [0.1] 6.8 [0.2] 7.0 [0.033] 7.1 [0.067] 7.3 [0.533] 7.4 [0.067]
Weston Geophysical	Source WGC-05	1.0	6.0 [0.61] 6.6 [0.36] 7.2 [0.03]	1.0	6.6 [0.276] 7.2 [0.724]
Woodard-Clyde Consultants	Source WCC-15+ Default	0.324	5.9 [0.33] 6.3 [0.34] 7.0 [0.33]	0.362	6.5 [0.1106] 6.75 [0.142] 7.0 [0.371] 7.25 [0.268] 7.5 [0.099] 7.75 [0.014]
	Source WCC-16	0.09	5.2 [0.33] 6.3 [0.34] 7.0 [0.33]	0.10	6.5 [0.1106] 6.75 [0.142] 7.0 [0.371] 7.25 [0.268] 7.5 [0.099] 7.75 [0.014]
	Source WCC-19	0.482	5.9 [0.33] 6.5 [0.34] 6.9 [0.33]	0.538	6.5 [0.1106] 6.75 [0.142] 7.0 [0.371] 7.25 [0.268] 7.5 [0.099] 7.75 [0.014]

* Values in brackets indicate weight assigned to each maximum magnitude



File path: S:\13300\13356_001\Figures\RAI Figures\RAI 02.05.02-3 Figure 1.mxd; Date: [01/19/2010]; User: Laura Glaser, AMEC Geomatrix, Inc.

Figure 1 – Seismic sources defined by the Bechtel team for Western Quebec Seismic Zone.

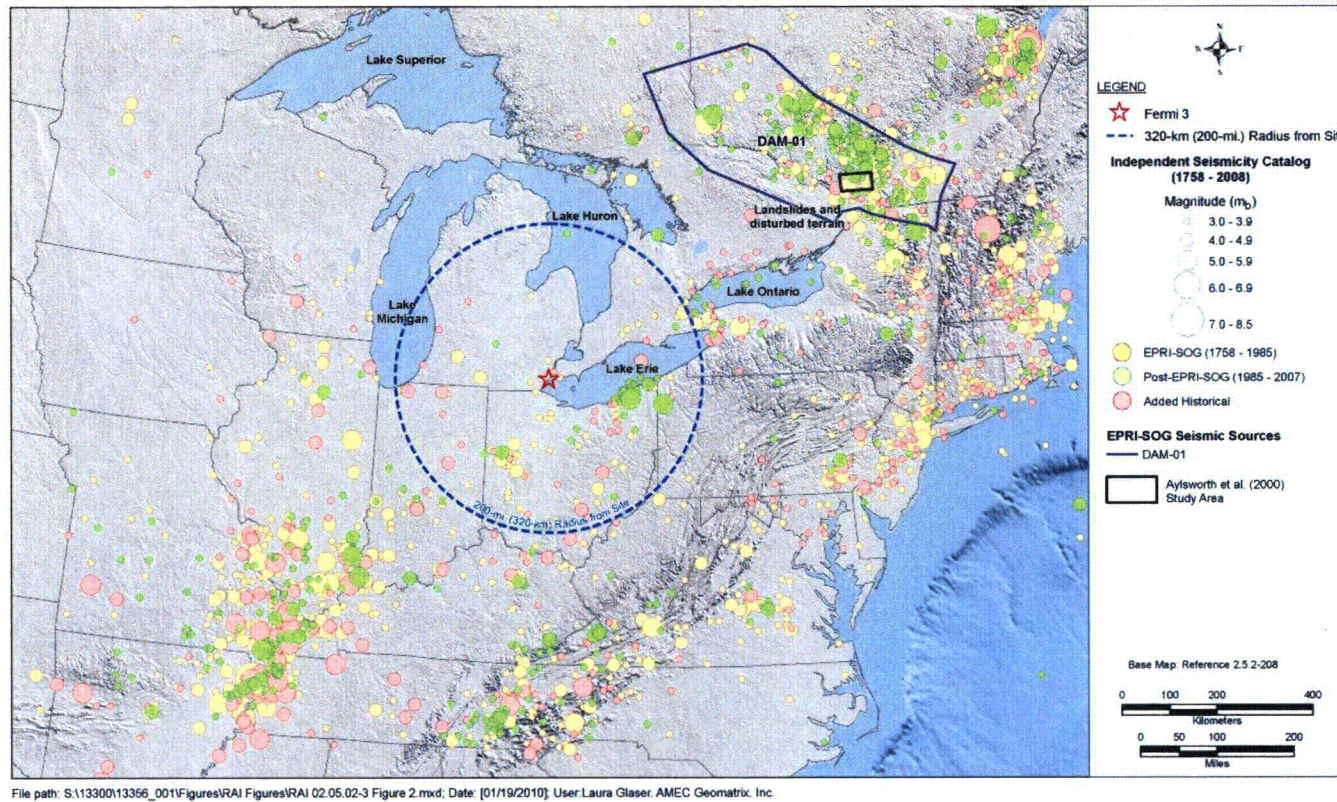


Figure 2 – Seismic sources defined by the Dames & Moore team for Western Quebec Seismic Zone.

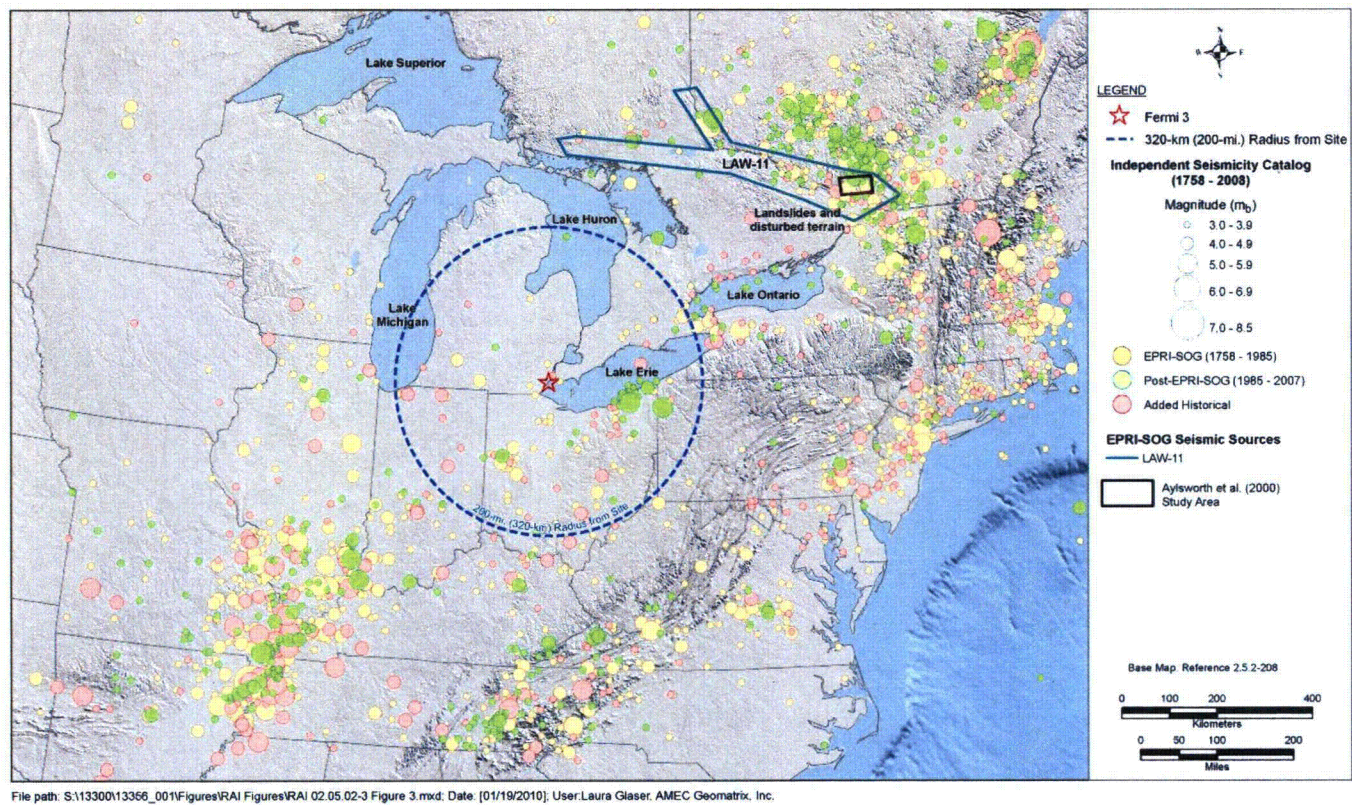


Figure 3 – Seismic sources defined by the Law Engineering team for Western Quebec Seismic Zone.

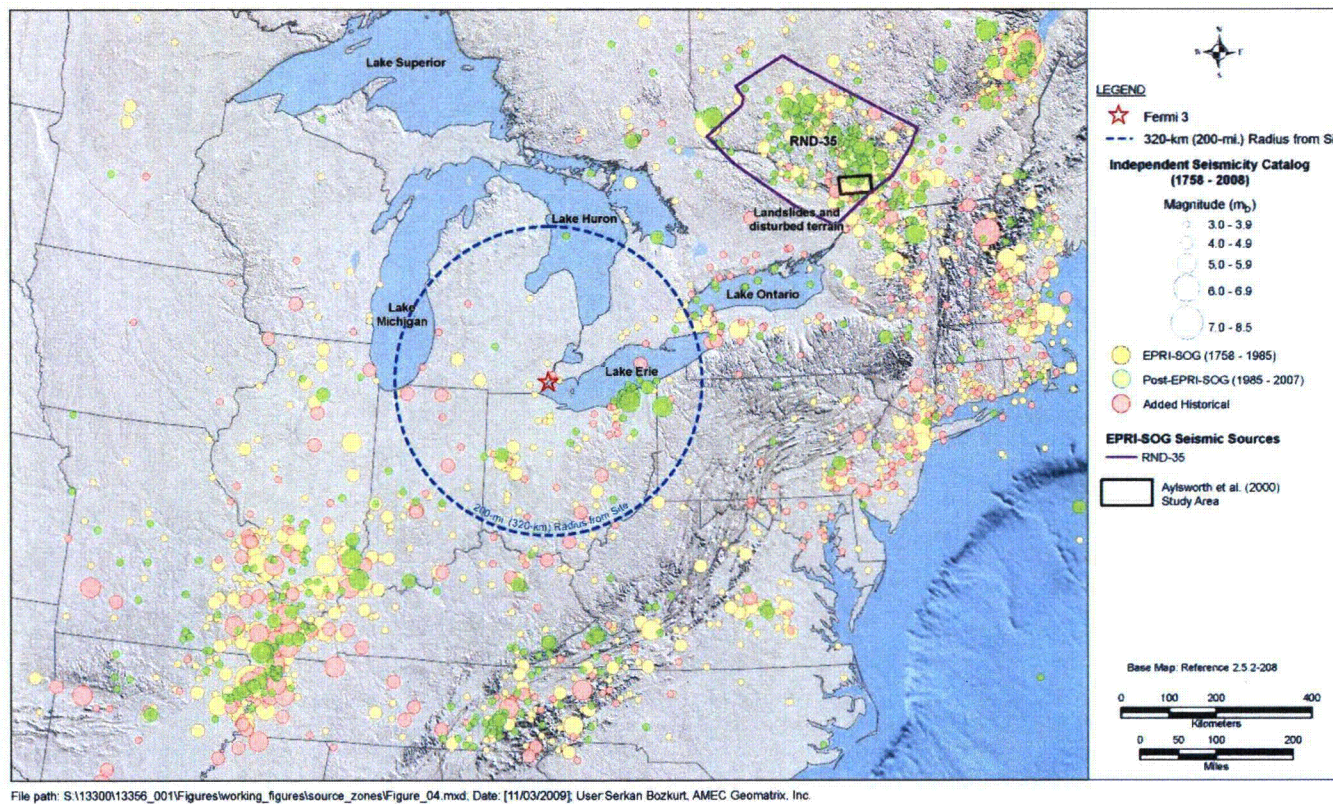


Figure 4 – Seismic sources defined by the Rondout Associates team for Western Quebec Seismic Zone.

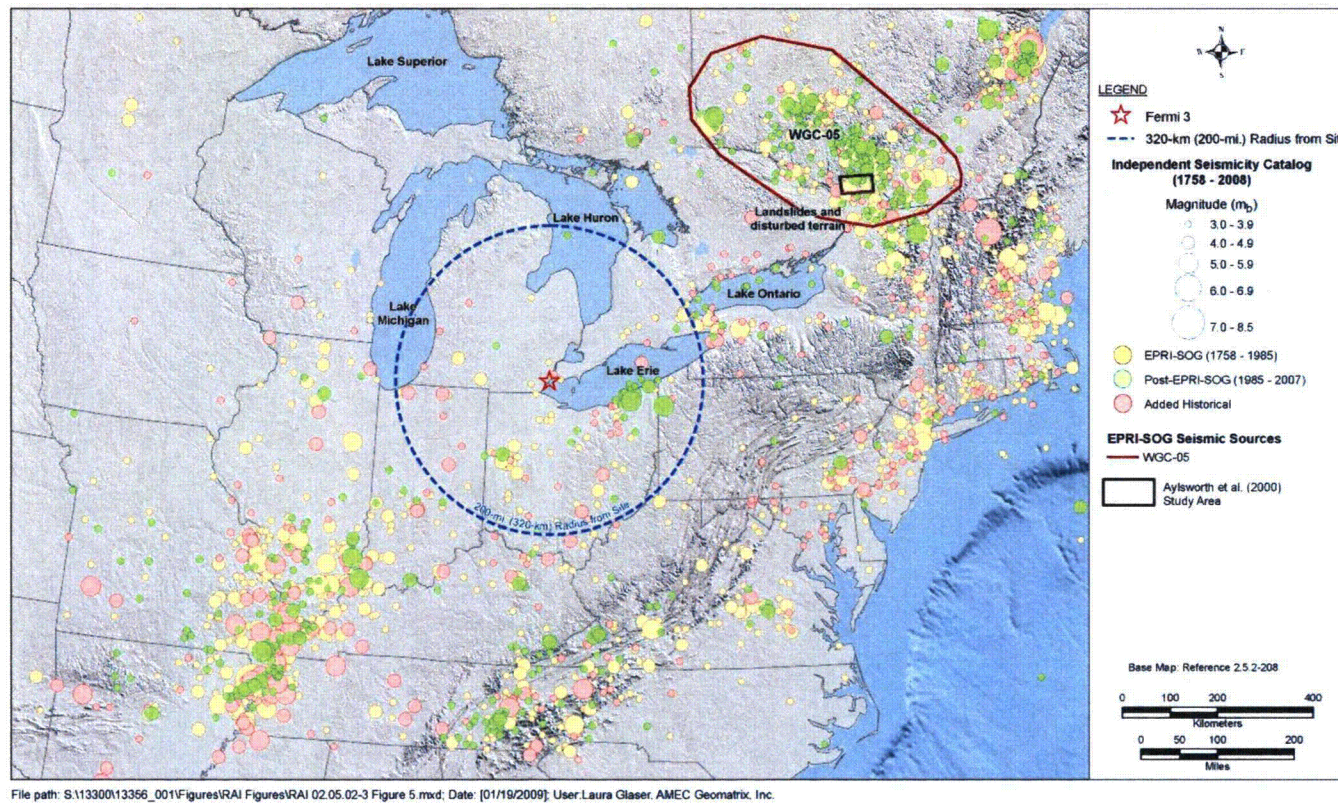
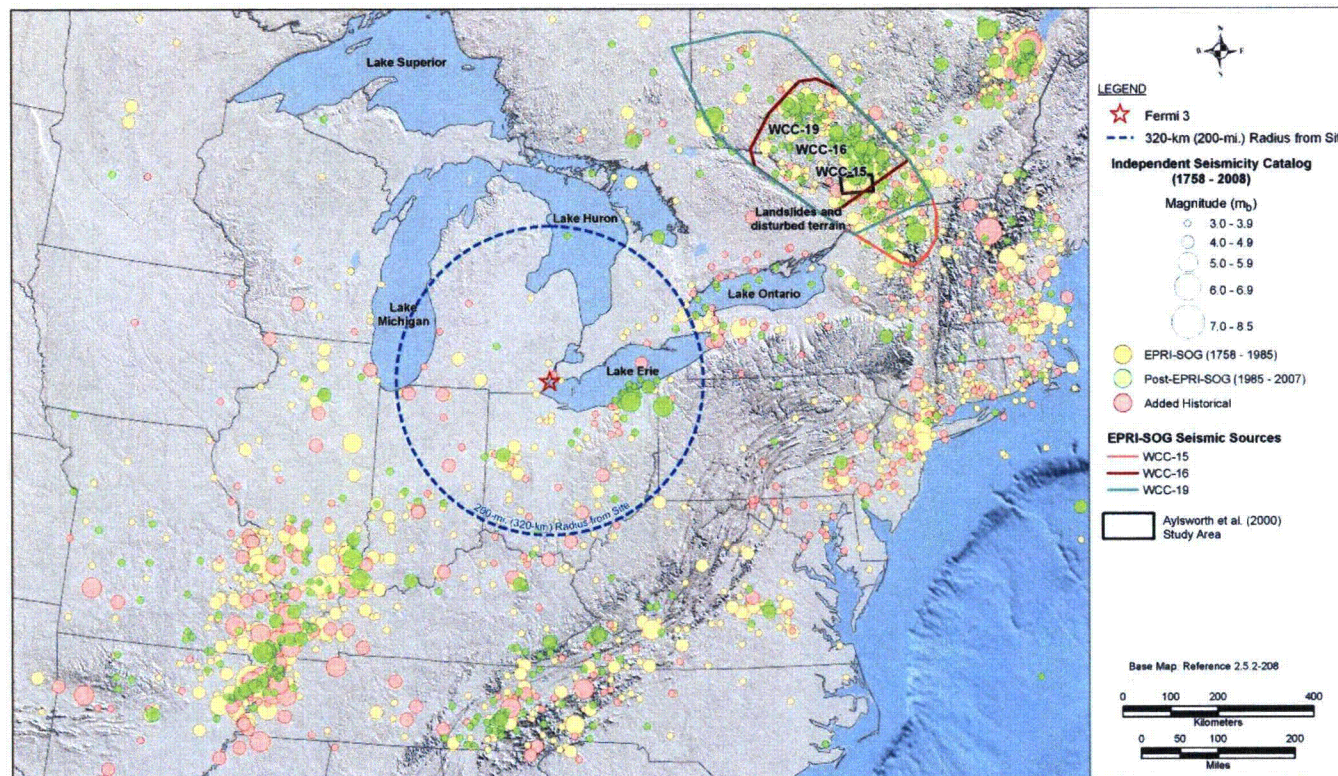


Figure 5 – Seismic sources defined by the Weston Geophysical team for Western Quebec Seismic Zone.



File path: S:\13300\13366_001\Figures\RAI Figures\RAI 02.05.02-3 Figure 6.mxd. Date: [01/19/2010]. User: Laura Glaser, AMEC Geomatrix, Inc.

Figure 6 – Seismic sources defined by the Woodward-Clyde team for Western Quebec Seismic Zone.

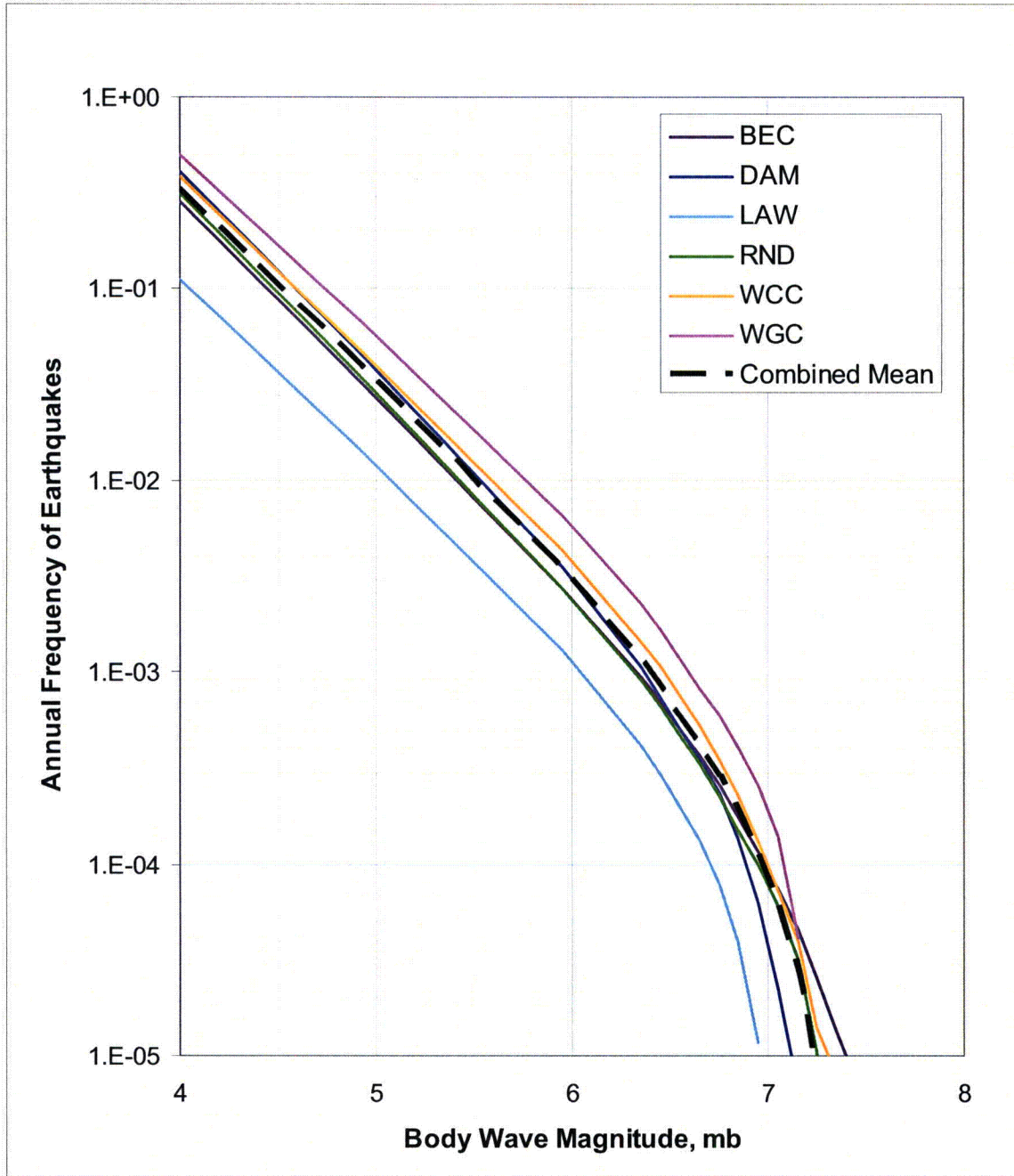


Figure 7 – Mean earthquake recurrence relationships for the each EPRI-SOG Expert Team’s collection of Western Quebec Seismic Zone sources and a combined mean recurrence relationship.

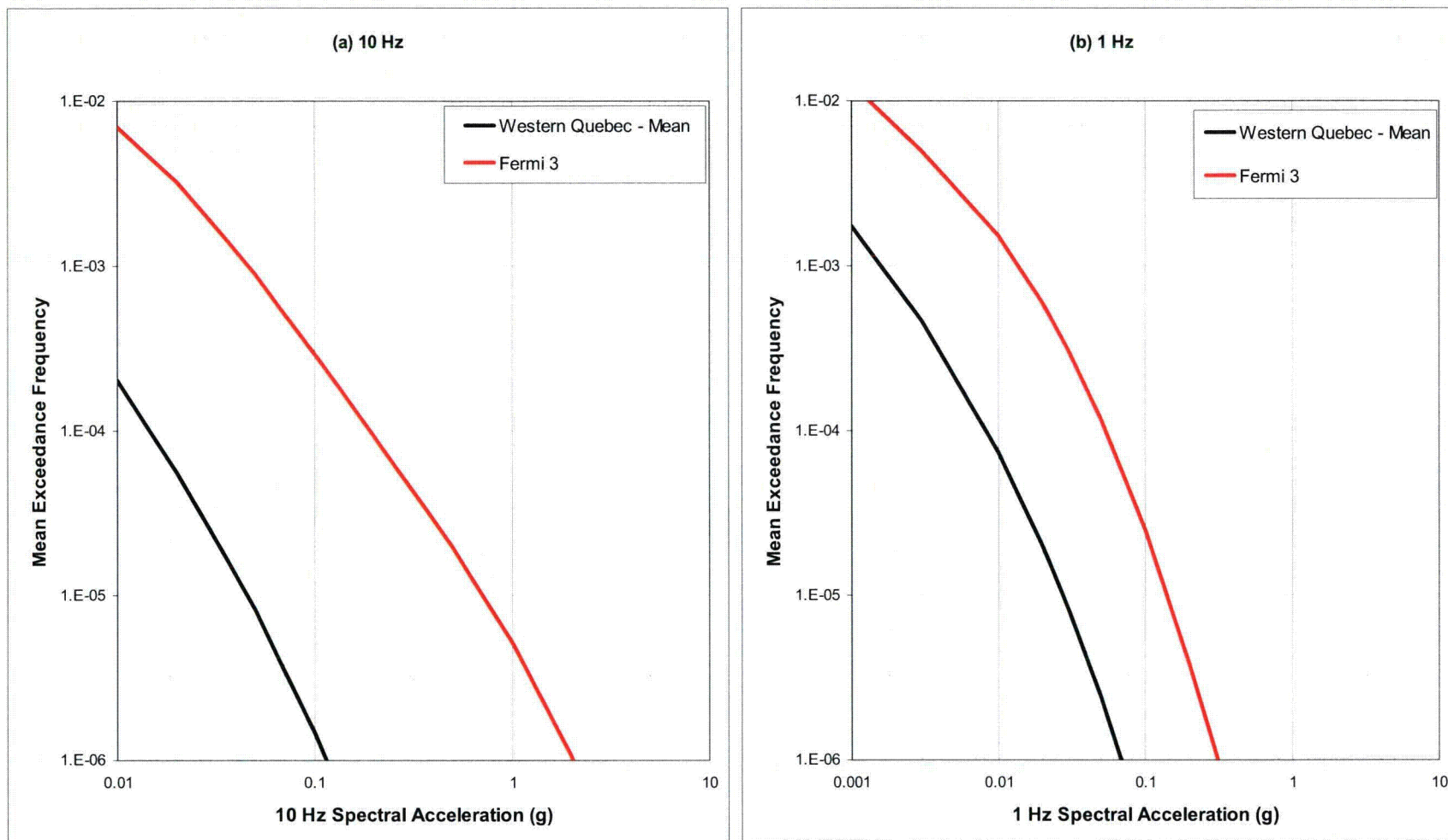


Figure 8 – Mean hazard from sensitivity analysis of the modified Western Quebec Seismic Zone EPRI-SOG sources compared to the total mean hazard computed for the FERMI 3 site. (a) 10 Hz spectral acceleration, (b) 1 Hz spectral acceleration.

Proposed COLA Revision

None

**Attachment 3
NRC3-10-0012**

**Response to RAI Letter No. 16
(eRAI Tracking No. 3918)**

RAI Question No. 02.05.02-04

RAI 02.05.02-04

FSAR section 2.5.2.4.2.1 and FSAR Figure 2.5.2–221 compare the EPRI 2004 ground motion models to newer ground motion models for the CEUS. The FSAR concludes that the newer ground motion models fall within the range of the EPRI models. However, it appears that two of the newer models (Atkinson and Boore, 2006, and Tavakoli and Pezeshk, 2005) fall close to (or above) the EPRI models at distances and frequencies relevant to seismic hazard at the Fermi site. For example, the median Atkinson and Boore (2006) model for a M 7.5 event, 1 Hz Spectral Acceleration, and distances of greater than 300 km, is above the EPRI Cluster 2 median and approaches the 95 percent level (FSAR Figure 2.5.2–221). The Tavakoli and Pezeshk (2005) model (M = 5) is also above the EPRI Cluster 3 median at short (less than 20 km) distances and high frequencies. The Tavakoli and Pezeshk model also exceeds the 95 percent level at very short distances. Please explain how the inclusion of these models instead of the EPRI Cluster 2 and 3 models would affect both low and high frequency seismic hazard at the Fermi site.

Response

FSAR Figure 2.5.2-221 compares the Electric Power Research Institute (EPRI) 2004 (FSAR Reference 2.5.2-259) ground motion models with the more recent models developed by Silva et al. (FSAR Reference 2.5.2-264), Atkinson and Boore (FSAR Reference 2.5.2-265), and Tavakoli and Pezeshk (FSAR Reference 2.5.2-266). As indicated in FSAR Section 2.5.2.4.2.1, the more recent models generally fall within the range of the EPRI 2004 models.

The EPRI 2004 ground motion models were developed by a SSHAC Level III assessment of viable ground motion prediction equations (GMPE) on the basis of their formulation and their consistency with available strong motion data for central and eastern North America (CENA). The major component of the EPRI 2004 model is specification of GMPEs in terms of four clusters that represent alternative model bases. Cluster 2 represents stochastic GMPEs developed on the basis of a double-corner model for the shape of the earthquake source spectra and Cluster 3 represents hybrid models that translate empirical western North America (WNA) GMPEs to CENA conditions. The Atkinson and Boore (FSAR Reference 2.5.2-265) GMPE represents a newer model of Cluster 2, although it uses a finite-fault stochastic approach instead of a double-corner point source model for the source. The Tavakoli and Pezeshk (FSAR Reference 2.5.2-266) GMPE represents a more recent GMPE of the Cluster 3 hybrid class. A sufficient assessment of the effect of including the newer models can be obtained by comparing the hazard computed using these two newer models with the hazard computed using the central median models for the two clusters to which they would be assigned.

Sensitivity hazard calculations were performed using the median EPRI 2004 models for Clusters 2 and 3 and using the Atkinson and Boore (FSAR Reference 2.5.2-265) and Tavakoli and Pezeshk (FSAR Reference 2.5.2-266) GMPEs. The EPRI 2006 (FSAR Reference 2.5.2-267) aleatory variability models were used in the calculations along with the three alternative models to convert m_b magnitudes to M magnitudes for ground motion estimation. The calculations were conducted using the updated seismic source model presented in FSAR Section 2.5.2.4.3.2.

Implementation of the PSHA calculations requires the use of models to translate epicentral (point-source) distances into the appropriate distance measures used by the GMPEs. Both the EPRI 2004 Cluster 3 models and the Tavakoli and Pezeshk (FSAR Reference 2.5.2-266) model use rupture distance as the distance measure. Therefore the EPRI 2004 (FSAR Reference 2.5.2-259) Cluster 3 distance adjustment and added aleatory variability models were used to compute the hazard from the Electric Power Research Institute and Seismicity Owners Group (EPRI-SOG) sources using the Tavakoli and Pezeshk (FSAR Reference 2.5.2-266) model. The EPRI 2004 Cluster 2 models use the Joyner-Boore distance measure. However, the Atkinson and Boore (Reference 2.5.2-265) uses rupture distance as the distance measure. Therefore, to be consistent with the ground motion measure used in the model development, the Cluster 3 distance adjustment and added aleatory variability models were used to compute the hazard from the EPRI-SOG sources using the Atkinson and Boore model (FSAR Reference 2.5.2-265). Hazard calculations were conducted for both hard rock conditions using a minimum magnitude of m_b 5.0 and for the site-specific ground motion response spectra (GMRS) elevation using the cumulative absolute velocity (CAV) model with site amplification effect.

Figures 1 and 2 compare the results obtained with the EPRI 2004 Cluster 2 median model to those obtained using the Atkinson and Boore (FSAR Reference 2.5.2-265) model for 10 Hz and 1 Hz spectral accelerations, respectively. The Atkinson and Boore (FSAR Reference 2.5.2-265) model produces lower 10 Hz hazard than the EPRI 2004 Cluster 2 model because for most distances the median model is lower (FSAR Figure 2.5.2-221). The Atkinson and Boore (FSAR Reference 2.5.2-265) 10 Hz model only exceeds the EPRI 2004 Cluster 2 model for M 7.5 earthquakes at very small source-to-site distances (FSAR Figure 2.5.2-221). As shown in FSAR Figures 2.5.2-242 through 2.5.2-245, there is little contribution to the high frequency hazard from large magnitude earthquakes at short distances. The Atkinson and Boore (FSAR Reference 2.5.2-265) 1 Hz model produces higher hard rock hazard than the EPRI 2004 Cluster 2 model because the low frequency hazard is dominated by large, distant earthquakes and the Atkinson and Boore (FSAR Reference 2.5.2-265) model is somewhat higher for these conditions. However, when the CAV model is applied, the Atkinson and Boore (FSAR Reference 2.5.2-265) model produces similar hazard to the EPRI 2004 Cluster 2 model because the Atkinson and Boore (FSAR Reference 2.5.2-265) model predicts lower peak ground accelerations, and thus lower probabilities that earthquakes will produce a CAV value in excess of 0.16 g-sec.

Figures 3 and 4 compare the results obtained with the EPRI 2004 Cluster 3 median model to those obtained using the Tavakoli and Pezeshk (FSAR Reference 2.5.2-266) model for 10 Hz and 1 Hz spectral accelerations, respectively. The Tavakoli and Pezeshk (FSAR Reference 2.5.2-266) 10 Hz model produces lower hazard than the EPRI 2004 Cluster 3 model for mean frequencies of exceedance greater than 10^{-5} and slightly higher hazard at lower mean frequencies of exceedance. The Tavakoli and Pezeshk (FSAR Reference 2.5.2-266) 10 Hz model predicts higher median motions than the EPRI Cluster 3 model only for smaller magnitude events at small source-to-site distances (see FSAR Figure 2.5.2-221) and these events become the major contributor to the high frequency hazard at low frequencies of exceedance (FSAR Figures 2.5.2-244 and 2.5.2-245). The Tavakoli and Pezeshk (FSAR Reference 2.5.2-266) 1 Hz model produces similar hard rock hazard to that for the EPRI 2004 Cluster 3 model for mean frequencies of exceedance greater than 10^{-5} and slightly higher hazard at lower frequencies of

exceedance. The higher hazard at low frequencies of exceedance is due to the higher predictions of the Tavakoli and Pezeshk (FSAR Reference 2.5.2-266) at short distances as these events become greater contributors to the hazard. A similar comparison between the results produced by the two models is shown for the CAV calculations. For this case, there are greater differences between the models due to greater differences in their predicted peak ground accelerations.

An evaluation of the overall effect of the newer models on the definition of the Fermi 3 site GMRS can be made by comparing the weighted average of the hazard results obtained using the EPRI and newer models for hazards computed using CAV. Using the EPRI 2004 ground motion model logic tree shown in FSAR Figure 2.5.2-220, the relative weights assigned to Cluster 2 and Cluster 3 are 0.614 and 0.386, respectively. Figure 5 shows comparisons of the weighted average hazard curves from Figures 1 through 4. The results labeled EPRI 2004 models were computed assigning weight of 0.614 to the Cluster 2 results and 0.386 to the Cluster 3 results. The results labeled post EPRI 2004 were computed assigning weight of 0.614 to the Atkinson and Boore (FSAR Reference 2.5.2-265) results and 0.386 to the Tavakoli and Pezeshk (FSAR Reference 2.5.2-266) results. The relative weights defined for the Cluster 2 and Cluster 3 EPRI 2004 models were assumed to apply to the newer models that fall within the same cluster classification. The weighed results for the EPRI 2004 models are equal to or higher than those for the post EPRI 2004 models for mean exceedance frequencies of 10^{-5} and higher. Thus, GMRS computed using the EPRI 2004 models would be higher than those computed using the post EPRI 2004 models. On the basis of this comparison, it is concluded that the use of the Atkinson and Boore (FSAR Reference 2.5.2-265) and Tavakoli and Pezeshk (FSAR Reference 2.5.2-266) models would not lead to a higher GMRS than presented in the FSAR.

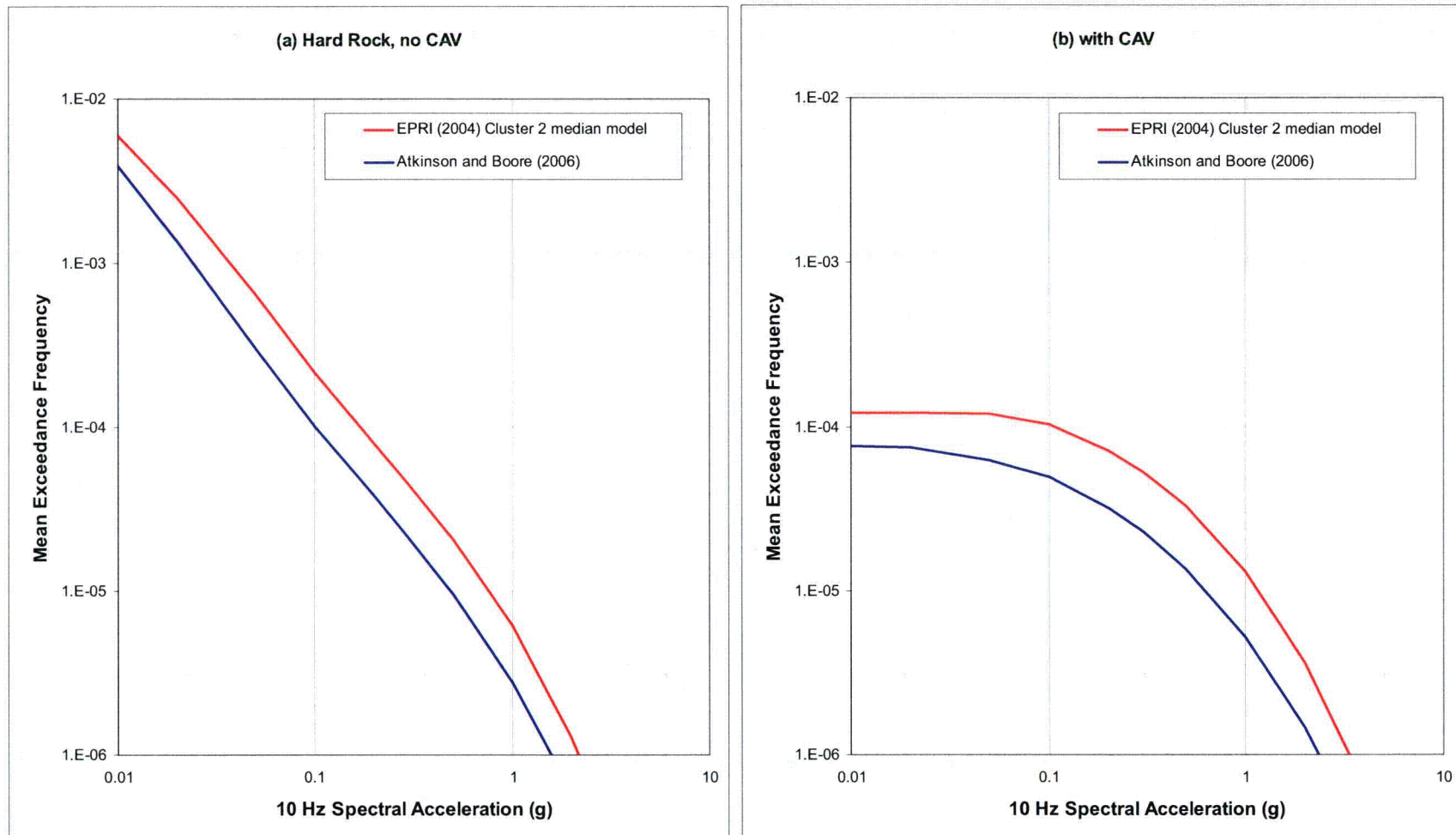


Figure 1 – Comparison of 10 Hz hazard results for the Fermi 3 seismic source model using the EPRI 2004 Cluster 2 median model and the Atkinson and Boore (FSAR Reference 2.5.2-265) model.

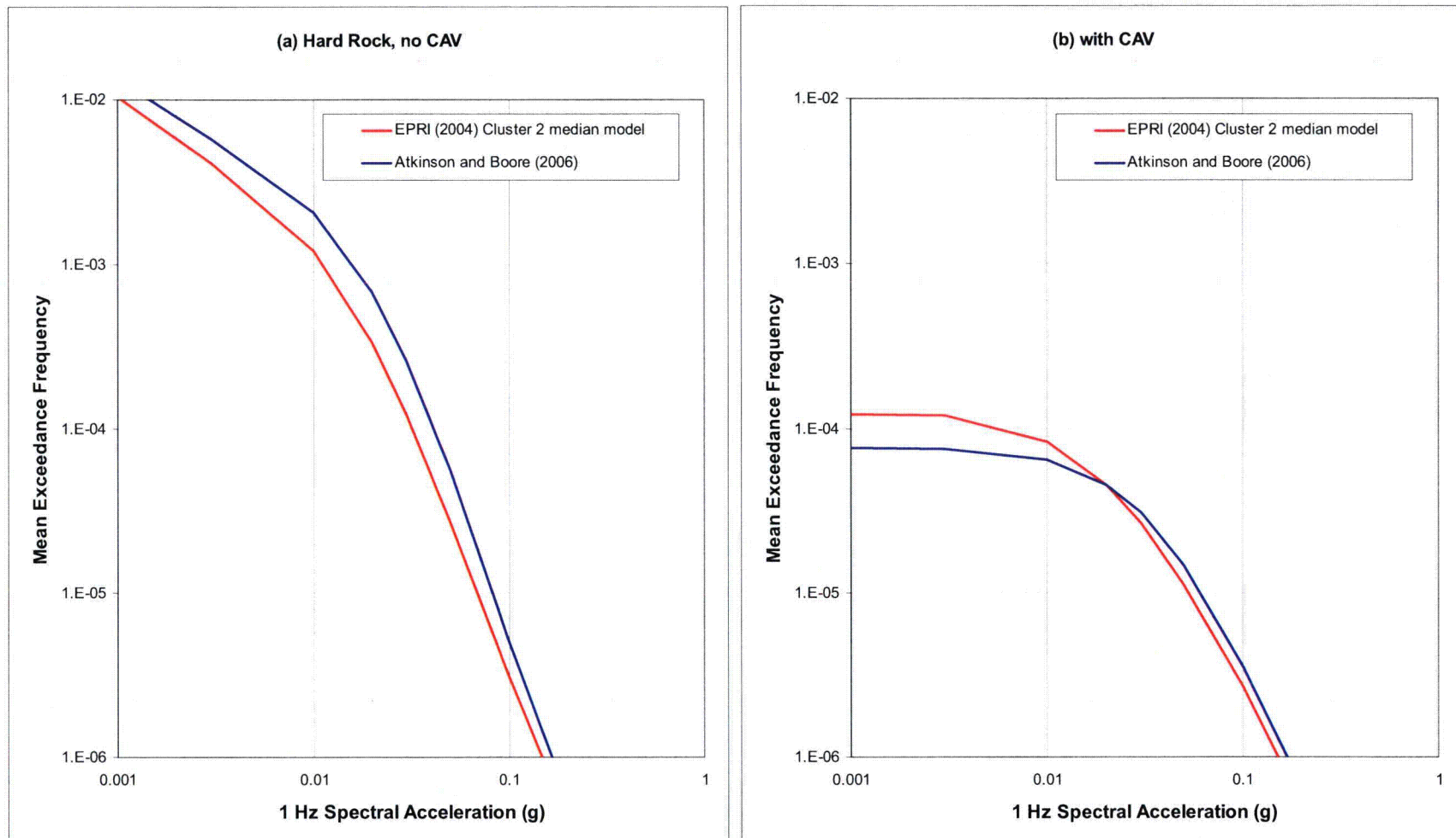


Figure 2 – Comparison of 1 Hz hazard results for the Fermi 3 seismic source model using the EPRI 2004 Cluster 2 median model and the Atkinson and Boore (FSAR Reference 2.5.2-265) model.

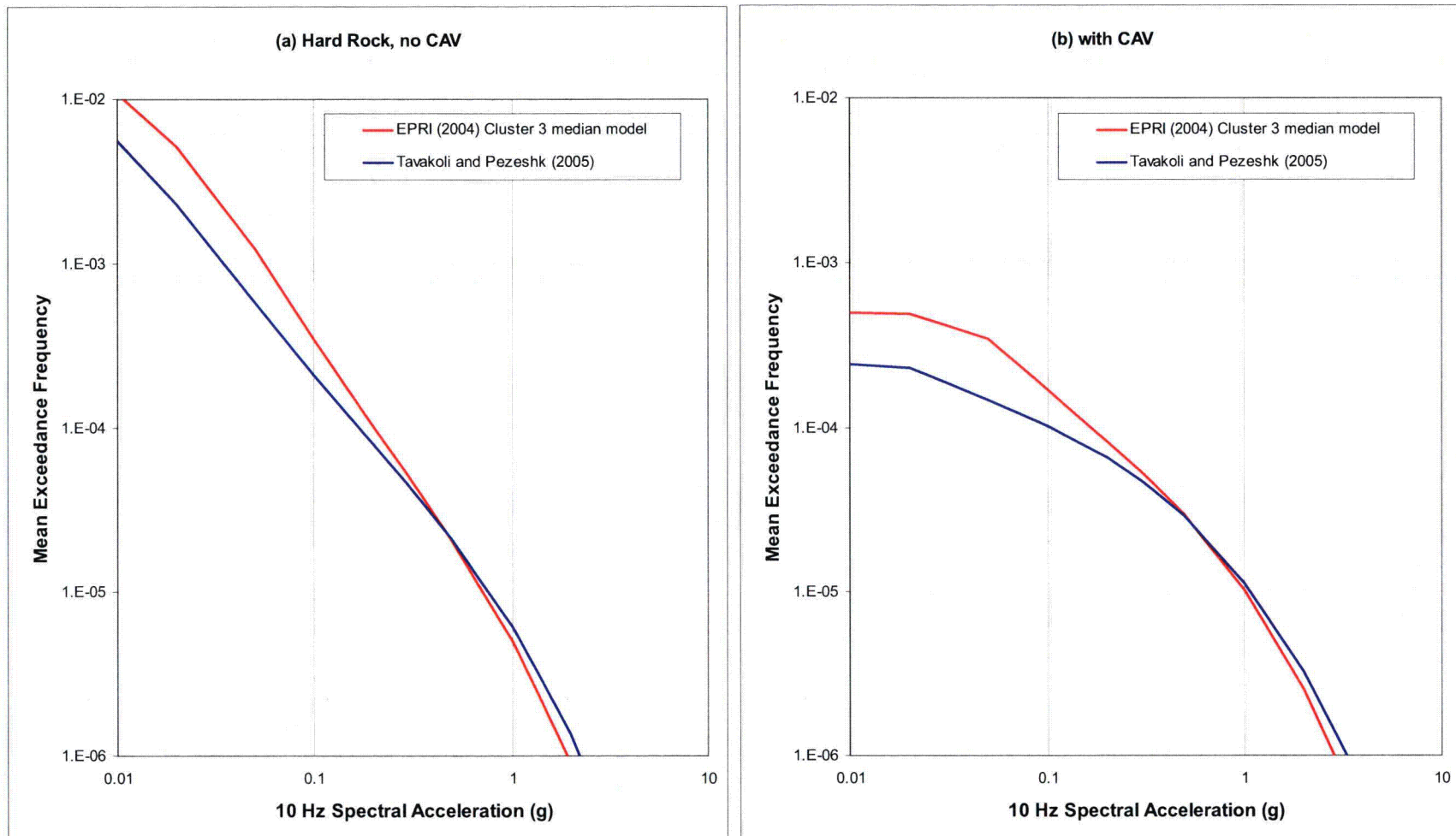


Figure 3 – Comparison of 10 Hz hazard results for the Fermi 3 seismic source model using the EPRI 2004 Cluster 3 median model and the Tavakoli and Pezeshk (FSAR Reference 2.5.2-266) model.

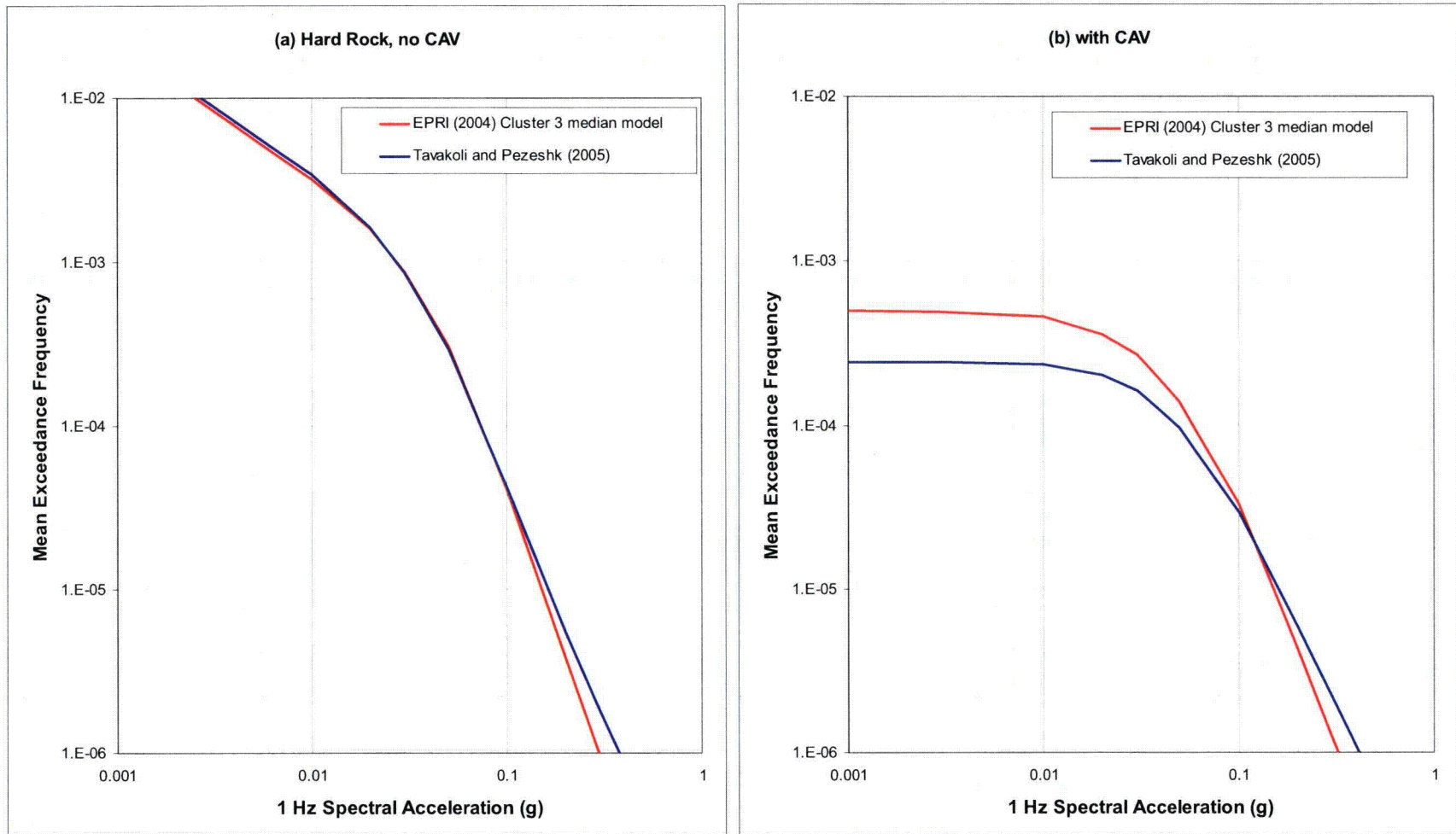


Figure 4 – Comparison of 1 Hz hazard results for the Fermi 3 seismic source model using the EPRI 2004 Cluster 3 median model and the Tavakoli and Pezeshk (FSAR Reference 2.5.2-266) model.

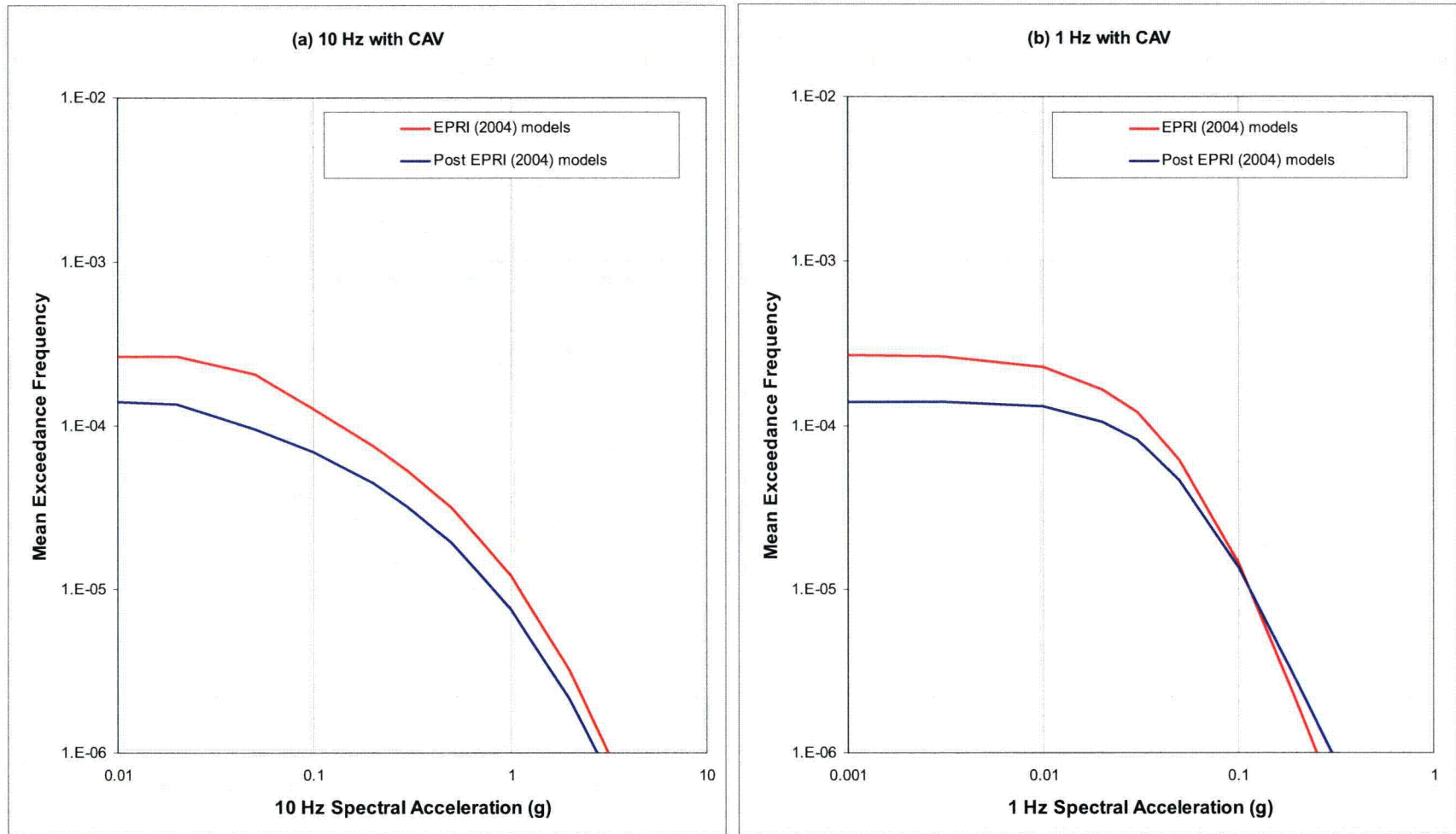


Figure 5 – Comparison of weighted average hazard results for the EPRI 2004 Cluster 2 and 3 models to the weighted average hazard results for the Atkinson and Boore (FSAR Reference 2.5.2-265) and Tavakoli and Pezeshk (FSAR Reference 2.5.2-266) models. Calculations are for the GMRS profile amplification and include the use of the CAV filter.

Proposed COLA Revision

The first sentence of the third to last paragraph in this FSAR section 2.5.2.4.2.1 incorrectly references Figure 2.5.2-220 rather than Figure 2.5.2-221. Complete Figure 2.5.2-221 is provided to replace FSAR Figure 2.5.2-221, which is half shown on the current Fermi 3 FSAR. Revisions to FSAR Section 2.5.2.4.2.1 and FSAR Figure 2.5.2-221 are shown in the attached markup.

Markup of Detroit Edison COLA
(following 3 pages)

The following markup represents how Detroit Edison intends to reflect this RAI response in a future submittal of the Fermi 3 COLA. However, the same COLA content may be impacted by revisions to the ESBWR DCD, responses to other COLA RAIs, other COLA changes, plant design changes, editorial or typographical corrections, etc. As a result, the final COLA content that appears in a future submittal may be different than presented here.

1 Hz median models for ground motion cluster 1 with the three single-corner stochastic models developed by Silva et al. (Reference 2.5.2-264). The updated models all fall well within the range of the EPRI (Reference 2.5.2-259) models.

The two plots in the center of Figure 2.5.2-220²²¹ compare the EPRI (Reference 2.5.2-259) 5th , 50th , and 95th percentile 10 Hz and 1 Hz median models for ground motion cluster 2 with the model developed by Atkinson and Boore (Reference 2.5.2-265). The Atkinson and Boore (Reference 2.5.2-265) model uses rupture distance as the distance measure, while the EPRI (Reference 2.5.2-259) cluster 2 models use Joyner-Boore distance. The comparisons shown on Figure 2.5.2-221 were made assuming that the top of rupture for the M 5 earthquake is at a depth of 4 km (2.5 mi.), based on a mean point-source depth of 6 km (3.7 mi.) (Reference 2.5.2-261). The median ground motions produced by the updated Atkinson and Boore (Reference 2.5.2-265) model fall within the range of the EPRI (Reference 2.5.2-259) cluster 2 medians except for distances less than about 7 km (4.3 mi.) for large-magnitude earthquakes.

The two plots on the right of Figure 2.5.2-221 compare the EPRI (Reference 2.5.2-259) 5th , 50th , and 95th percentile 10 Hz and 1 Hz median models for ground motion cluster 3 with the model developed by Tavakoli and Pezeshk (Reference 2.5.2-266). The Tavakoli and Pezeshk (Reference 2.5.2-266) model predictions generally fall within the range of the EPRI (Reference 2.5.2-259) cluster 3 medians except for small magnitudes at short rupture distances.

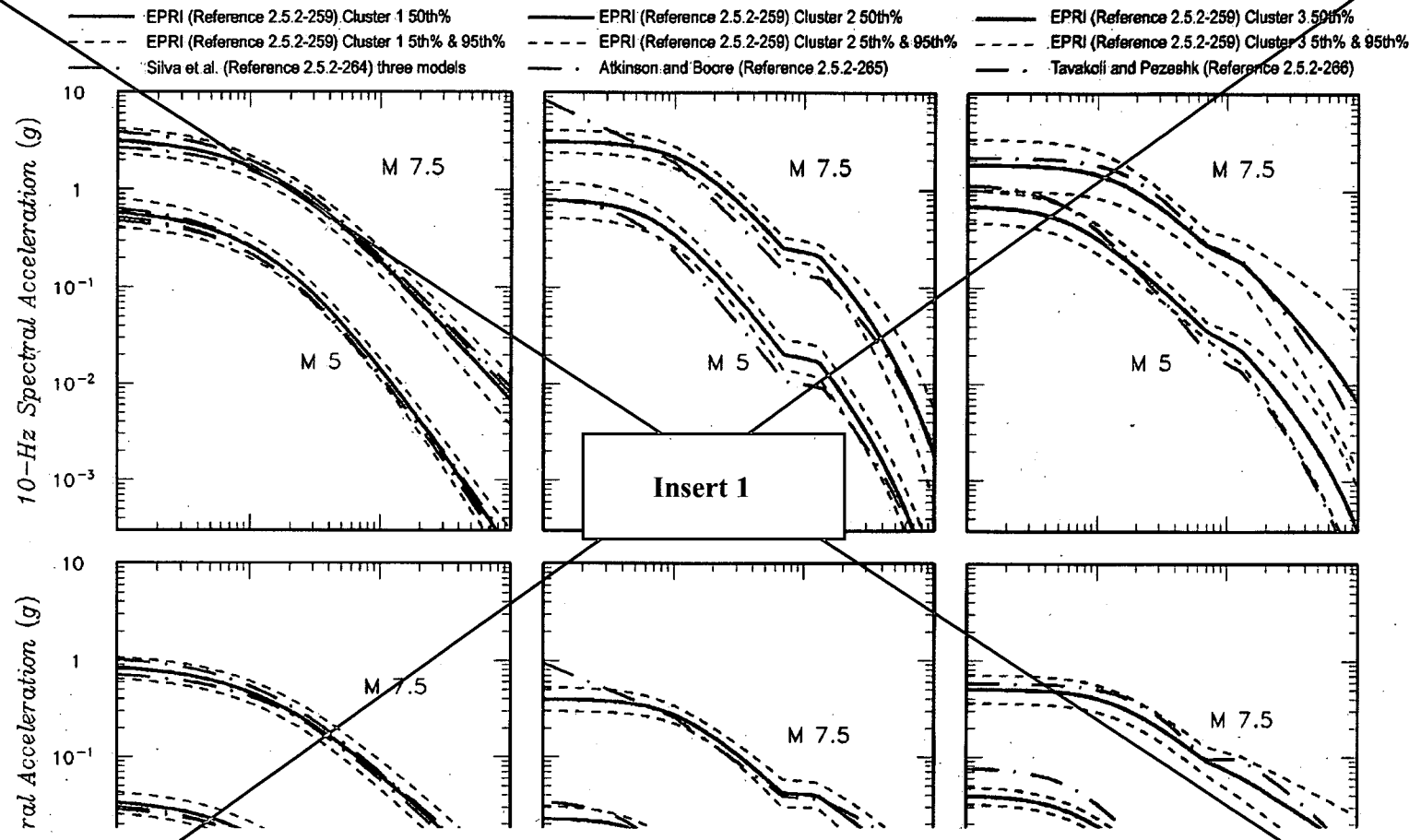
As presented in Subsection 2.5.2.4.4, large-magnitude earthquakes at very small distances are not a significant contributor to the hazard. Also, small-magnitude earthquakes have only a small contribution to the low-frequency hazard. On the basis of the comparisons shown on Figure 2.5.2-221, it is concluded that the EPRI (Reference 2.5.2-259) median ground motion models are appropriate for use in computing the hazard for the Fermi 3 site.

2.5.2.4.2.2 Models for Ground Motion Aleatory Variability

The EPRI (Reference 2.5.2-259) study also provided a characterization of the aleatory variability in CEUS ground motions based on an assessment of information available at the time. More recently, EPRI conducted a study focused in part on evaluating the appropriate aleatory

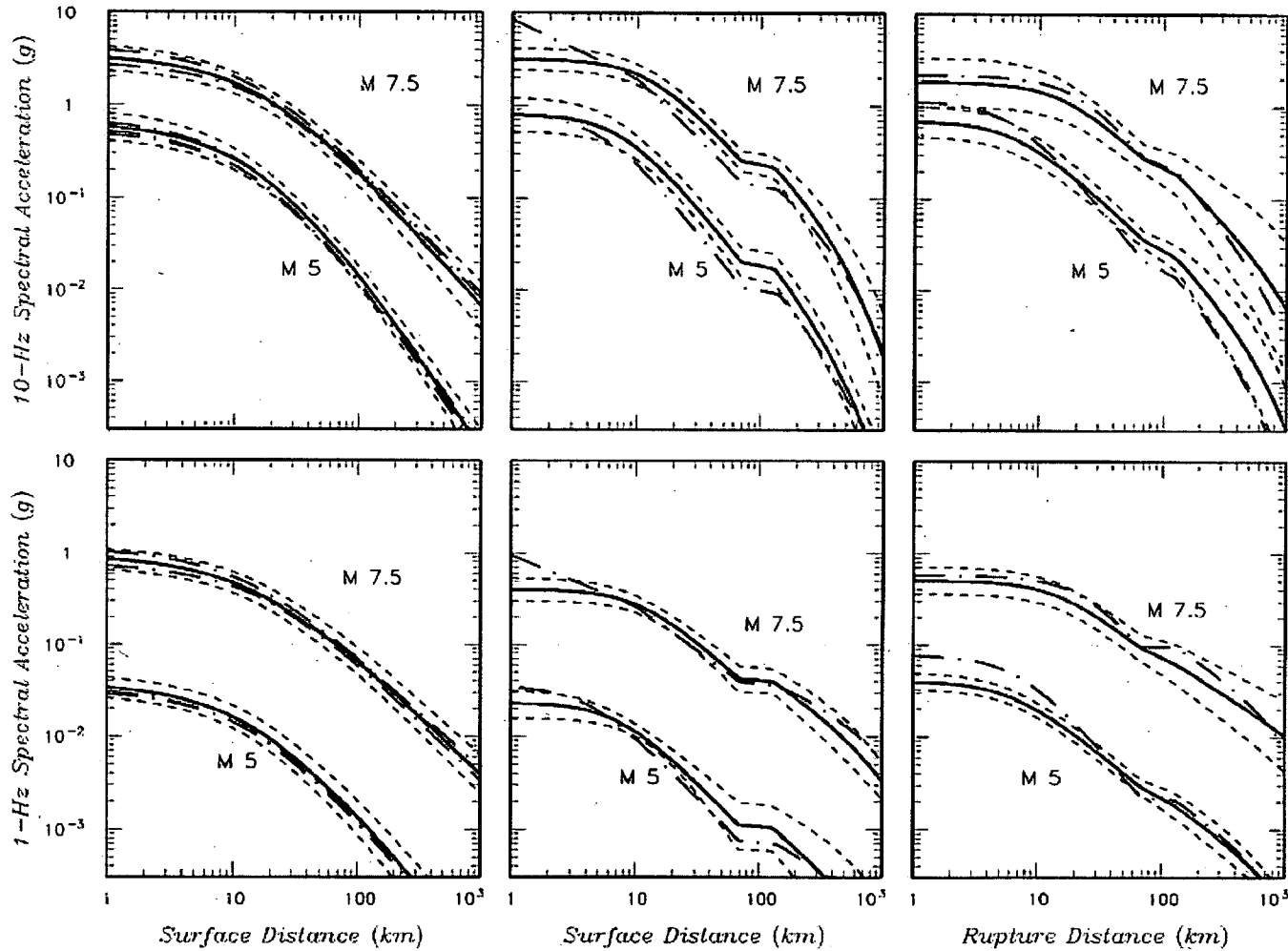
Figure 2.5.2-221 Comparison of Median Ground Motion Models Used in the PSHA with Recently Published Models

[EF3 COL2.0-27-A]



Insert 1

- EPRI (Reference 2.5.2-259) Cluster 1 50th%
- - - EPRI (Reference 2.5.2-259) Cluster 1 5th% & 95th%
- Silva et al. (Reference 2.5.2-264) three models
- EPRI (Reference 2.5.2-259) Cluster 2 50th%
- - - EPRI (Reference 2.5.2-259) Cluster 2 5th% & 95th%
- Atkinson and Boore (Reference 2.5.2-265)
- EPRI (Reference 2.5.2-259) Cluster 3 50th%
- - - EPRI (Reference 2.5.2-259) Cluster 3 5th% & 95th%
- Tavakoli and Pezashk (Reference 2.5.2-266)



**Attachment 4
NRC3-10-0012**

**Response to RAI Letter No. 16
(eRAI Tracking No. 3938)**

RAI Question No. 02.05.02-08

RAI 02.05.02-08

In order for the staff to verify the adequacy of the Fermi 3 site PSHA relative to the seismicity in the Anna, Ohio and Northeast Ohio areas, please provide the input source parameters (e.g. activity rates) as well as the specific source geometries used by each of the EPRI Teams to model these two potential sources. In addition, provide the corresponding PSHA hazard curves for these two sources.

Response

The seismic sources modeling the seismicity in the Anna, Ohio, and Northeastern Ohio areas have been selected for each of the six Electric Power Research Institute and Seismicity Owners Group (EPRI-SOG) Expert Teams. For each source the following are provided:

- Seismic source parameters specified in the original EPRI-SOG format (Provided as ASCII files on the enclosed CD).
- Probabilistic seismic hazard curves calculated for two spectral periods (1 Hz and 10 Hz) with and without cumulative absolute velocity (CAV) (Provided as plots in this response.)

List of Sources

The specific seismic sources that cover the Anna and Northeastern Ohio areas are discussed below and are listed in Tables 1 through 6 and shown on Figures 1 through 6. Table 7 lists the source designations used in this response and the corresponding names used in the FSAR Section 2.5.2. The sources are also shown on FSAR Figures 2.5.2-204 through 2.5.2-209.

Bechtel Team

The Electric Power Research Institute (EPRI) (Reference 2.5.2-202) seismic sources for the Bechtel team covering the Anna, Ohio, and Northeastern Ohio areas are: background source BBZ6; source B-N1 (Anna, Ohio area); and the combined source BC06 (Sources BEC-27 and BEC-N1 on FSAR Figure 2.5.2-204). Background source BBZ6 also covers the areas of B-N1 and BC06. The background source is always active ($P^* = 1$), source B-N1 has P^* of 0.6. The combined source BC06 receives a weight of 0.12 (Table 1). The Bechtel team (Reference 2.5.2-201, volume 10) assigned probabilities of activity of 0.6 and 0.2 to sources BEC-N1 and BEC-27, respectively and also stated that these were independent probabilities. These interpretations produce four alternatives: BEC-N1 alone active with probability 0.48, BEC-27 alone active with probability 0.08, both active (the combined source BC06) with probability 0.12, and neither active with probability 0.32. In defining the source set for the Fermi site calculation, EPRI (Reference 2.5.2-202) found that the option of BEC-27 alone active contributed less than one percent to the total hazard and this option was not included in the Bechtel team source set used at that time. The probability mass of 0.08 was assigned to neither source active case in order to maintain the correct probability that BEC-N1 is active (0.48 plus 0.12 sums to 0.6). Testing done in developing the source set for the Fermi 3 probabilistic seismic hazard analysis (PSHA) also produced the same result and the source combinations for BEC-N1 and BEC-27 used by EPRI (Reference 2.5.2-202) and listed in Table 1 below were used for the Fermi 3 PSHA

reported in FSAR Section 2.5.2.4. Figure 1 shows the geometry of the three zones and the location of the Fermi 3 site (yellow star) for reference.

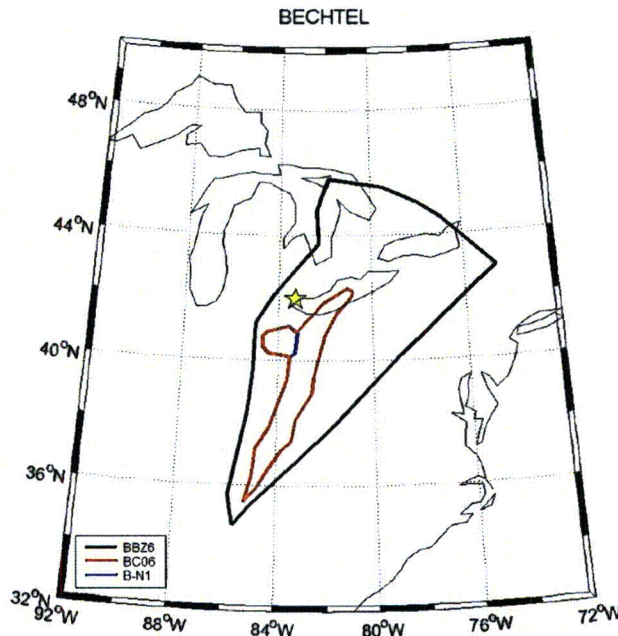


Figure 1 – Geometry of the Bechtel sources that cover the Anna, Ohio, and Northeastern Ohio areas.

Source Combination	Weight Assigned to Source Combination
BBZ6+ B-N1	0.48
BBZ6 + BC06	0.12
BBZ6	0.4

Note: The source designation corresponds to the one used in attached EPRI-SOG source parameters files. Refer to Table 7 for the corresponding designations in FSAR.

Dames & Moore Team

The EPRI (Reference 2.5.2-202) seismic sources for the Dames & Moore team that cover the Anna, Ohio, and Northeastern Ohio areas are: D-08 (Eastern Marginal Basin), D-12 (Anna, Ohio), and DB70 (Wisconsin-Michigan Block). Sources D-12 and DB70 are always active (probability of activity P* of 1), while source D-08 is reported having P* of 0.08. However, based on the occurrence of two post-EPRI earthquakes of m_b 5.0 and 5.2 (respectively in 1986 and in 1998) the probability of activity for this source was increased to 1 for the Fermi 3 PSHA

(FSAR Table 2.5.2-202). Figure 2 shows the geometry of these zones and the location of the Fermi 3 site (yellow star) for reference. Table 2 lists the source combinations used in the hazard calculations.

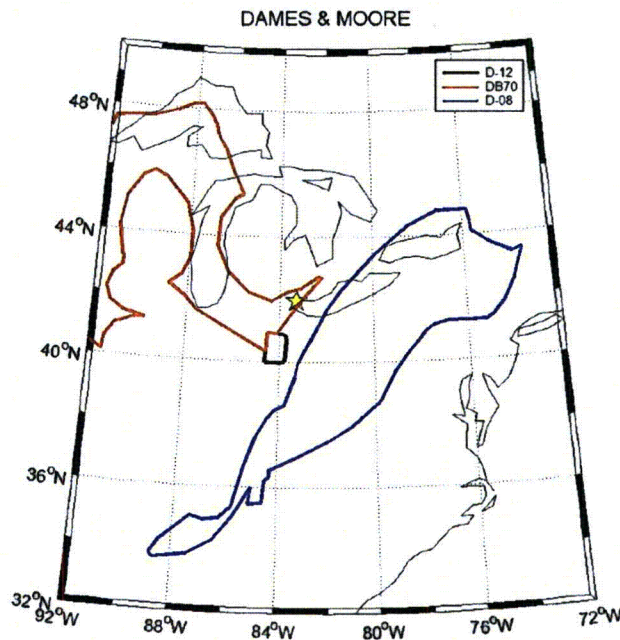


Figure 2 – Geometry of the Dames & Moore sources that cover the Anna, Ohio, and Northeastern Ohio areas.

Table 2 Dames & Moore Team Source Zone Combinations for the Anna, Ohio, and Northeastern Ohio areas	
Source Combination	Weight Assigned to Source Combination
D-08 + D-12 + DB70	1.0
Note: The source designation corresponds to the one used in attached EPRI-SOG source parameters files. Refer to Table 7 for the corresponding designations in FSAR.	

Law Engineering Team

The EPRI (Reference 2.5.2-202) seismic sources for the Law team that cover the Anna, Ohio and Northeastern Ohio areas are L112 (Ohio-Pennsylvania Block), and L115 (Indiana Block). Both sources have a probability of activity P* of 1 (FSAR Table 2.5.2-203). Figure 3 shows the geometry of these zones and the location of the Fermi 3 site (yellow star) for reference. Table 3 lists the source combinations used in the hazard calculations.

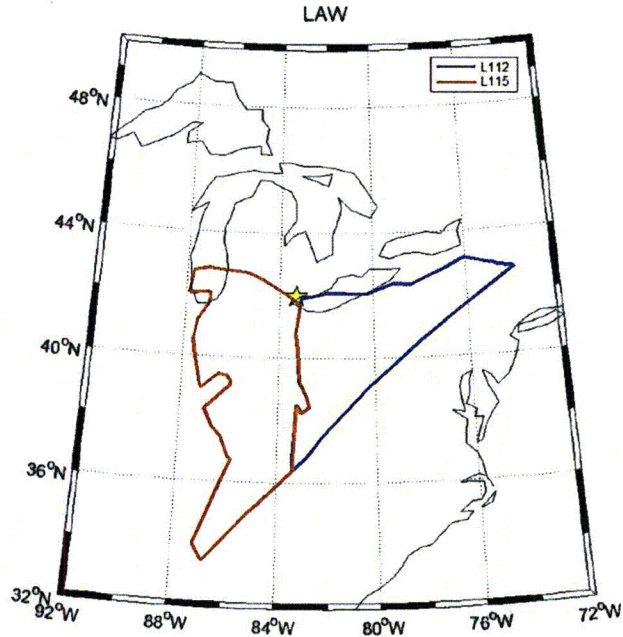


Figure 3 – Geometry of the Law Engineering team sources that cover the Anna, Ohio, and Northeastern Ohio areas.

Table 3 Law Engineering Team Source Zone Combinations for the Anna, Ohio, and Northeastern Ohio areas	
Source Combination	Weight Assigned to Source Combination
L112 + L115	1.0
Note: The source designation corresponds to the one used in attached EPRI-SOG source parameters files. Refer to Table 7 for the corresponding designations in FSAR.	

Rondout Team

The EPRI (Reference 2.5.2-202) seismic sources for the Rondout team that model the seismicity in the Anna, Ohio, and Northeastern Ohio areas are zones: R-08 (Anna, Ohio), R-10 (Southeast Michigan), R-11 (Northwestern Ohio), and R-12 (Cleveland, Ohio). Source R-08 is always active, with P* of 1. Source R-10 has P* of 0.95, source R-11 has P* of 0.87, and source R-12 has P* of 0.78 (FSAR Table 2.5.2-204). Figure 4 shows the geometry of these zones and the location of the Fermi 3 site (yellow star) for reference. Table 4 lists the source combinations used in the hazard calculations.

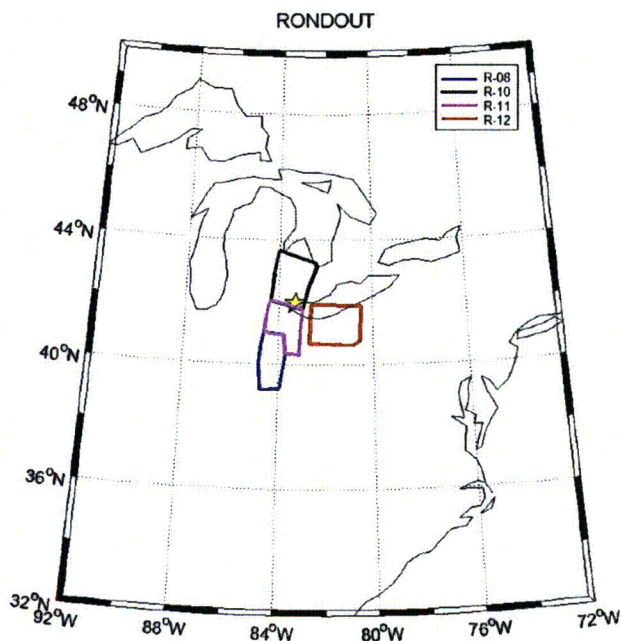


Figure 4 – Geometry of the Rondout team sources that cover the Anna, Ohio, and Northeastern Ohio areas.

Source Combination	Weight Assigned to Source Combination
R-08 + R-10 + R-11+ R-12	0.6447
R-08 + R-10 + R-11	0.1818
R-08 + R-10 + R-12	0.0963
R-08 + R-10	0.0272
R-08 + R-11 + R-12	0.0339
R-08 + R-11	0.0096
R-08 + R-12	0.0051
R-08	0.0014

Note: The source designation corresponds to the one used in attached EPRI-SOG source parameters files. Refer to Table 7 for the corresponding designations in FSAR.

Weston Geophysical Team

The EPRI (Reference 2.5.2-202) seismic sources for the Weston team that model the seismicity of the Anna, Ohio, and Northeastern Ohio areas are zones G-29 (Anna, Ohio), and WGC-101 (Southern Ontario-Ohio-Indiana). Source G-29 has a probability of activity P* of 0.93, and source WGC-101 has P* of 1 (FSAR Table 2.5.2-205). Source WGC-101 is represented by four alternative complementary sources (GC13, GC14, GC15, and GC16) that represent Source

WGC-101 with various zones cut out of it for the cases when they are active. Figure 5 shows the geometry of these zones and the location of the Fermi 3 site (yellow star) for reference. Note that Sources GC13, GC14, GC15, and GC16 encompass essentially the same area. Table 5 lists the source combinations used in the hazard calculations.

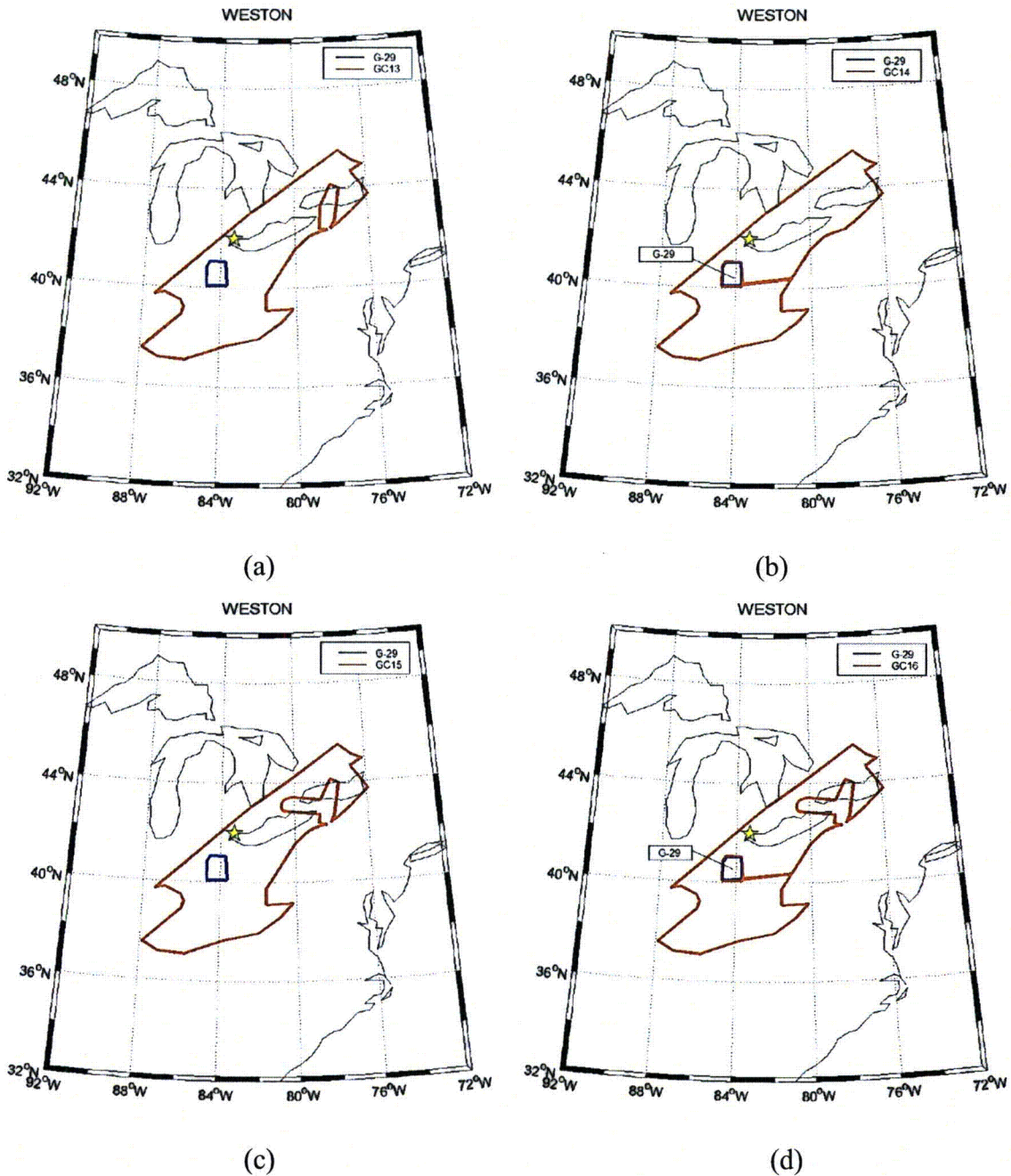


Figure 5 – Geometry of the Weston Geophysical team sources that cover the Anna, Ohio, and Northeastern Ohio areas. The four alternative complementary sources that represent source WGC-101 (GC13, GC14, GC15, and GC16) are shown in plots a, b, c, and d, respectively. In each plot the geometry of source G-29 is shown by the solid, blue line.

Table 5 Weston Geophysical Team Source Zone Combinations for the Anna, Ohio, and Northeastern Ohio areas	
Source Combination	Weight Assigned to Source Combination
GC13	0.0488
G-29 + GC14	0.1012
GC15	0.0252
G-29 + GC16	0.8288

Note: The source designation corresponds to the one used in attached EPRI-SOG source parameters files. Refer to Table 7 for the corresponding designations in FSAR.

Woodward-Clyde Team

The EPRI (Reference 2.5.2-202) seismic sources for the Woodward-Clyde team that model the seismicity of the Anna, Ohio, and Northeastern Ohio areas are zones W-35 (NE Ohio Gravity & NOTA), W-36 (Michigan-Ohio Gravity High), W-37 (Bowling Green-Auglaize Fault Systems), W-38 (Champaign-Anna Fault), W-39 (Anna, Ohio, Geophysical Intersection & none of the above zone, a source with the same geometry [NOTA]), and the background zone WB67. Source W-35 has an assessed P* of 0.548 given by the sum of the probabilities for zones 35 and NOTA. Sources W-36, W-37, W-38, and W-39 are considered dependent and mutually exclusive. Their P* values are respectively: 0.090, 0.072, 0.065, and 0.773 (FSAR Table 2.5.2-206). The probability of activity of zone 39 is calculated considering the NOTA zone. The background zone WB67 is always active (P* of 1) and covers the entire area around the site. Figure 6 shows the geometry of these zones and the location of the Fermi 3 site (yellow star) for reference. Table 6 lists the source combinations used in the hazard calculations.

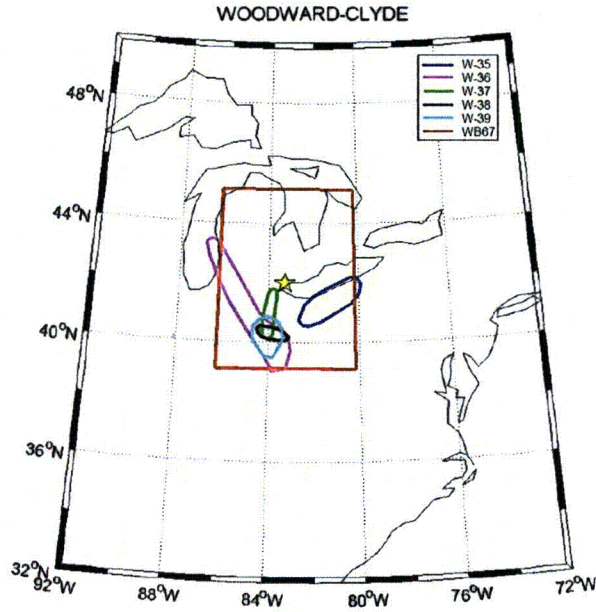


Figure 6 – Geometry of the Woodward-Clyde team sources that cover the Anna, Ohio, and Northeastern Ohio areas.

Source Combination	Weight Assigned to Source Combination
WB67 + W-35 + W-36	0.0619
WB67 + W-35 + W-37	0.0418
WB67 + W-35 + W-38	0.0384
WB67 + W-35 + W-39	0.4309
WB67 + W-36	0.0461
WB67 + W-37	0.0312
WB67 + W-38	0.0286
WB67 + W-39	0.3211

Note: The source designation corresponds to the one used in attached EPRI-SOG source parameters files. Refer to Table 7 for the corresponding designations in FSAR.

Table 7 Source Designations Used in This Response and Corresponding Designations in Fermi 3 FSAR			
Source Designation in This Response	Source Designation in FSAR Section 2.5.2	FSAR Table Number	FSAR Figure Number
BBZ6	BEC-BZ6	2.5.2-201	2.5.2-204
B-N1	BEC-N1	2.5.2-201	2.5.2-204
BC06 ⁽¹⁾	BEC-27 and BEC-N1 ⁽¹⁾	2.5.2-201	2.5.2-204
D-08	DAM-08	2.5.2-202	2.5.2-205
D-12	DAM-12	2.5.2-202	2.5.2-205
DB70	DAM-70	2.5.2-202	2.5.2-205
L112	LAW-112	2.5.2-203	2.5.2-206
L115	LAW-115	2.5.2-203	2.5.2-206
R-08	RND-08	2.5.2-204	2.5.2-207
R-10	RND-10	2.5.2-204	2.5.2-207
R-11	RND-11	2.5.2-204	2.5.2-207
R-12	RND-12	2.5.2-204	2.5.2-207
G-29	WGC-29	2.5.2-205	2.5.2-208
GC13, GC14, GC15, GC16 ⁽²⁾	WGC-101 ⁽²⁾	2.5.2-205	2.5.2-208
W-35	WCC-35	2.5.2-206	2.5.2-209
W-36	WCC-36	2.5.2-206	2.5.2-209
W-37	WCC-37	2.5.2-206	2.5.2-209
W-38	WCC-38	2.5.2-206	2.5.2-209
W-39	WCC-39	2.5.2-206	2.5.2-209
WB67	WCC-B67	2.5.2-206	2.5.2-209

Notes:

1. Source BEC-27 is represented in the calculation by the combined source BC06.
2. Source WGC-101 is represented in the calculation by its complementary sources GC13, GC14, GC15, GC16.

Seismic Source Parameters in EPRI-SOG Format

The seismic source parameters for the sources listed in Tables 1 through 6 are provided in the original EPRI-SOG (Reference 2.5.2-201) format used by the EPRI-SOG program EQHAZ. A detailed description of the format of these files is provided in EPRI-SOG (Reference 2.5.2-201, Volume 3). Three files are provided for each EPRI-SOG expert team:

- One containing the basic data on the maximum magnitude distribution and seismicity option distribution (files XXX.BAS).
- One containing the geometry of the sources (files XXX.GEO).
- One containing the seismicity parameters (files XXX.SEI).

The file name XXX designates a three character code indicating the EPRI-SOG expert team: BEC for the Bechtel team, DAM for the Dames & Moore team, LAW for the Law Engineering team, RND for the Rondout team, WGC for the Weston Geophysical team, and WCC for the Woodward-Clyde team. The files are in ASCII format and can be opened with a text editor or Notepad. The files are contained in on the enclosed CD.

The data contained in these files is described below using the files for the Bechtel team.

Basic Data File

For the Bechtel team, the file "BEC.BAS" contains the following information:

```
TEAM=BEC  SITE=67      FERMI 3
-83.262    41.961
B-N1
10  1      9
1
4 5.4 .10 5.7 .40 6.0 .40 6.6 .10
3 1 .33  2 .34  4 .33 0 0 0
BBZ6
10  1     19
1
4 5.4 .10 5.7 .40 6.0 .40 6.6 .10
3 1 .33  2 .34  3 .33 0 0 0
BC06
10  1     26
1
4 5.4 .10 5.7 .40 6.0 .40 6.6 .10
3 1 .33  2 .34  4 .33 0 0 0
q
```

Details of the meaning of the parameters are provided in EPRI-SOG (Reference 2.5.2-201, volume 3). The meaning of the data on each line is as follows:

- The first line is a header record.
- The second line specifies the longitude and latitude of the Fermi 3 site.
- The third line gives the name of the first source.
- The fourth line contains the point source depth used in the EPRI-SOG calculations, the number of source pieces used for the source (typically only 1) and the number of vertices that define the source geometry for each source piece in file BEC.GEO.
- The fifth line specifies a code for each source piece used to indicate whether the source piece is additive (1) or subtractive or a hole in a larger source (-1).
- The sixth line specifies the number of alternative maximum magnitude values and then pairs of maximum magnitude and assigned weight.
- The seventh line specifies the number of seismicity options, pairs of seismicity option number and assigned weight, and then a code for each seismicity option indicating how the seismicity parameters are defined in file BEC.SEI.

The fourth through the seventh line are then repeated for each additional source. A “q” for the source name indicates the end of the sources for a specific team.

Source Geometry File

For the Bechtel team the file “BEC.GEO” contains the following information.

```
'B-N1' $$$$$ ESRI      58 BECHTEL          N1  **BECDBM 104  1 057 00**          9  57
  83.19  40.90  83.28  40.26  83.43  40.14  84.38  40.24  84.64  40.46
  84.64  40.80  84.44  40.95  83.54  41.11  83.19  40.90
'BBZ6' $$$$$ ESRI      7 BECHTEL          BZ6  **BECDBM 155  1 022 00**          19  22
  85.65  34.75  85.85  35.71  85.19  38.30  85.02  39.48  84.94  41.21
  84.15  42.12  82.31  43.73  82.36  44.80  81.89  45.78  79.46  45.52
  78.05  45.06  76.89  44.50  74.61  42.91  78.82  40.21  80.47  38.91
  81.69  37.92  83.12  36.81  84.97  35.40  85.65  34.75
'BC06' $$$$$          BECHTEL          C06  **BECDBM          1 006 00**          26 10  1
  80.84  42.20  81.11  42.30  82.06  41.87  83.22  40.92  83.54  41.11
  84.44  40.95  84.64  40.80  84.64  40.46  84.38  40.24  83.51  40.15
  83.60  39.40  84.34  37.84  84.85  37.17  84.97  36.28  85.24  35.49
  84.76  35.90  84.29  36.50  83.79  37.12  83.39  37.43  83.22  38.10
  82.55  38.94  82.49  39.46  82.03  40.82  81.48  41.54  80.89  42.03
  80.84  42.20
```

The meaning of the data for each source is described using the first source in this file as an example, as follows:

- The first line is a header record with the source name given at the beginning.
- The second and third indented lines for the first source contain longitude-latitude pairs for each of the vertices defining the source polygon. The number of vertices is specified in the BEC.BAS file.

This information is repeated for each source specified in the BEC.BAS file.

Seismicity Parameter File

For the Bechtel team the file “BEC.SEI” contains the following information.

```
45  0  1  4
14 26 14 27 15 26 15 27
-1.15 0.576 -1.15 0.576 -1.14 0.573 -1.15 0.577
-1.15 0.576 -1.15 0.576 -1.14 0.573 -1.15 0.577
45  0  2  4
14 26 14 27 15 26 15 27
-1.15 0.577 -1.17 0.579 -1.04 0.562 -1.24 0.590
45  0  3  4
14 26 14 27 15 26 15 27
-1.05 0.766 -1.06 0.773 -0.94 0.710 -1.13 0.815
56  0  1  76
10 28 10 29 10 30 10 31 10 32 10 33 11 28 11 29 11 30 11 31 11 32 11 33
11 34 12 27 12 28 12 29 12 30 12 31 12 32 12 33 12 34 12 35 12 36 13 26
13 27 13 28 13 29 13 30 13 31 13 32 13 33 13 34 13 35 13 36 14 26 14 27
14 28 14 29 14 30 14 31 14 32 14 33 14 34 15 26 15 27 15 28 15 29 15 30
15 31 15 32 15 33 16 25 16 26 16 27 16 28 16 29 16 30 16 31 17 25 17 26
17 27 17 28 17 29 17 30 18 25 18 26 18 27 18 28 18 29 19 25 19 26 19 27
19 28 20 25 20 26 21 25
-1.64 1.073 -1.64 1.073 -1.64 1.074 -1.64 1.075 -1.64 1.075 -1.64 1.075 -1.64 1.074 -1.64 1.074 -1.64 1.074 -1.64 1.075
-1.64 1.075 -1.64 1.076 -1.64 1.076 -1.64 1.075 -1.64 1.076 -1.64 1.076 -1.64 1.075 -1.64 1.072 -1.64 1.072 -1.64 1.075
-1.64 1.077 -1.64 1.076 -1.64 1.075 -1.64 1.074 -1.64 1.075 -1.64 1.076 -1.64 1.077 -1.64 1.075 -1.64 1.071 -1.64 1.068
-1.64 1.074 -1.64 1.076 -1.64 1.076 -1.64 1.075 -1.64 1.071 -1.64 1.072 -1.64 1.075 -1.64 1.076 -1.64 1.075 -1.64 1.074
-1.64 1.074 -1.64 1.074 -1.64 1.076 -1.64 1.064 -1.64 1.067 -1.64 1.073 -1.64 1.075 -1.64 1.077 -1.64 1.076 -1.64 1.076
```

```

-1.64 1.075 -1.64 1.069 -1.64 1.069 -1.64 1.069 -1.64 1.072 -1.64 1.074 -1.64 1.077 -1.64 1.077 -1.64 1.072 -1.64 1.072
-1.64 1.072 -1.64 1.073 -1.64 1.075 -1.64 1.076 -1.64 1.074 -1.64 1.074 -1.64 1.074 -1.64 1.075 -1.64 1.074
-1.64 1.073 -1.64 1.072 -1.64 1.073 -1.64 1.072 -1.64 1.071 -1.64 1.071
56 0 2 76
10 28 10 29 10 30 10 31 10 32 10 33 11 28 11 29 11 30 11 31 11 32 11 33
11 34 12 27 12 28 12 29 12 30 12 31 12 32 12 33 12 34 12 35 12 36 13 26
13 27 13 28 13 29 13 30 13 31 13 32 13 33 13 34 13 35 13 36 14 26 14 27
14 28 14 29 14 30 14 31 14 32 14 33 14 34 15 26 15 27 15 28 15 29 15 30
15 31 15 32 15 33 16 25 16 26 16 27 16 28 16 29 16 30 16 31 17 25 17 26
17 27 17 28 17 29 17 30 18 25 18 26 18 27 18 28 18 29 19 25 19 26 19 27
19 28 20 25 20 26 21 25
-1.92 1.093 -1.86 1.085 -1.86 1.097 -1.85 1.101 -1.99 1.097 -2.07 1.092 -1.97 1.104 -1.89 1.106 -1.78 1.105 -1.77 1.100
-1.91 1.093 -2.08 1.087 -2.14 1.084 -1.86 1.105 -1.95 1.121 -1.91 1.128 -1.59 1.120 -1.15 1.091 -1.64 1.068 -1.99 1.074
-2.08 1.082 -2.19 1.075 -2.17 1.069 -1.60 1.073 -1.71 1.095 -1.78 1.127 -1.75 1.146 -1.61 1.136 -1.46 1.088 -1.38 1.041
-1.87 1.073 -2.17 1.080 -2.21 1.075 -2.13 1.065 -1.51 1.033 -1.29 1.061 -1.62 1.115 -1.28 1.153 -1.66 1.144 -1.83 1.119
-1.91 1.094 -2.01 1.082 -2.13 1.081 -1.21 0.957 -1.31 1.014 -1.44 1.099 -1.54 1.140 -1.82 1.156 -1.92 1.144 -1.97 1.119
-2.05 1.095 -1.54 0.975 -1.54 0.991 -1.52 1.022 -1.34 1.082 -1.67 1.123 -1.86 1.151 -1.89 1.150 -1.76 0.991 -1.71 1.000
-1.57 1.027 -1.56 1.075 -1.80 1.114 -1.85 1.133 -1.83 0.990 -1.83 0.999 -1.70 1.024 -1.72 1.055 -1.75 1.088 -1.74 0.972
-1.62 0.975 -1.48 0.985 -1.66 1.037 -1.55 0.951 -1.36 0.940 -1.42 0.940
56 0 3 76
10 28 10 29 10 30 10 31 10 32 10 33 11 28 11 29 11 30 11 31 11 32 11 33
11 34 12 27 12 28 12 29 12 30 12 31 12 32 12 33 12 34 12 35 12 36 13 26
13 27 13 28 13 29 13 30 13 31 13 32 13 33 13 34 13 35 13 36 14 26 14 27
14 28 14 29 14 30 14 31 14 32 14 33 14 34 15 26 15 27 15 28 15 29 15 30
15 31 15 32 15 33 16 25 16 26 16 27 16 28 16 29 16 30 16 31 17 25 17 26
17 27 17 28 17 29 17 30 18 25 18 26 18 27 18 28 18 29 19 25 19 26 19 27
19 28 20 25 20 26 21 25
-1.91 1.107 -1.85 1.074 -1.85 1.126 -1.84 1.150 -1.98 1.149 -2.07 1.140 -1.95 1.145 -1.87 1.146 -1.77 1.147 -1.76 1.142
-1.90 1.134 -2.07 1.124 -2.14 1.117 -1.84 1.177 -1.94 1.207 -1.89 1.212 -1.58 1.183 -1.15 1.099 -1.65 1.041 -1.99 1.081
-2.08 1.112 -2.19 1.084 -2.17 1.061 -1.60 1.107 -1.70 1.162 -1.76 1.227 -1.72 1.256 -1.59 1.217 -1.46 1.069 -1.40 0.936
-1.88 1.072 -2.17 1.101 -2.21 1.082 -2.12 1.044 -1.52 1.004 -1.29 1.073 -1.60 1.194 -1.26 1.267 -1.64 1.221 -1.82 1.157
-1.91 1.104 -2.01 1.086 -2.13 1.098 -1.26 0.789 -1.33 0.937 -1.43 1.154 -1.52 1.228 -1.80 1.256 -1.91 1.228 -1.96 1.173
-2.05 1.120 -1.58 0.878 -1.56 0.927 -1.53 0.981 -1.33 1.108 -1.65 1.183 -1.84 1.252 -1.87 1.247 -1.78 0.939 -1.73 0.959
-1.58 1.003 -1.55 1.104 -1.78 1.181 -1.83 1.216 -1.86 0.942 -1.85 0.959 -1.72 1.004 -1.72 1.057 -1.75 1.127 -1.77 0.885
-1.66 0.884 -1.51 0.876 -1.67 1.011 -1.60 0.816 -1.41 0.764 -1.48 0.774
64 0 1 23
13 29 13 30 14 26 14 27 14 28 14 29 14 30 15 26 15 27 15 28 15 29 16 27
16 28 17 26 17 27 17 28 18 26 18 27 19 25 19 26 19 27 20 25 20 26
-1.44 0.967 -1.44 0.967 -1.44 0.960 -1.44 0.962 -1.44 0.966 -1.44 0.968 -1.44 0.967 -1.44 0.956 -1.44 0.962 -1.44 0.967
-1.44 0.968 -1.44 0.964 -1.44 0.967 -1.44 0.966 -1.44 0.966 -1.44 0.966 -1.45 0.967 -1.45 0.967 -1.44 0.966 -1.45 0.967
-1.44 0.967 -1.44 0.966 -1.44 0.966
64 0 2 23
13 29 13 30 14 26 14 27 14 28 14 29 14 30 15 26 15 27 15 28 15 29 16 27
16 28 17 26 17 27 17 28 18 26 18 27 19 25 19 26 19 27 20 25 20 26
-1.31 1.110 -1.24 1.123 -1.05 0.870 -1.17 0.914 -1.41 1.032 -1.16 1.106 -1.25 1.116 -0.96 0.846 -1.27 0.922 -1.42 1.007
-1.36 1.063 -1.57 0.936 -1.52 0.982 -1.84 0.950 -1.71 0.951 -1.73 0.958 -1.99 0.956 -1.96 0.957 -1.96 0.952 -2.01 0.955
-1.98 0.954 -1.95 0.951 -1.91 0.946
64 0 3 23
13 29 13 30 14 26 14 27 14 28 14 29 14 30 15 26 15 27 15 28 15 29 16 27
16 28 17 26 17 27 17 28 18 26 18 27 19 25 19 26 19 27 20 25 20 26
-1.28 1.239 -1.20 1.260 -1.06 0.824 -1.17 0.909 -1.39 1.125 -1.13 1.235 -1.21 1.253 -0.98 0.759 -1.27 0.958 -1.40 1.103
-1.32 1.186 -1.56 1.002 -1.49 1.085 -1.82 1.030 -1.69 1.026 -1.71 1.049 -1.96 1.034 -1.94 1.042 -1.94 1.000 -1.99 1.018
-1.96 1.016 -1.93 0.993 -1.88 0.978

```

The seismicity parameter data is organized in blocks of input parameters for each seismic source and seismicity option specified in the BEC.BAS file. The first block is for the first seismicity option for the first source, the second block is for the second seismicity option for the first source, and so on, until data for all of the seismicity options for the first source are input. The process then repeats for the second and succeeding sources. Each input block contains the following input information

- The first line contains three values that are not used. The fourth value is the number of one degree longitude by one degree latitude cells or partial cells contained within the source polygon specified in file BEC.GEO.
- The second line contains the latitude code and longitude code pairs for the southeast corner of each cell. The actual latitude is obtained by subtracting the latitude code from

55 degrees and the longitude (west positive) is obtained by subtracting the longitude code from 110 degrees. If the seismicity option codes are set to 3 on the seventh line of the XXX.BAS file, as they are for the Rondout Team, then this line is not used, as the entire source is used with uniform rate.

- The third line contains “a” and “b” value pairs for each cell or partial cell. The “a” value typically represents the \log_{10} of the annual frequency of earthquakes in magnitude range $3.3 \leq m_b < 3.9$ for a one degree longitude by one degree latitude cell at the equator (area 12,364.3 km², [4,773.9 mi²]), depending on the seismicity option code specified in the BEC.BAS file. If the seismicity option codes are set to 3 on the seventh line of the XXX.BAS file, as they are for the Rondout Team, then the “a” value applies to the entire source.

The above description is for cases where a seismicity option 0 is specified in the basic data input file. This is the case for all of the EPRI-SOG teams except the Rondout team. The Rondout team used seismicity option 3 in which a uniform seismicity rate is applied to the entire source zone. In this case, the seismicity parameter file becomes simpler. There is only a single line of data for each source and seismicity parameter option. This line contains the “a” and “b” value applied to the entire source area. As a result, the RND.SEI file has the following form.

```
-1.08 0.810  
-1.38 0.890  
-1.69 1.040  
-2.95 0.900  
-1.69 1.040  
-1.08 0.810  
-1.20 1.110  
-1.24 1.130
```

Seismic Hazard Curves

Seismic hazard curves have been calculated for each of the sources that model the seismicity of the Anna, Ohio, and Northeastern Ohio areas. PSHA has been conducted for two spectral frequencies (10 Hz and 1 Hz), with and without CAV. These hazard curves represent the motion at the GMRS elevation. The seismic hazard curves are shown in attached Figures 7 through 29. Each hazard curve represents the mean hazard from the source conditional on the source being active (the curves have not been multiplied by P*). The hazard curves are labeled by the source name followed by the character “c” for hazard computed using CAV and by the character “n” for hazard computed without using CAV.

Figure 7 shows the mean hazard curves obtained for the Bechtel Team background zone BBZ6. The plot on the left shows the results for 10 Hz, while the one on the right shows the curves obtained for 1 Hz spectral acceleration. In each plot the solid line represents the results obtained with CAV and dashed line the corresponding curve without CAV. Figures 8 and 9 show the mean seismic hazard curves obtained for the Bechtel Team sources BC06 and B-N1.

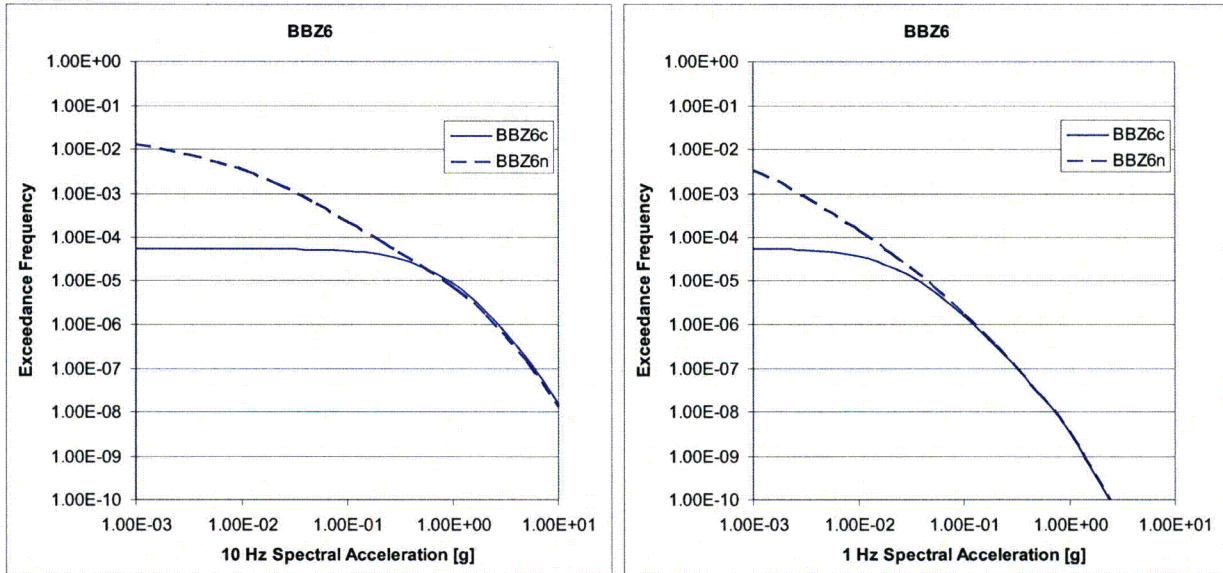


Figure 7 – Mean 10 Hz and 1 Hz hazard curves computed for Bechtel source BBZ6 with and without CAV.

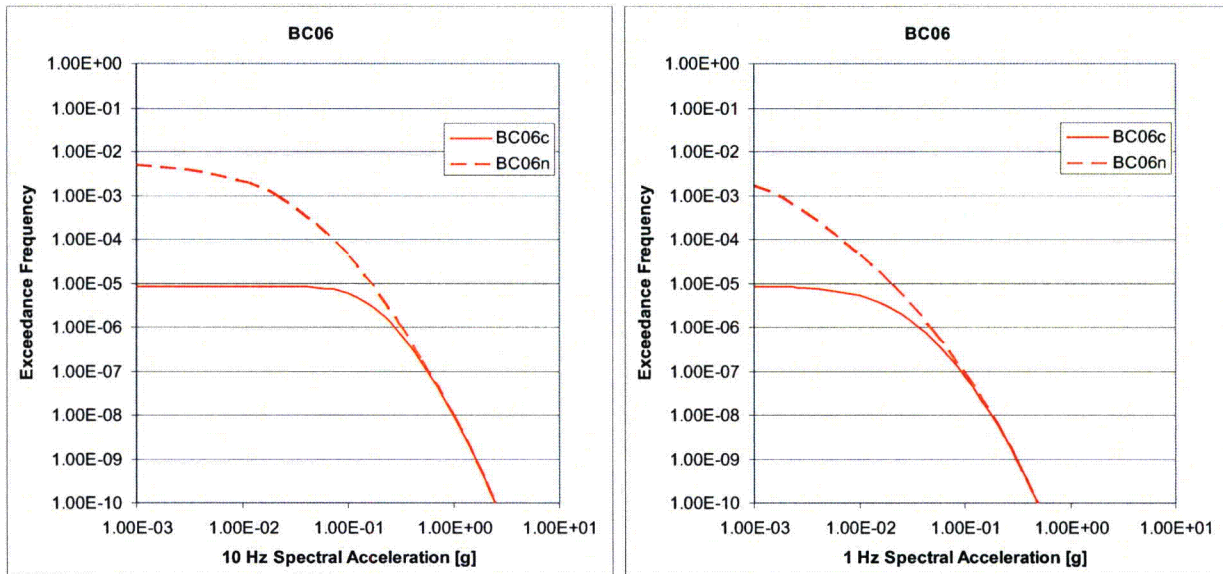


Figure 8 – Mean 10 Hz and 1 Hz hazard curves computed for Bechtel source BC06 with and without CAV.

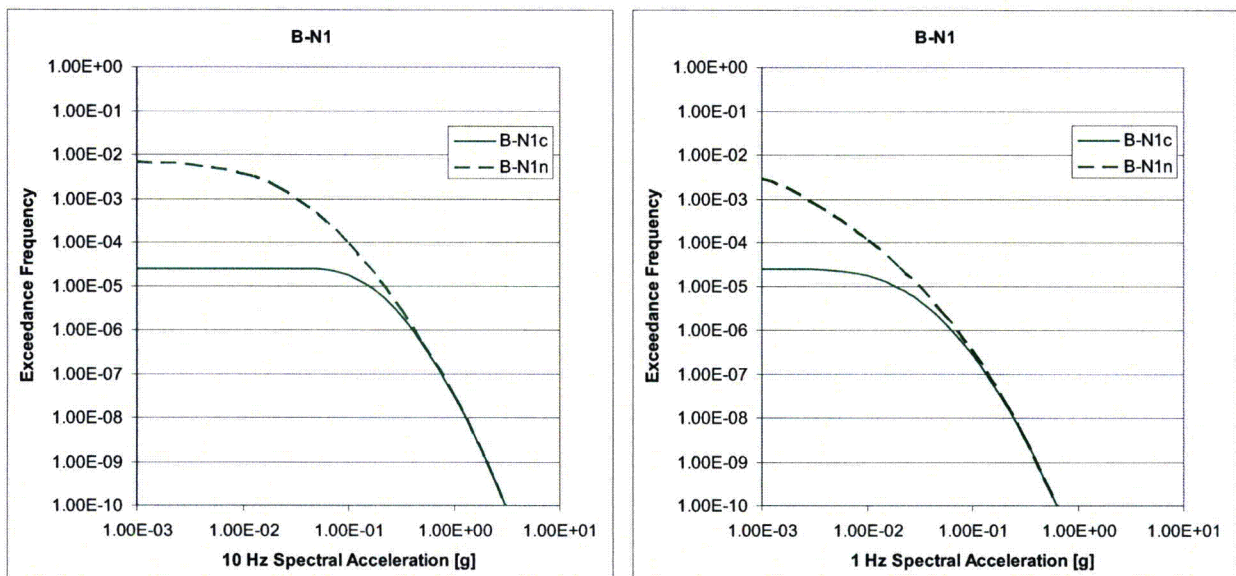


Figure 9 – Mean 10 Hz and 1 Hz hazard curves computed for Bechtel source B-N1 with and without CAV.

Figures 10, 11, and 12 show the mean hazard curves obtained for the Dames & Moore Team source zones D-08, D-12, and DB70.

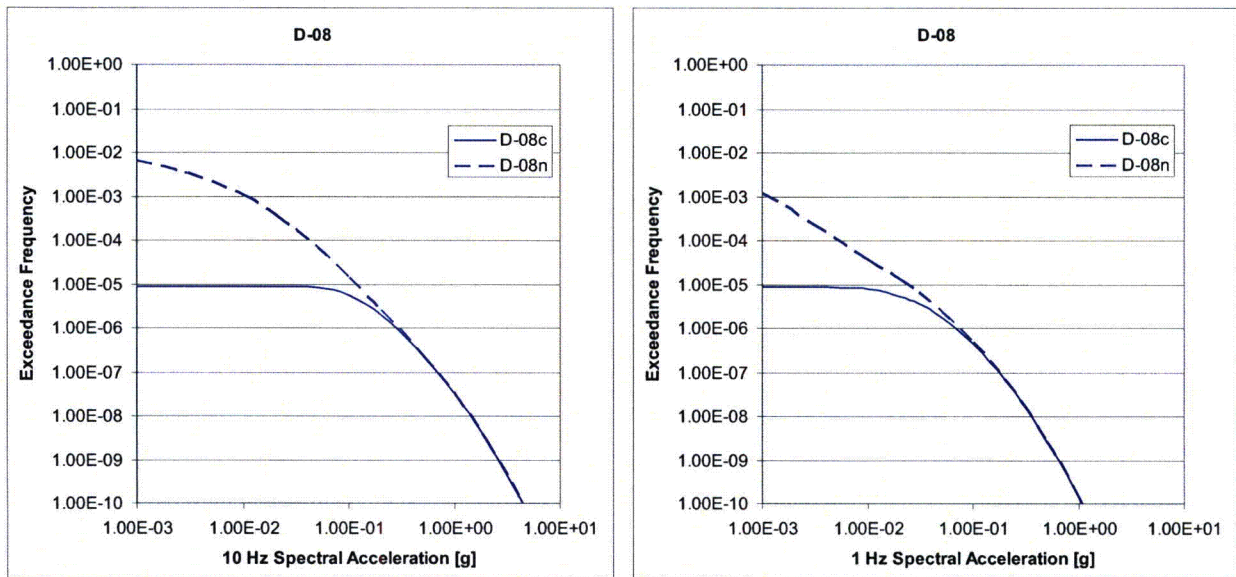


Figure 10 – Mean 10 Hz and 1 Hz hazard curves computed for Dames & Moore source D-08 with and without CAV.

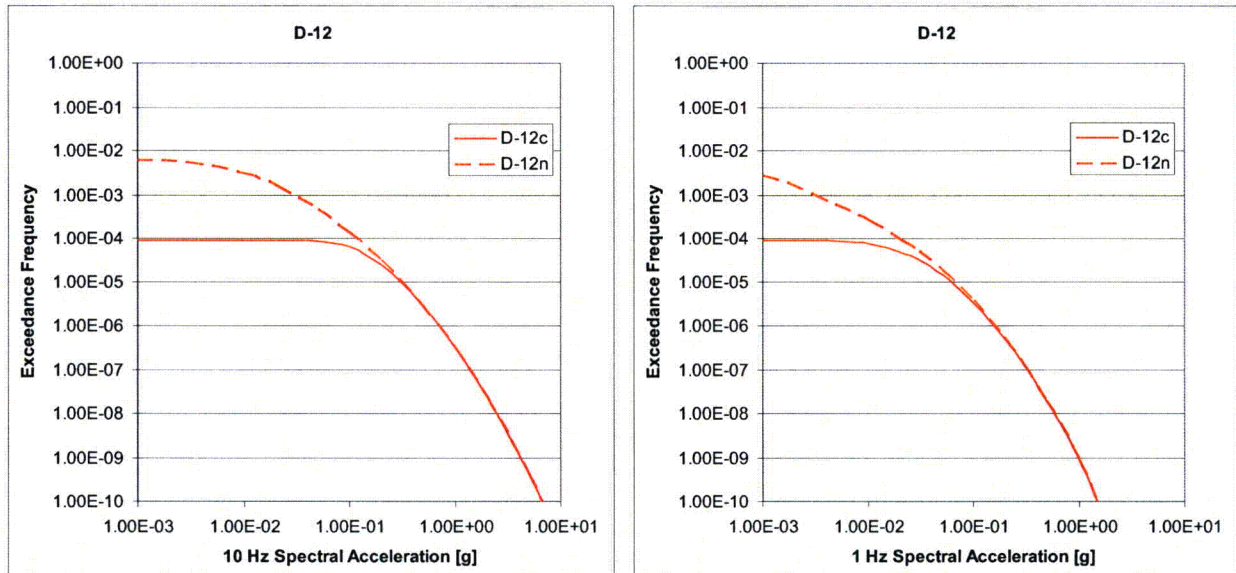


Figure 11 – Mean 10 Hz and 1 Hz hazard curves computed for Dames & Moore source D-12 with and without CAV.

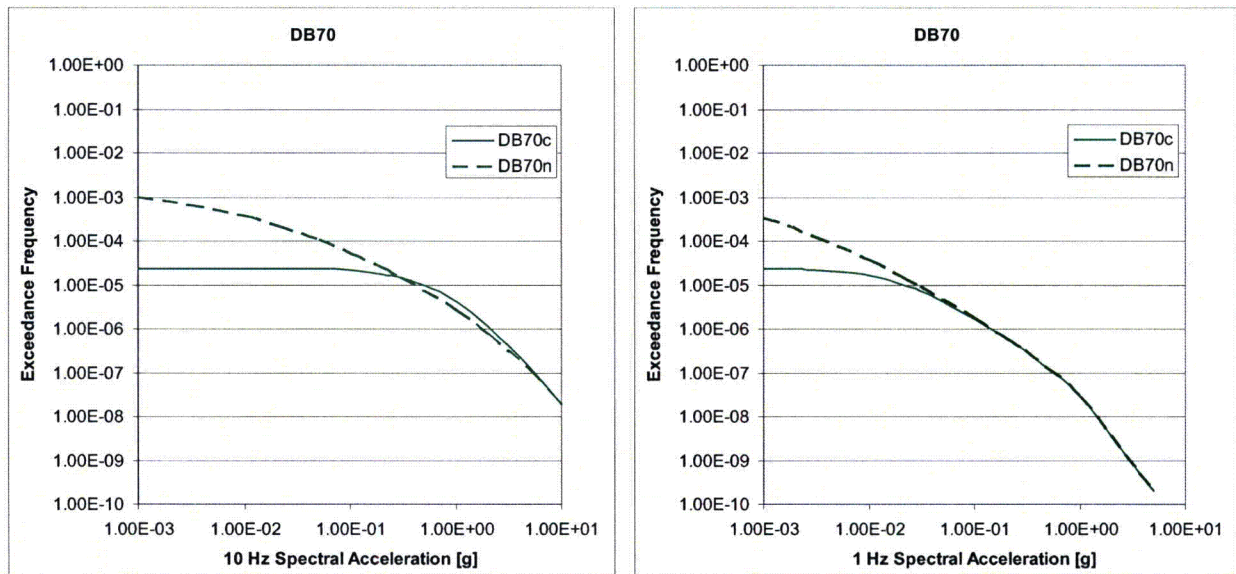


Figure 12 – Mean 10 Hz and 1 Hz hazard curves computed for Dames & Moore source DB70 with and without CAV.

Figures 13 and 14 show the mean hazard curves obtained for Law Team sources L112 and L115.

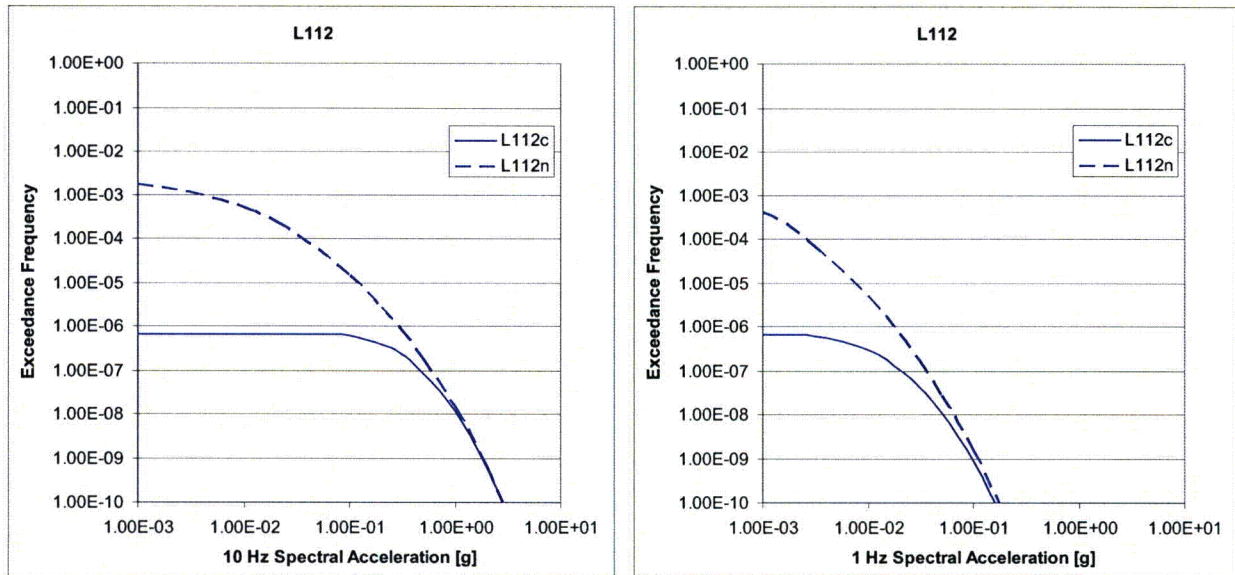


Figure 13 – Mean 10 Hz and 1 Hz hazard curves computed for Law source L112 with and without CAV.

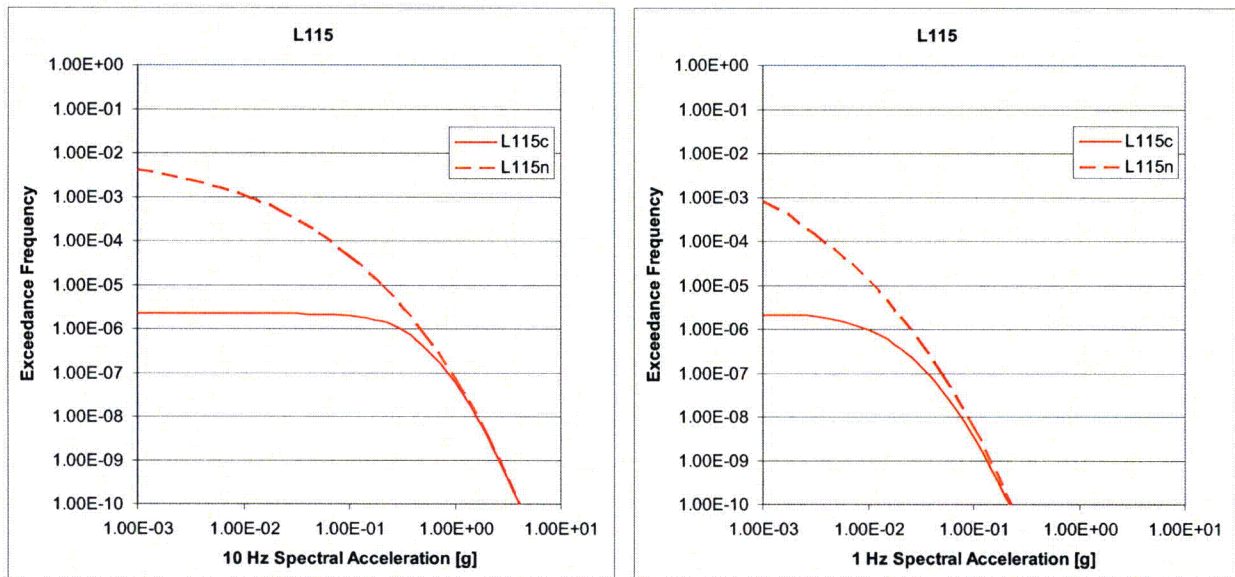


Figure 14 – Mean 10 Hz and 1 Hz hazard curves computed for Law source L115 with and without CAV.

Figures 15, 16, 17, and 18 show the mean hazard curves obtained for Rondout Team sources R-08, R-10, R-11, and R-12.

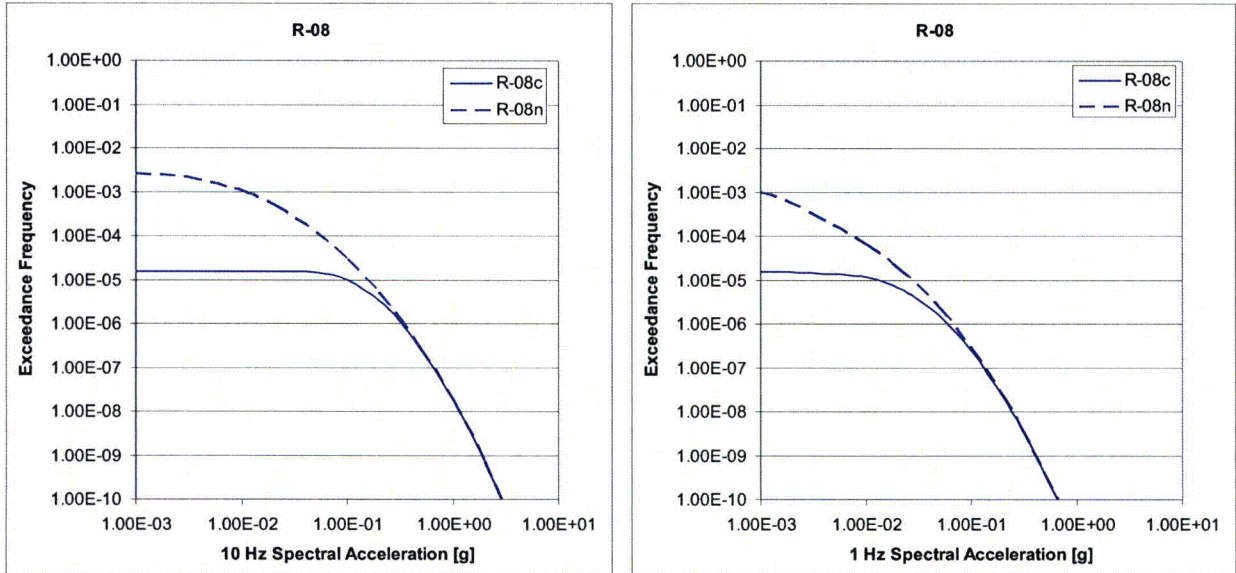


Figure 15 – Mean 10 Hz and 1 Hz hazard curves computed for Rondout source R-08 with and without CAV.

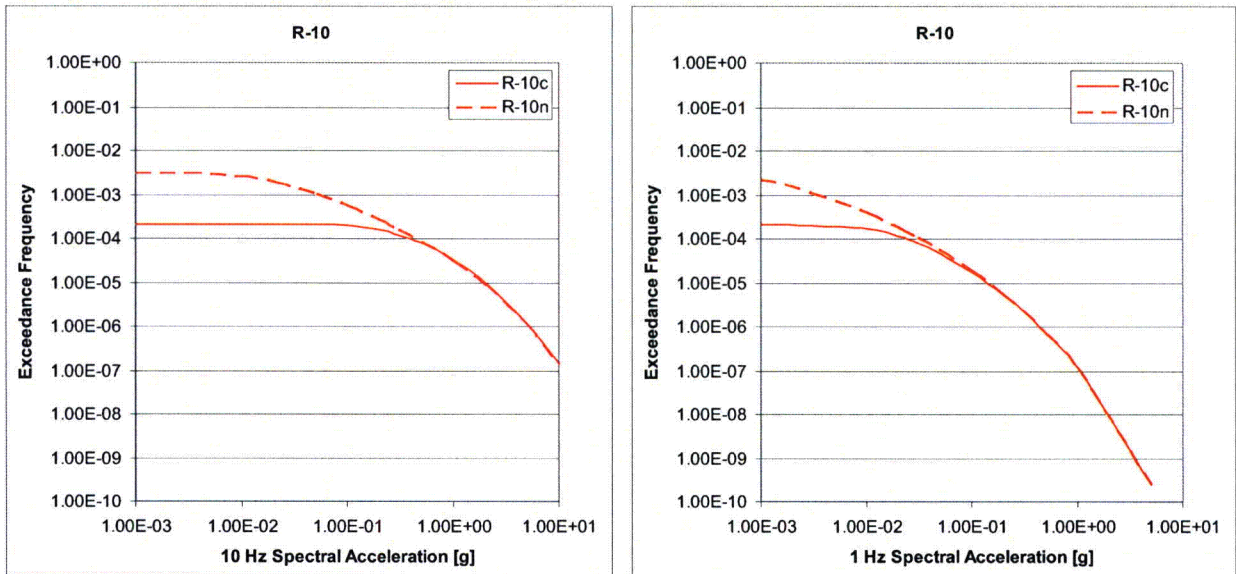


Figure 16 – Mean 10 Hz and 1 Hz hazard curves computed for Rondout source R-10 with and without CAV.

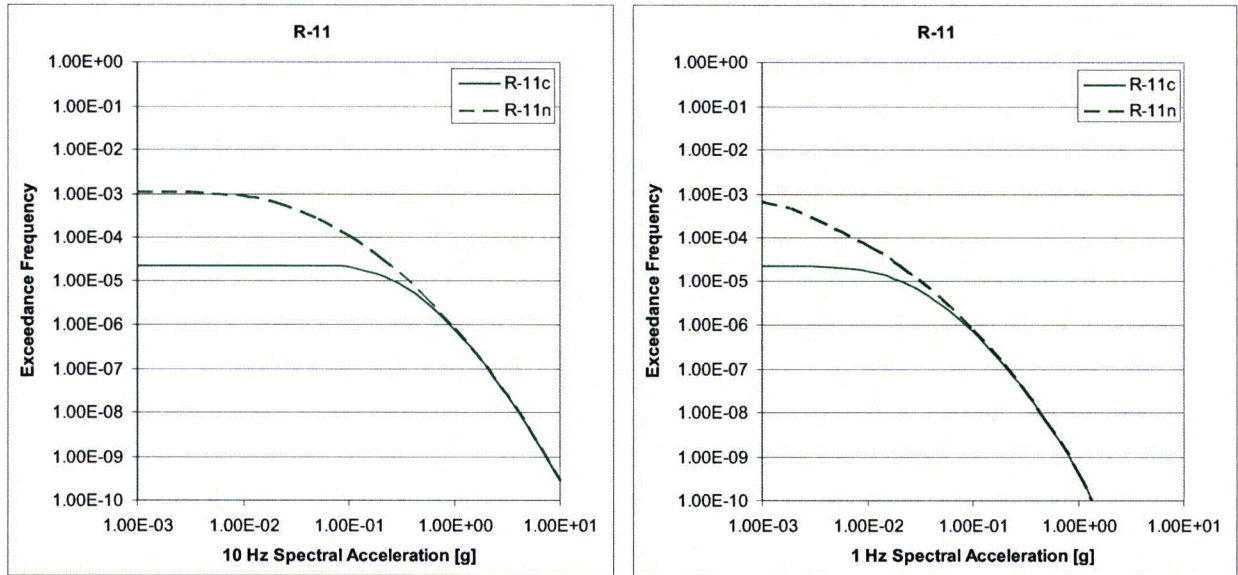


Figure 17 – Mean 10 Hz and 1 Hz hazard curves computed for Rondout source R-11 with and without CAV.

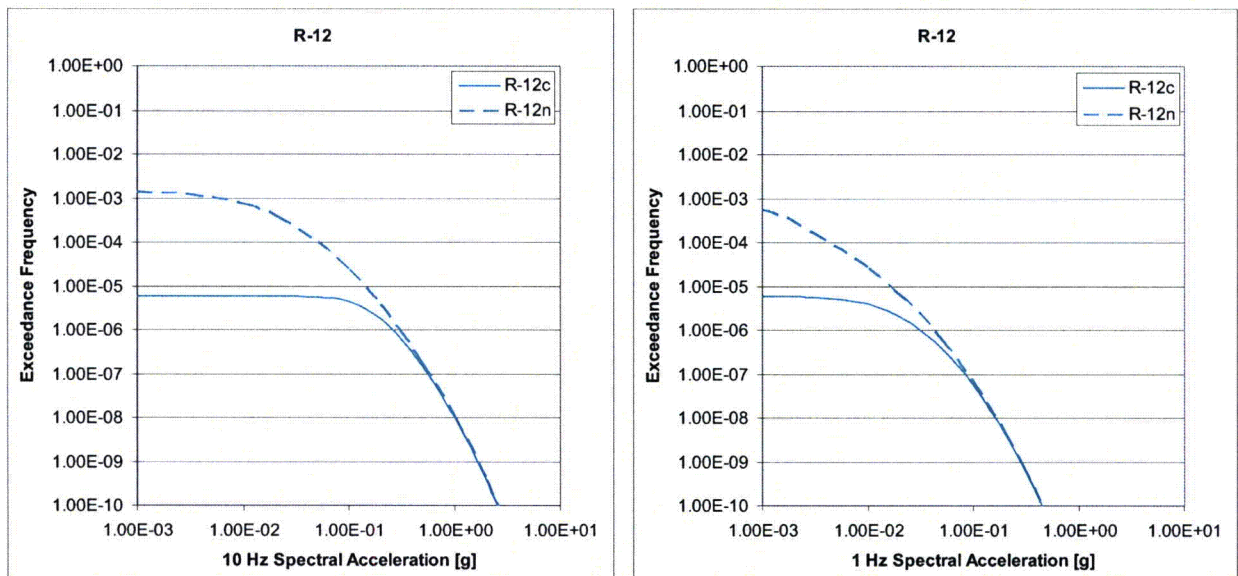


Figure 18 – Mean 10 Hz and 1 Hz hazard curves computed for Rondout source R-12 with and without CAV.

Figures 19, 20, 21, 22, 23, and 24 show the mean hazard curves obtained for the Woodward-Clyde sources W-35, W-36, W-37, W-38, W-39, and background zone WB67.

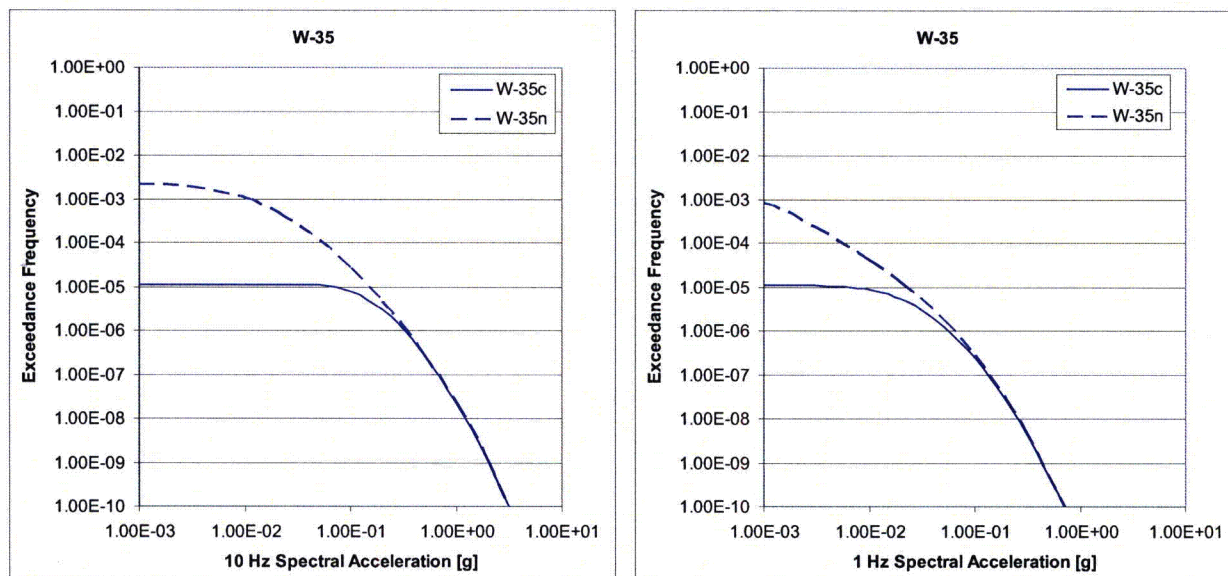


Figure 19 – Mean 10 Hz and 1 Hz hazard curves computed for Woodward-Clyde source W-35 with and without CAV.

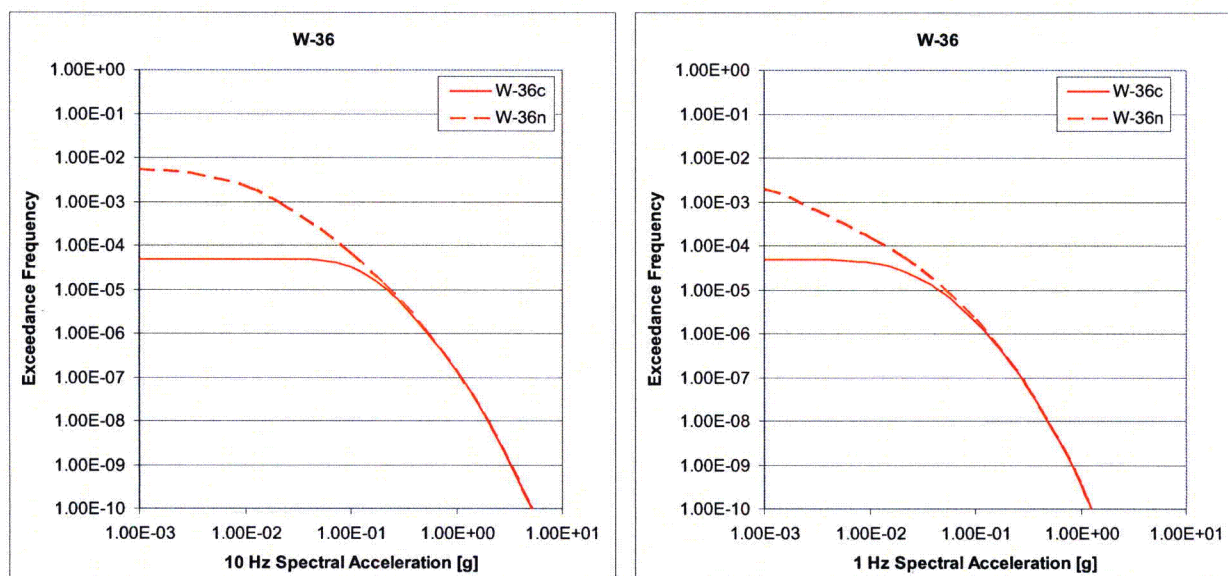


Figure 20 – Mean 10 Hz and 1 Hz hazard curves computed for Woodward-Clyde source W-36 with and without CAV.

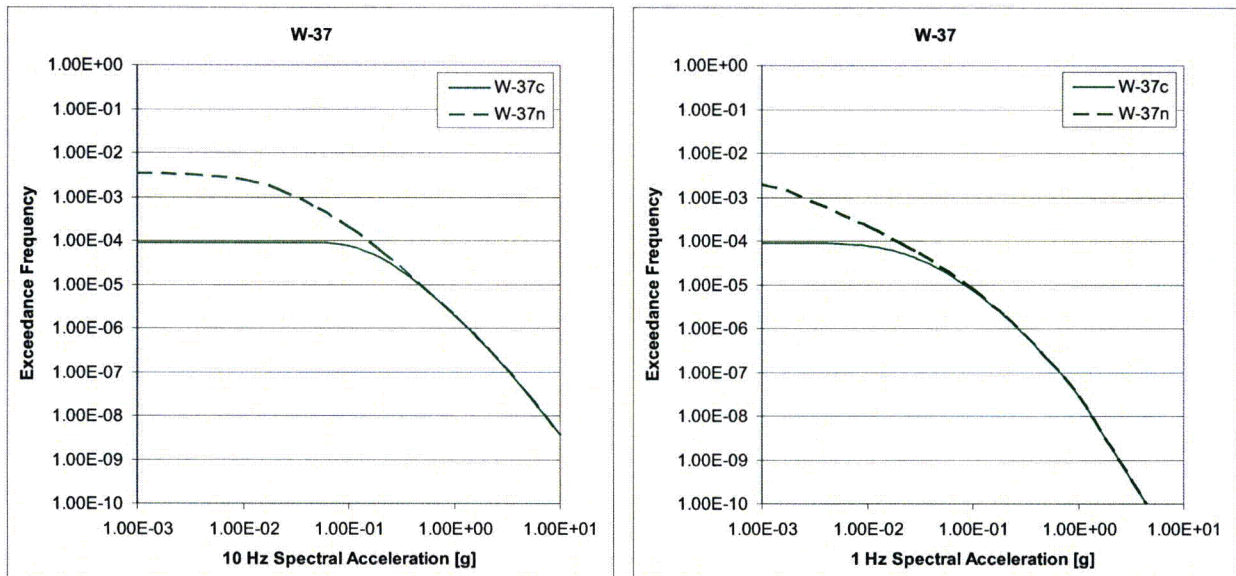


Figure 21 – Mean 10 Hz and 1 Hz hazard curves computed for Woodward-Clyde source W-37 with and without CAV.

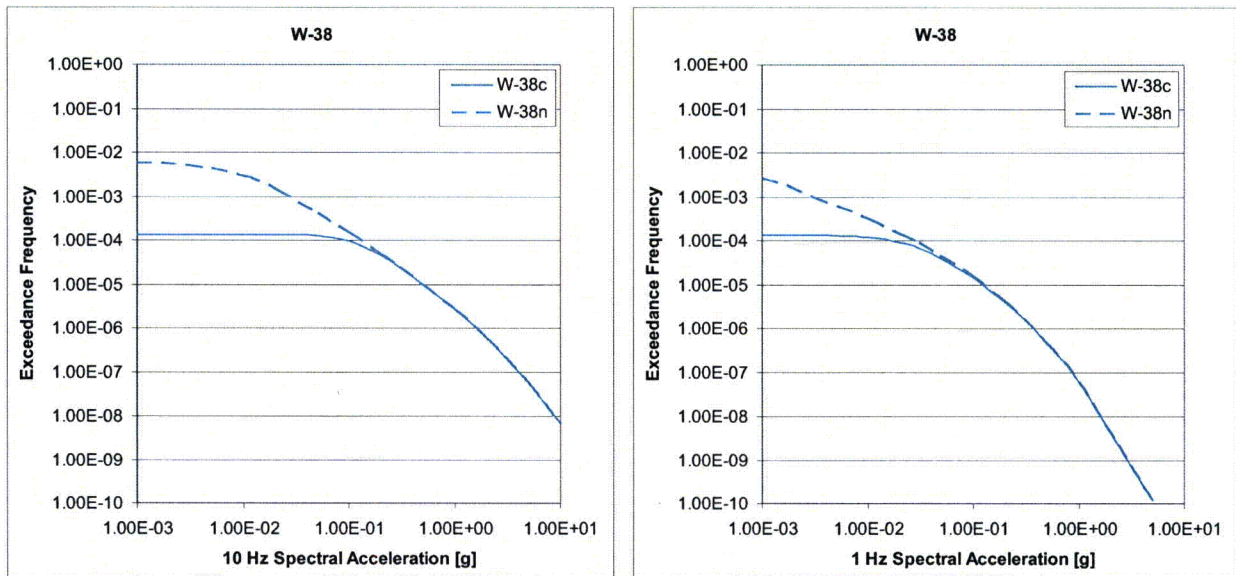


Figure 22 – Mean 10 Hz and 1 Hz hazard curves computed for Woodward-Clyde source W-38 with and without CAV.

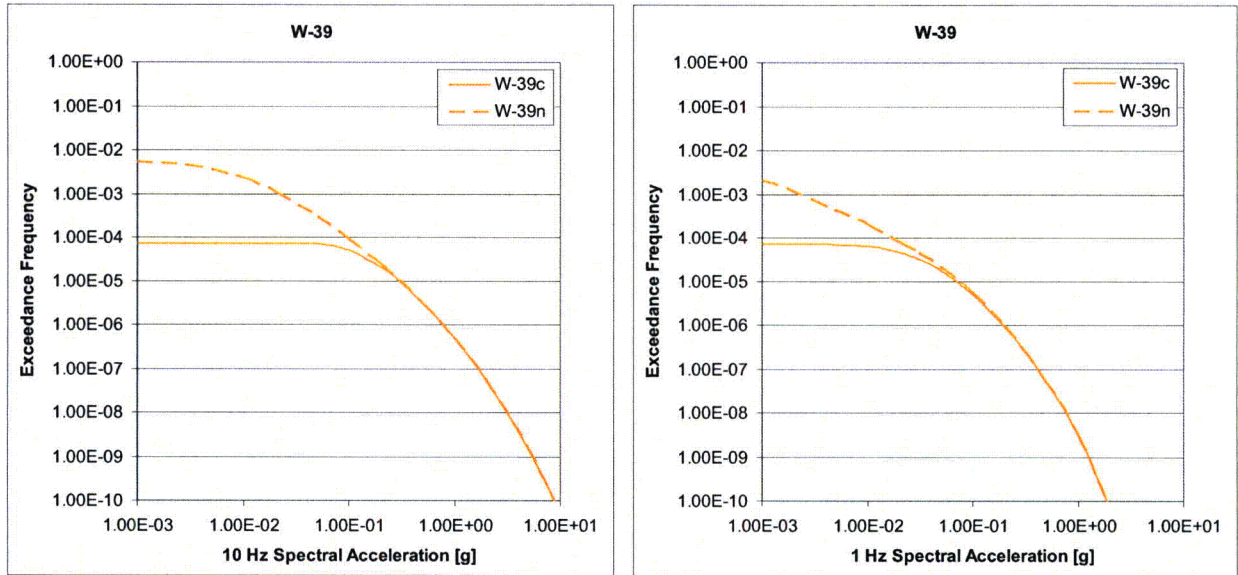


Figure 23 – Mean 10 Hz and 1 Hz hazard curves computed for Woodward-Clyde source W-39 with and without CAV.

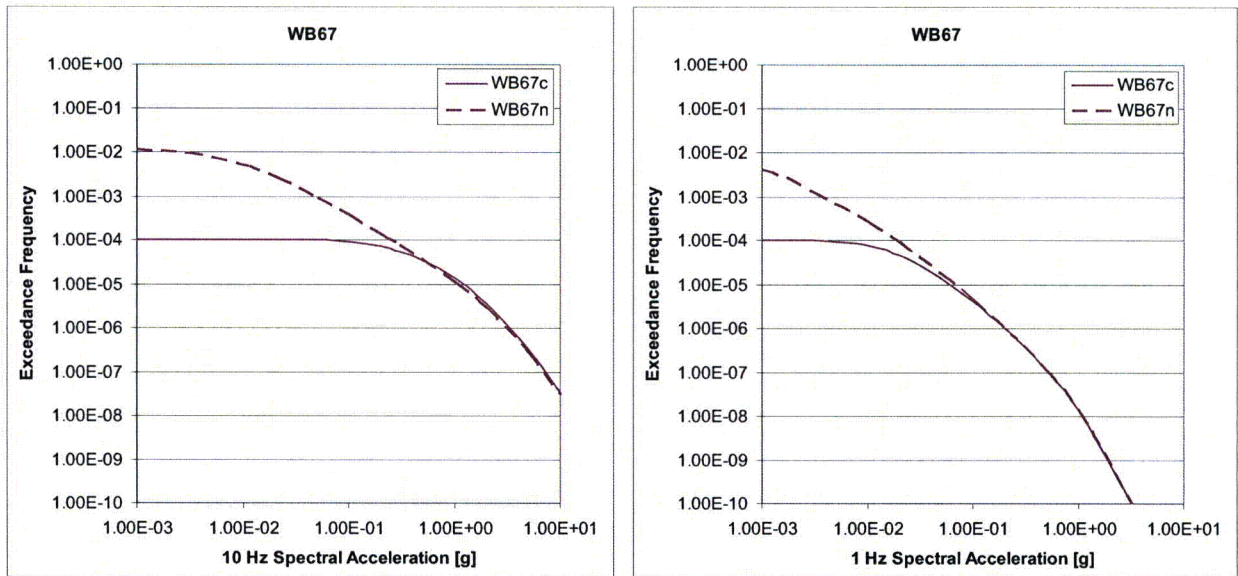


Figure 24 – Mean 10 Hz and 1 Hz hazard curves computed for Woodward-Clyde background source WB67 with and without CAV.

Figures 25, 26, 27, 28, and 29 show the mean hazard curves obtained for the Weston Geophysical Team source zones G-29 and GC13, GC14, GC15, GC16 which are different geometries of source WGC-101.

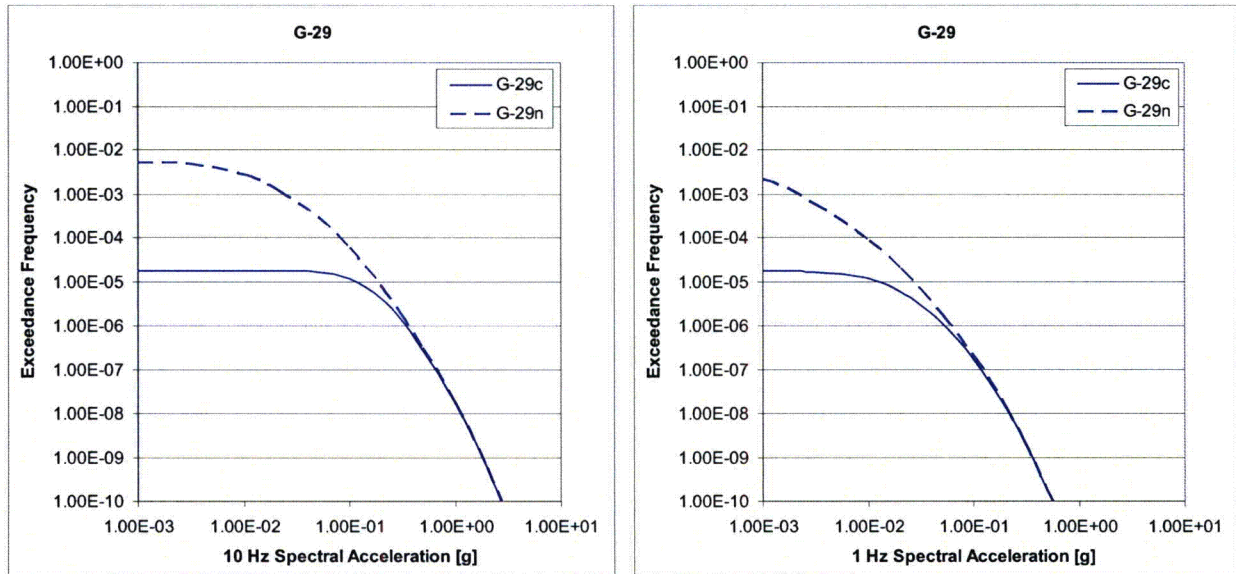


Figure 25 – Mean 10 Hz and 1 Hz hazard curves computed for Weston Geophysical source G-29 with and without CAV.

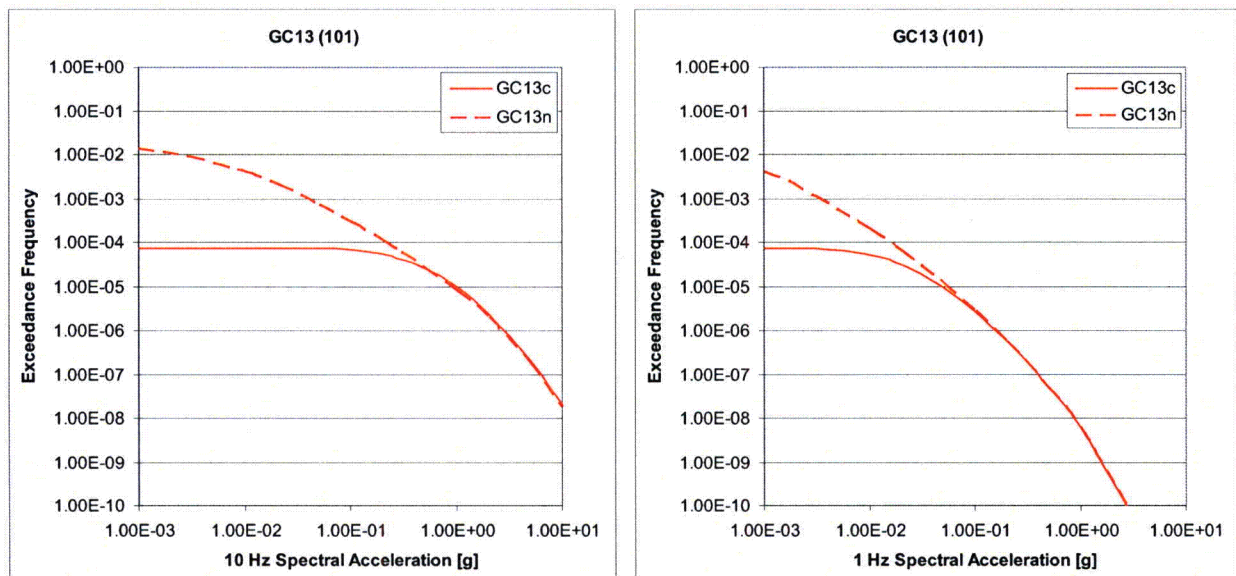


Figure 26 – Mean 10 Hz and 1 Hz hazard curves computed for Weston Geophysical combined source GC13 with and without CAV.

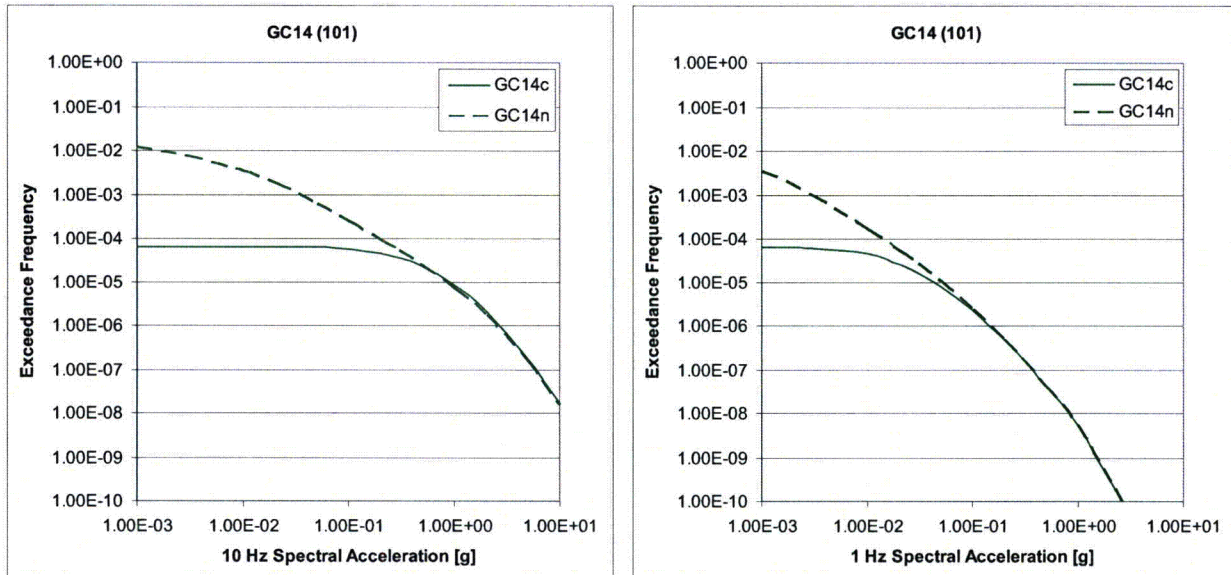


Figure 27 – Mean 10 Hz and 1 Hz hazard curves computed for Weston Geophysical combined source GC14 with and without CAV.

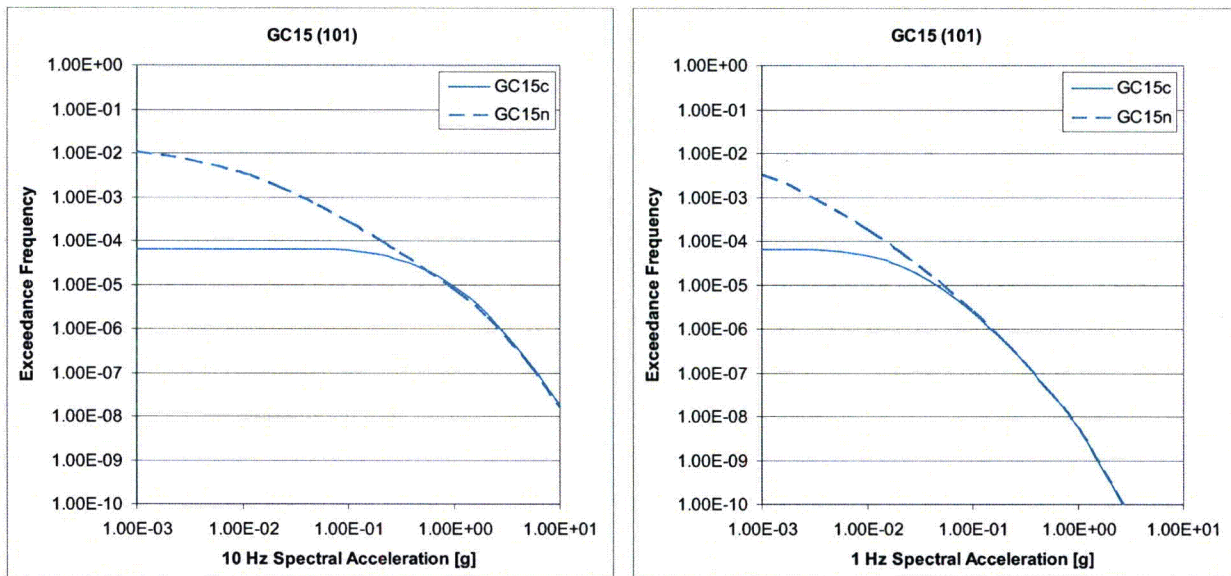


Figure 28 – Mean 10 Hz and 1 Hz hazard curves computed for Weston Geophysical combined source GC15 with and without CAV.

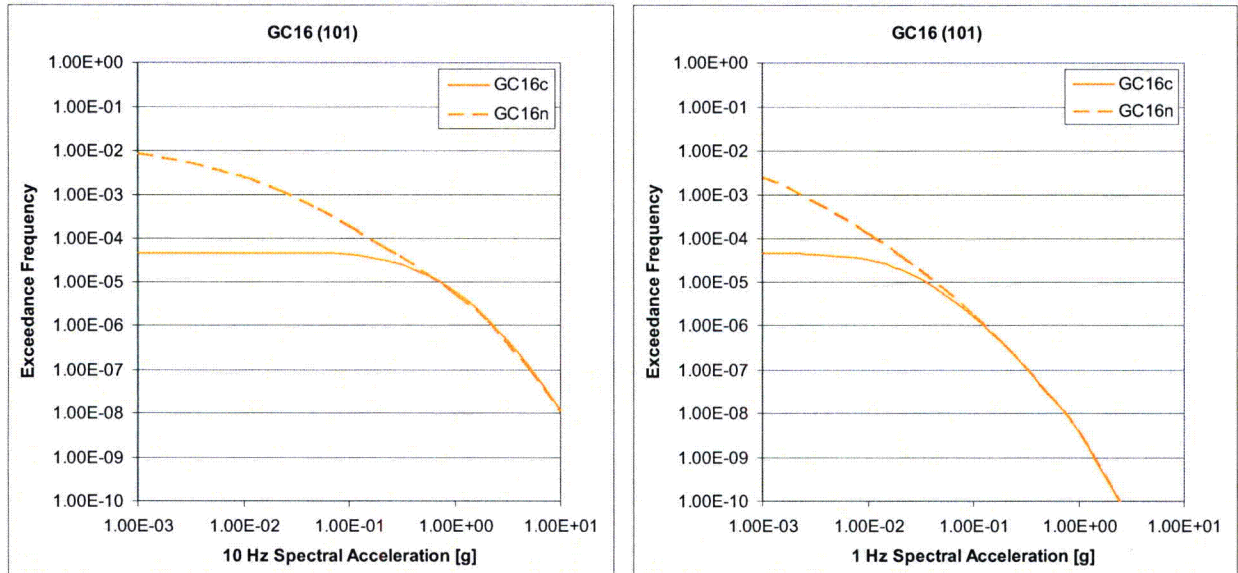


Figure 29 – Mean 10 Hz and 1 Hz hazard curves computed for Weston Geophysical combined source GC16 with and without CAV.

Proposed COLA Revision

None

Attachment 4
NRC3-10-0012

Enclosure 1 .
Inventory of CD
(following page)

Attachment 4 to
NRC3-10-0012
Page 28

Volume in drive D is NRC3-10-0006
Volume Serial Number is F19E-4A84

Directory of D:\

02/10/2010	07:52 PM	3,251	BEC.BAS	
02/10/2010	07:52 PM	3,251	BEC.GEO	
02/10/2010	07:52 PM	3,251	BEC.SEI	
02/10/2010	07:50 PM	3,251	DAM.BAS	
02/10/2010	07:50 PM	3,251	DAM.GEO	
02/10/2010	07:50 PM	3,251	DAM.SEI	
02/10/2010	07:50 PM	3,251	LAW.BAS	
02/10/2010	07:50 PM	3,251	LAW.GEO	
02/10/2010	07:50 PM	3,251	LAW.SEI	
02/10/2010	07:51 PM	3,251	RND.BAS	
02/10/2010	07:51 PM	3,251	RND.GEO	
02/10/2010	07:51 PM	3,251	RND.SEI	
02/10/2010	07:51 PM	3,251	WCC.BAS	
02/10/2010	07:51 PM	3,251	WCC.GEO	
02/10/2010	07:51 PM	3,251	WCC.SEI	
02/10/2010	07:52 PM	3,251	WGC.BAS	
02/10/2010	07:52 PM	3,251	WGC.GEO	
02/10/2010	07:52 PM	3,251	WGC.SEI	

18 File(s) 58,518 bytes

Total Files Listed:
18 File(s) 58,518 bytes
0 Dir(s) 0 bytes free

**Attachment 5
NRC3-10-0012**

**Response to RAI Letter No. 16
(eRAI Tracking No. 3936)**

RAI Question No. 02.05.04-27

RAI 02.05.04-27

ESBWR DCD rev. 6 has changed significantly from the revision used in the preparation of the Fermi FSAR. The following changes refer to Table 2.0-1 of the latest revision of the ESBWR DCD and its corresponding notes:

- a. FSAR Section 2.5.4.11 "Design Criteria" states "DCD Table 2.0-1 requires that that $\phi' > 30^\circ$." As per revision 6, the angle of internal friction for both in-situ and backfill is updated from $\phi' > 30^\circ$ to $\phi' > 35^\circ$. Please demonstrate that both in-situ material and backfill meet this updated requirement.*
- b. Note 7 stipulates the criteria needed to compare the maximum dynamic bearing demand with the allowable bearing pressure. FSAR Table 2.5.4-227 illustrates the results of the Bearing Capacity Analysis. Please make corresponding changes in Table 2.5.4-227 in order to incorporate the new requirements set forth in Note 7 of the revised DCD.*
- c. Note 8 establishes a new method to estimate the minimum shear wave velocity. Equation 2 in FSAR Section 2.5.4.7.2 states the method used to calculate the equivalent shear wave velocity under each Category I structure. According to revision 6 of the DCD, said equation is no longer valid. Please demonstrate that your shear wave velocity at minus one sigma from the mean is enveloped by the site-related minimum shear wave velocity parameter.*

Response

- a. FSAR Section 2.5.4.11 "Design Criteria" states "DCD Table 2.0-1 requires that [SIC] $\phi' > 30^\circ$." As per revision 6, the angle of internal friction for both in-situ and backfill is updated from $\phi' > 30^\circ$ to $\phi' > 35^\circ$. Please demonstrate that both in-situ material and backfill meet this updated requirement.*

With the exception of the Firewater Service Complex (FWSC), the in situ material below the Category I structure foundations will be Bass Islands Group dolomite bedrock. The FWSC will be supported on lean concrete on Bass Islands Group dolomite bedrock.

Fermi 3 FSAR, Section 2.5.4.2.1.2.1, states:

"The residual friction angle along discontinuities ranges between 33 and 74 degrees, with a mean of 52 degrees."

"The rock mass properties and Mohr-Coulomb parameters for the Bass Islands Group, based on Hoek-Brown criterion are presented in Table 2.5.4-207 and Table 2.5.4-208, respectively. The upper bound, mean, and lower bound are presented for each property."

FSAR Table 2.5.4-208 shows that the estimated friction angle for the Bass Islands Group dolomite bedrock ranges between 42 and 53 degrees, with a mean of 48 degrees. Therefore, the friction angle of Bass Islands Group dolomite bedrock will be greater than 35 degree based on laboratory direct shear tests performed on samples with discontinuities from the Bass Islands Group and empirical correlations using Hoek-Brown criterion.

Fermi 3 FSAR, Section 2.5.4.5.4.2, states:

“Backfill for the Fermi 3 may consist of concrete fill or a sound, well graded granular backfill.”

“Engineered granular backfill materials are placed in controlled lifts and compacted. Within confined areas or close to foundation walls, smaller compactors are used to prevent excessive lateral pressures against the walls from stress caused by heavy compactors.”

“A quality control sampling and testing program is developed to verify that concrete fill and granular backfill material properties conform to the specified design parameters. Sufficient laboratory compaction and grain size distribution tests are performed to account for variations in fill material. A test fill program may be included for the purposes of determining an optimum size of compaction equipment, number of passes, lift thickness, and other relevant data for achievement of the specified compaction.”

Placing the well graded granular backfill in controlled lifts with compaction will result in a dense to very dense consistency engineered backfill surrounding the embedded walls of Seismic Category I structures. Tables 1 and 2 show that for dense to very dense granular soils, the relative density ranges from 65 to 100 percent. Figure 1 shows that with a relative density greater than 65 percent, the angle of internal friction of well graded granular soils (SW and GW) will be greater than 35 degrees. Table 2 also shows that the angle of internal friction of dense to very dense medium to coarse grained granular soils will be greater than 35 degrees.

Table 1
Correlations of Soil Relative Density with Consistency
of Granular Soils
(Excerpt from Reference 1)

TABLE 4.4 CONSISTENCY OF COARSE-GRAINED SOILS
VARIOUS RELATIVE DENSITIES (Lambe and Whitman, 1969;
Adapted by permission of John Wiley and Sons, Inc.)^a

Relative Density, D_r , (%)	Classification
0 - 15	Very loose
15 - 35	Loose
35 - 65	Medium dense ^b
65 - 85	Dense
85 - 100	Very dense

^a Other classification systems have been proposed by others that use these terms, but with different values for the corresponding relative densities.

^b Lambe and Whitman used the term "medium," but "medium dense" is probably better because "medium" usually refers to the grain size

Table 2
Correlations of Soil Properties with Consistency of Granular Soils
(Excerpt from Reference 2)

TABLE 3-4
Empirical values for ϕ , D_r , and unit weight of granular soils based on
the SPT at about 6 m depth and normally consolidated [approximately,
 $\phi = 28^\circ + 15^\circ D_r$ ($\pm 2^\circ$)]

Description	Very loose	Loose	Medium	Dense	Very dense
Relative density D_r	0	0.15	0.35	0.65	0.85
SPT N_{60} fine	1-2	3-6	7-15	16-30	> 30
medium	2-3	4-7	8-20	21-40	> 40
coarse	3-6	5-9	10-25	26-45	> 45
ϕ fine	26-28	28-30	30-34	33-38	> 38
medium	27-28	30-32	32-36	36-42	< 50
coarse	28-30	30-34	33-40	40-50	> 50
γ_{wet} , kN/m ³	11-16*	14-18	17-20	17-22	20-23

* Excavated soil or material dumped from a truck has a unit weight of 11 to 14 kN/m³ and must be quite dense to weigh much over 21 kN/m³. No existing soil has a $D_r = 0.00$ nor a value of 1.00. Common ranges are from 0.3 to 0.7.

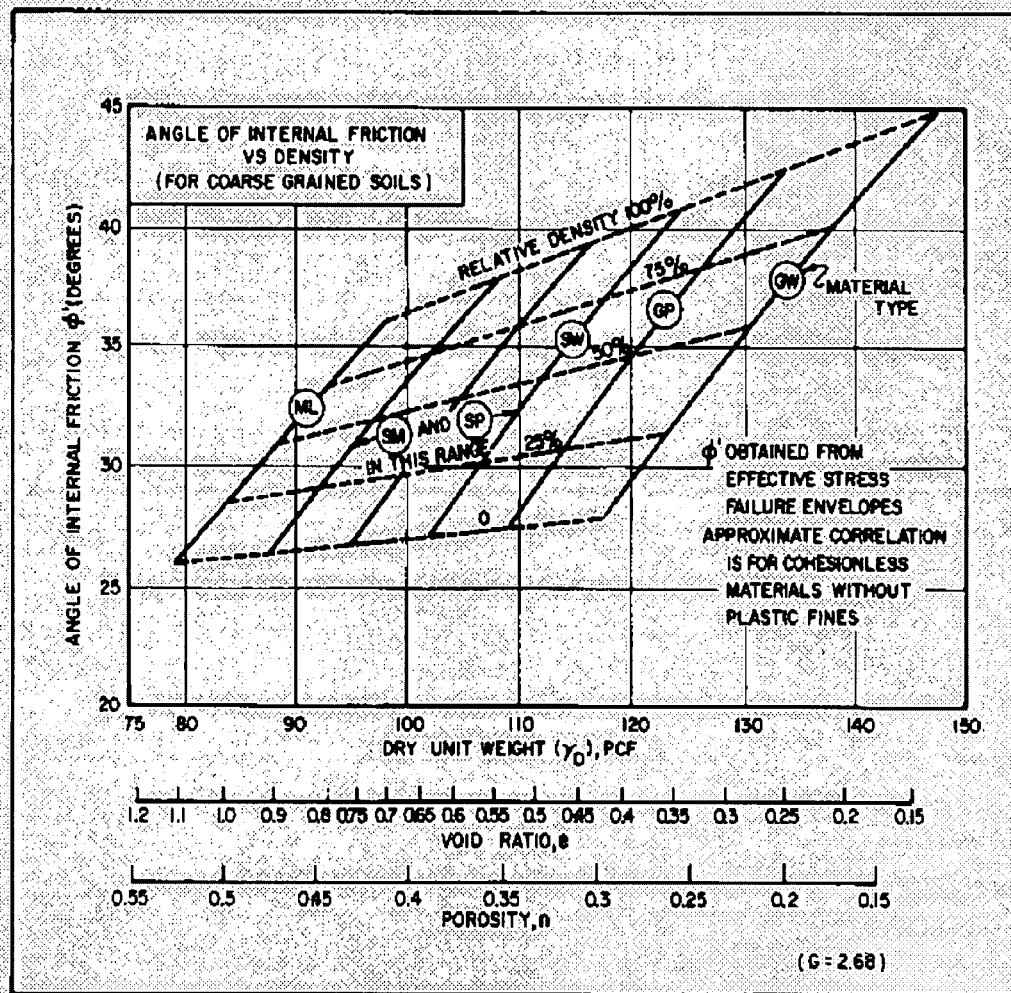


FIGURE 7
 Correlations of Strength Characteristics for Granular Soils

Figure 1 – Correlation of Angle of Internal Friction of Soil with Relative Density (Excerpt from FSAR Reference 2.5.4-242).

References

1. Coduto, D.P., (1999), "Geotechnical Engineering Principles and Practices," Prentice-Hall, Inc.
2. Bowles, J.E., (1996), "Foundation Analysis and Design," 5th Edition, McGraw-Hill Companies, Inc.

- b. *Note 7 stipulates the criteria needed to compare the maximum dynamic bearing demand with the allowable bearing pressure. FSAR Table 2.5.4-227 illustrates the results of the Bearing Capacity Analysis. Please make corresponding changes in Table 2.5.4-227 in order to incorporate the new requirements set forth in Note 7 of the revised DCD.*

ESBWR DCD, Revision 6, Tier 2, Chapter 2, Note 7 in Table 2.0-1, states:

“At the foundation level of Seismic Category I structures. The static bearing pressure is the average pressure. The dynamic bearing pressure is the toe pressure. To compare with the maximum bearing demand, the allowable bearing pressure is developed from the site-specific bearing capacity divided by a factor of safety appropriate for the design load combination. The maximum dynamic bearing demand to be compared with the site-specific allowable dynamic bearing pressure is the larger value or a linearly interpolated value of the applicable range of shear wave velocities at the foundation level. The shear wave velocities of soft, medium and hard soils are 300 m/sec (1000 ft/sec), 800 m/sec (2600 ft/sec) and greater than or equal to 1700 m/sec (5600 ft/sec), respectively.”

The terms “minimum static bearing capacity” and “minimum dynamic bearing capacity” used in ESBWR DCD, Revision 5 are replaced with the terms “maximum static bearing demand” and “maximum dynamic bearing demand”, respectively, in ESBWR DCD, Revision 6. The maximum static bearing demand values for Reactor/Fuel Building (R/FB), Control Building (CB) and Firewater Service Complex (FWSC) in ESBWR DCD, Revision 6, are the same as the minimum static bearing capacity values in ESBWR DCD, Revision 5. However, the maximum dynamic bearing demand values have been modified in ESBWR DCD, Revision 6, compared to the minimum dynamic bearing capacity values in ESBWR DCD, Revision 5 as follows:

- The maximum dynamic bearing demand values for the R/FB and CB have been reduced significantly for all soft, medium, and hard soil sites.
- The maximum dynamic bearing demand values for the FWSC have been increased slightly for the soft and medium soil sites and increased significantly for the hard soil site.

Fermi 3 FSAR, Section 2.5.4.3, states:

“As shown on Figure 2.5.4-202 and Figure 2.5.4-203, the base of the R/FB foundation lies on Bass Islands Group.”

“As shown on Figure 2.5.4-202, the base of the CB foundation is also founded on Bass Islands Group.”

“The FWSC foundation base is within fill material as shown on Figure 2.5.4-202; however, the existing subsurface materials including fill, lacustrine and glacial till are to be removed and backfill consisting of lean concrete will reestablish the foundation grade of the FWSC.”

Fermi 3 FSAR, Section 2.5.4.2.1.2.1, states:

“The mean V_p for the Bass Islands Group varies from 4,023 to 4,389 m/s (13,200 to 14,400 fps), and the mean V_s varies from 2,012 to 2,225 m/s (6,600 to 7,300 fps).....”

Fermi 3 FSAR Section 2.5.4.5.4.2, states:

“.....The lean concrete fill will have a mean 28-day compressive strength of equal to, or greater than, 2000 psi with a mean shear wave velocity of equal to, or greater than, 3,600 ft/s.....”

Both R/FB and CB are founded on Bass Islands Group with a mean shear wave velocity greater than 5,600 feet/second. Therefore, the maximum dynamic bearing demand for hard soil is compared to the site-specific allowable bearing capacity.

The FWSC is founded on lean concrete with mean shear wave velocity greater than 3,600 feet/second. The mean shear wave velocity of the lean concrete falls between the shear wave velocities of medium and hard soils as defined in the ESBWR DCD. Therefore, using the more conservative approach for comparing the maximum dynamic bearing demand to the site-specific allowable dynamic bearing capacity for the FWSC, the larger maximum dynamic bearing demand for hard soil is selected to compare to the site-specific allowable bearing capacity.

Fermi 3 FSAR, Section 2.5.4.10.1, states:

“Table 2.5.4-227 shows the results of the bearing capacity analyses using methods 1 and 2. Both methods were used to check against the static bearing capacity requirement in the Referenced DCD. Using Terzaghi’s approach, the allowable bearing capacity is estimated by dividing the ultimate bearing capacity by a factor of safety of 3. The allowable bearing capacity calculated based on both methods is greater than the minimum static bearing capacity required in the Referenced DCD as shown in Table 2.5.4-227”

“..... Using Terzaghi’s approach, the calculated ultimate bearing capacity was divided by a factor of safety of 2.25 to obtain the allowable dynamic bearing pressure. The dynamic factor of safety is established by dividing the static factor of safety by 1.33.....”

FSAR Table 2.5.4-227 will be updated to reflect the changes to the maximum dynamic bearing demand values in ESBWR DCD, Revision 6, as shown in the attached markup. The allowable dynamic bearing capacity calculated based on Terzaghi’s approach is greater than the maximum dynamic bearing demand required in ESBWR DCD, Revision 6, as shown in the revised FSAR Table 2.5.4-227.

- c. *Note 8 establishes a new method to estimate the minimum shear wave velocity. Equation 2 in FSAR Section 2.5.4.7.2 states the method used to calculate the equivalent shear wave velocity under each Category I structure. According to revision 6 of the DCD, said equation is no longer valid. Please demonstrate that your shear wave velocity at minus one sigma from the mean is enveloped by the site-related minimum shear wave velocity parameter.*

ESBWR DCD, Revision 6, Tier 2, Chapter 2, Note 8 in Table 2.0-1, states:

“This is the minimum shear wave velocity of the supporting foundation material associated with seismic strains for lower bound soil properties at minus one sigma from the mean.....”

Fermi 3 FSAR, Section 2.5.2.5.1.3, states:

“The data from the Fermi site display low to moderate variability in velocity at shallow depth with a $\sigma_{\ln(V_s)}$ of approximately 0.1, increasing to 0.2 in the Salina Group Unit F. These values are similar to those obtained from analyses of individual firm soil sites (Reference 2.5.2-286), and these values were used to develop randomized velocity profiles. The locations of velocity layer boundaries were randomized to vary uniformly within the range of layer thickness observed in the site borings.”

“Sixty randomized Vs profiles were generated for the GMRS profile. Figure 2.5.2-258 and Figure 2.5.2-259 show the randomized velocity profiles. The statistics of the randomized profiles are compared to the input target values for median velocity and standard deviation (sigma) of $\ln(V_s)$ on Figure 2.5.2-260.”

Fermi 3 FSAR, Section 2.5.2.5.3, states:

“The process described above for developing the GMRS profile amplification functions was repeated for the three FIRS profiles. For the R/FB and CB profiles, the analyses were performed with all material above the foundation elevation removed.”

To consider variation and uncertainties in dynamic soil properties, a suite of 60 randomized soil profiles were generated for soil amplification analyses. Soil amplification analyses were performed for the R/FB, CB and FWSC soil profiles and the response motions at the foundation level were obtained for the 10^{-4} and 10^{-5} input ground motions. At each of the loading levels for the input ground motions used in the SHAKE analyses, the iterated shear wave velocities for each layer of the 60 randomized profiles were sorted into rank order (from the lowest to highest value), and the 16th, 50th and 84th percentiles shear wave velocity profiles at seismic strains were determined. The 16th percentiles of the randomized shear wave velocities at seismic strains represent mean minus one standard deviation (the lower bound soil properties) referenced by ESBWR DCD, Revision 6.

The 16th percentiles of the randomized shear wave velocities at seismic strains for foundation materials below the R/FB, CB and FWSC are shown on attached Figures 2, 3 and 4, respectively. These figures show that the 16th percentiles shear wave velocities at seismic strains, for foundation materials below the R/FB, CB and FWSC, are greater than 1,000 feet/second.

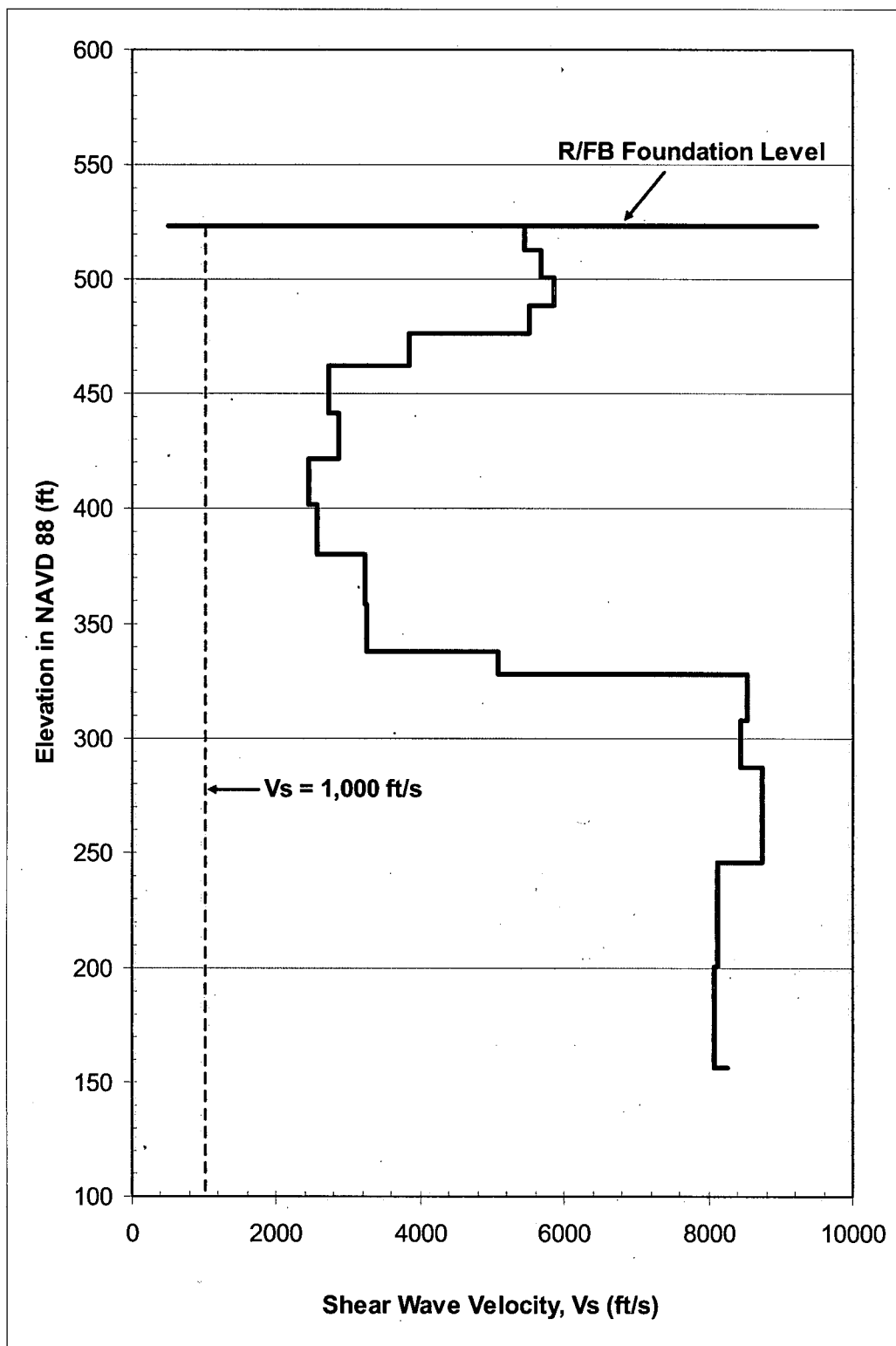


Figure 2 – The 16th Percentiles Shear Wave Velocities at Seismic Strains for Foundation Materials Below the R/FB.

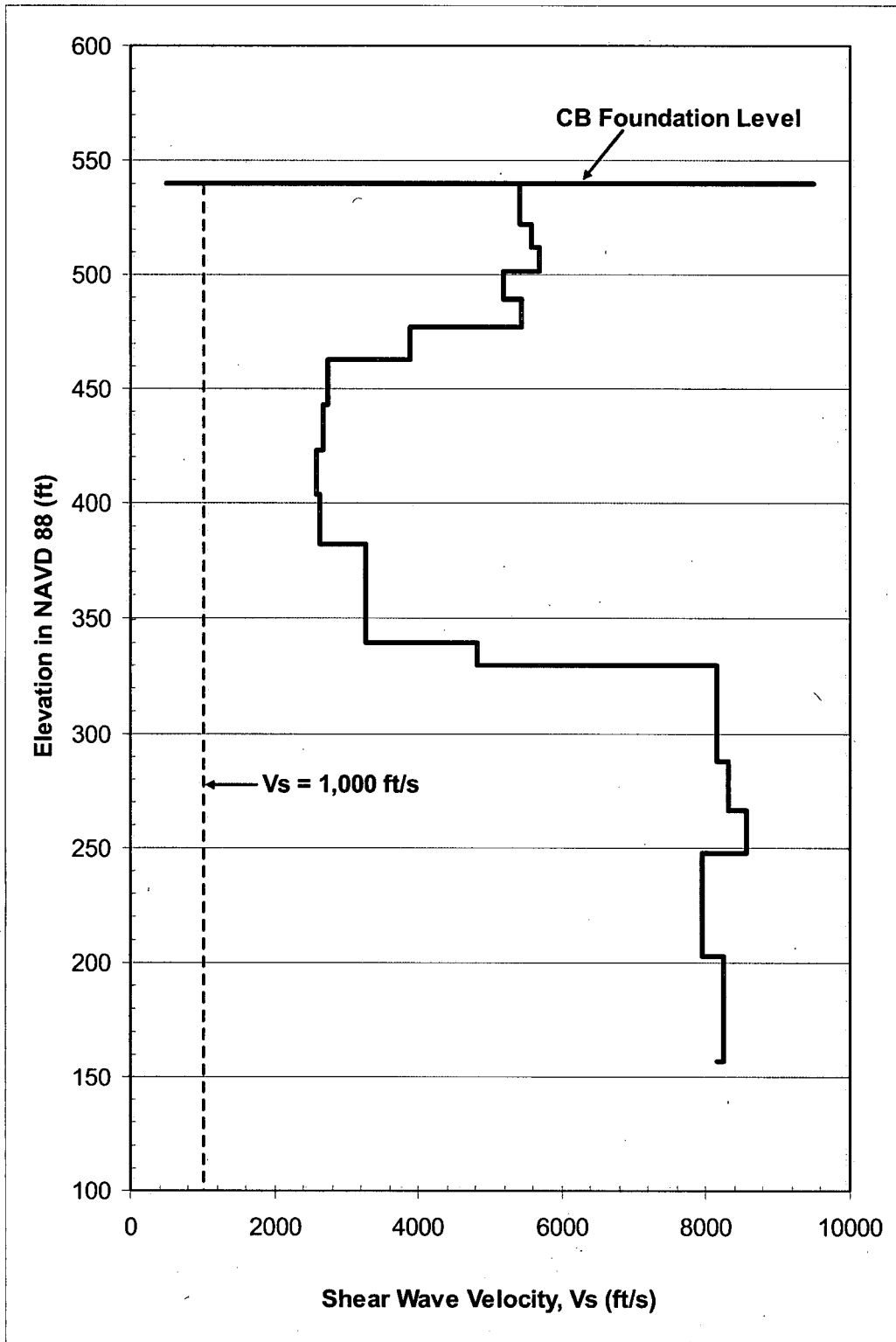


Figure 3 – The 16th Percentiles Shear Wave Velocities at Seismic Strains for Foundation Materials Below the CB.

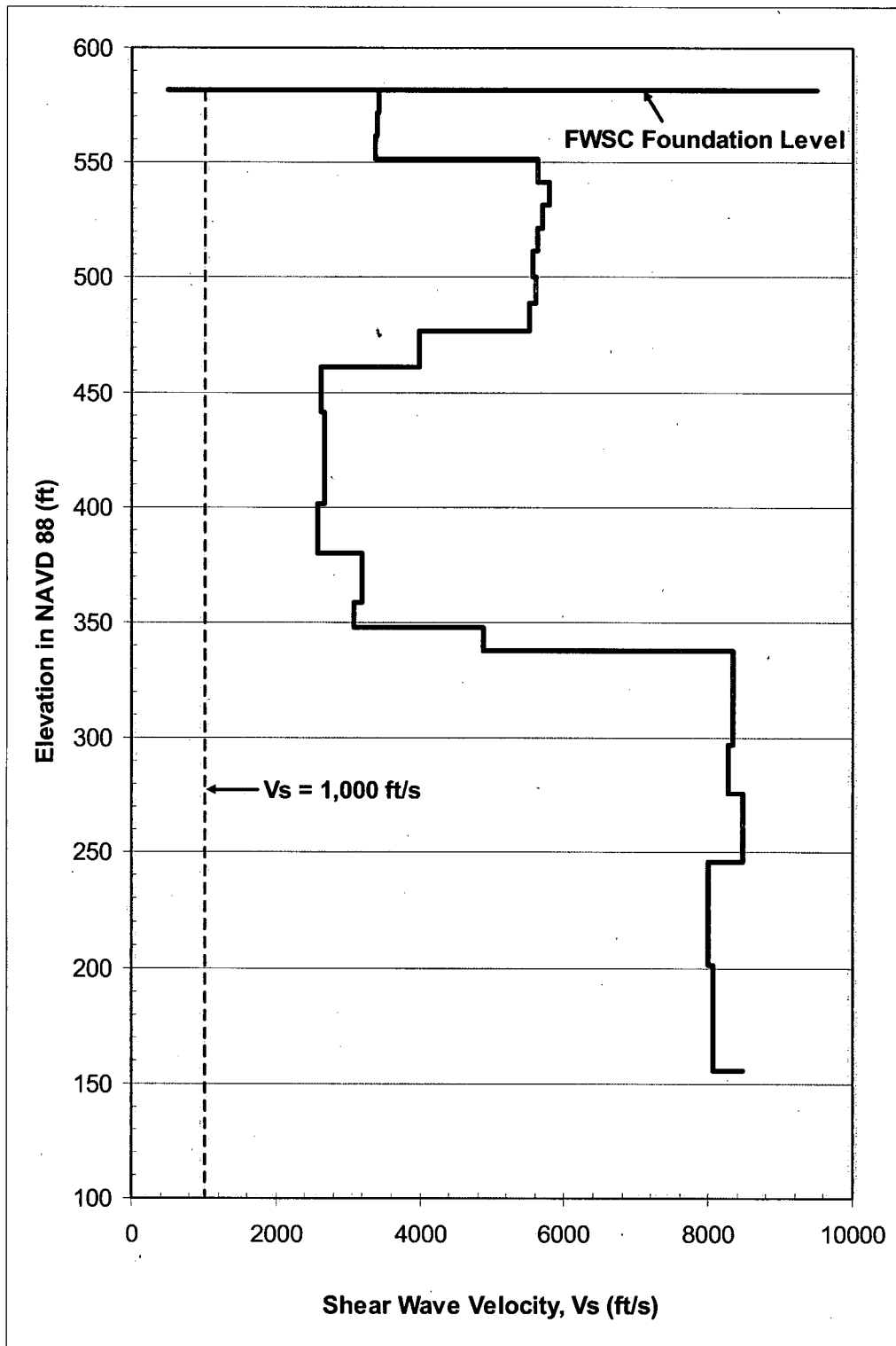


Figure 4 – The 16th Percentiles Shear Wave Velocities at Seismic Strains for Foundation Materials Below the FWSC.

Proposed COLA Revision

Revisions to FSAR text, and FSAR Tables 2.5.4-227 and 2.0-201 are shown in the attached markup.

Markup of Detroit Edison COLA
(following 11 pages)

The following markup represents how Detroit Edison intends to reflect this RAI response in a future submittal of the Fermi 3 COLA. However, the same COLA content may be impacted by revisions to the ESBWR DCD, responses to other COLA RAIs, other COLA changes, plant design changes, editorial or typographical corrections, etc. As a result, the final COLA content that appears in a future submittal may be different than presented here.

shown on Figure 2.5.4-224. The V_s profiles of overburden from SASW survey are presented on Figure 2.5.4-225. The variability of seismic wave velocities is present in Subsection 2.5.4.2.2. The average values of seismic wave velocities are summarized in Table 2.5.4-202.

Insert 1

~~The equivalent shear wave velocity, V_{eq} , is calculated to achieve the same wave traveling time over the depth equal to the embedment depth plus 2 times the largest foundation plan dimension below the foundation. Equation 2 from the Referenced DCD was used to calculate the equivalent shear wave velocity under each Seismic Category I structure using the subsurface information and the minimum average shear wave velocity in Table 2.5.4-202.~~

$$V_{eq} = \frac{\sum d_i}{\sum \frac{d_i}{V_i}} \quad \text{[Eq. 2]}$$

~~The equivalent shear wave velocities under the Reactor/Fuel Building, Control Building and FWSC are 1,768, 1,219 and 1,524 m/s (5,800, 4,000 and 5,000 fps), respectively, which is greater than the required 305 m/s (1,000 fps) in the Referenced DCD.~~

2.5.4.7.3 Dynamic Laboratory Testing

The laboratory testing program for dynamic properties is discussed in Subsection 2.5.4.2.3. No dynamic laboratory testing was performed in bedrock units. Some dynamic laboratory tests were performed on undisturbed glacial till samples; however, these results are not required for Seismic Category I structures, as these are all supported directly on bedrock, or on lean concrete fill extending to the bedrock.

Four RCTS tests were performed on glacial till after evaluating sample disturbance and quality by reviewing the results of X-ray radiography and one-dimensional consolidation tests for evaluating sample disturbance and quality. The RCTS tests were performed on undisturbed samples obtained using thin-wall tubes. Prior to the RCTS testing, the thin-wall tubes of all samples to be tested were subjected to X-ray radiography to evaluate the level of sample disturbance. Subsequently, good quality sample intervals were identified and selected for RCTS and one-dimensional consolidation testing. One-dimensional consolidation tests were first performed prior to RCTS testing for sample quality evaluation using the Specimen Quality Designation (SQD) (Reference

$$N_c = 2N_\phi^{1/2}(N_\phi + 1) \quad [\text{Eq. 4}]$$

$$N_\gamma = N_\phi^{1/2}(N_\phi^2 - 1) \quad [\text{Eq. 5}]$$

$$N_q = N_\phi^2 \quad [\text{Eq. 6}]$$

$$N_\phi = \tan^2(45 + \phi/2) \quad [\text{Eq. 7}]$$

where:

ϕ = angle of internal friction for the bedrock mass.

However, in cases where the shear failure is likely to develop along planes of discontinuity or through highly fractured bedrock masses, cohesion is not relied upon to provide resistance to failure (Reference 2.5.4-243). In such cases the ultimate bearing capacity can be estimated from Equation 6 as shown below:

$$q_{ult} = 0.5\gamma BN_\gamma + \gamma DN_q \quad [\text{Eq. 8}]$$

All terms are as previously defined. The ultimate bearing capacity is estimated by using the foundation correction shape factor (Reference 2.5.4-243).

For large foundations that are founded at great depths below grade, these equations can give very large bearing capacity values, even when a factor of safety of 3 is included for allowable bearing value. In such situations, settlement considerations normally governs design.

The Uniform Building Code (Method 2) calculates the allowable bearing pressure on rock as 20 percent of q_u .

Table 2.5.4-227 shows the results of the bearing capacity analyses using methods 1 and 2. Both methods were used to check against the static bearing capacity requirement in the Referenced DCD. Using Terzaghi's approach, the allowable bearing capacity is estimated by dividing the ultimate bearing capacity by a factor of safety of 3. The allowable bearing capacity calculated based on both methods is greater than the ~~minimum static bearing capacity~~ required in the Referenced DCD as shown in Table 2.5.4-227.

maximum static bearing demand



was



~~Methods 1 and 2 were~~ also used to check against the dynamic bearing capacity requirement. Using Terzaghi's approach, the calculated ultimate bearing capacity was divided by a factor of safety of 2.25 to obtain the allowable dynamic bearing pressure. The dynamic factor of safety is established by dividing the static factor of safety by 1.33. The allowable

Terzaghi's approach

maximum
dynamic
bearing demand

dynamic bearing pressure based on both methods was greater than the ~~minimum dynamic bearing capacity~~ required in the Referenced DCD as shown in Table 2.5.4-227.

2.5.4.10.2 Rebound Due to Excavation and Settlement Analysis

All Seismic Category I structures are founded on either bedrock or lean concrete overlying bedrock (Subsection 2.5.4.3); therefore, only linear elastic deformation is considered for settlement analysis. The parameter of interest for linear elastic settlement in the bedrock is E, which is addressed herein.

The E values of bedrock units at the Fermi 3 site obtained by various methods are summarized in Table 2.5.4-228. The various methods used to determine the E of bedrock units are 1) stress-strain curve from laboratory unconfined compression tests, 2) wave equation obtained by solving 3-dimensional equations of motion (using mean V_s from P-S suspension), 3) empirical approach using the Hoek-Brown criterion, and 4) stress-strain curve from results of pressuremeter testing.

For the Bass Islands Group and Salina Group Unit F, the largest E is the average E obtained from laboratory tests, because the unconfined compression tests were performed on intact rock samples which do not take the fractured nature of the bedrock mass into consideration. The E calculated from average V_s is lower, because the average V_s is more representative of the bedrock mass. The ratio of the E, based on laboratory tests, to the E, based on average V_s , is approximately 1.6 for the Bass Islands Group (average RQD is 54 percent) and 4.0 for the Salina Group Unit F (average RQD is 13 percent). The E calculated from average V_s and laboratory tests are both greater than the upper bound E using the Hoek-Brown criterion. The average E, based on the pressuremeter tests in Salina Group Unit F, falls within the upper and lower bound E based on Hoek-Brown criterion.

For Salina Group Unit E (average RQD is 72 percent) and Unit C (average RQD is 97 percent), the E of bedrock based on the average V_s are greater than the average E measured from laboratory unconfined compression tests. The ratio of the E based on laboratory tests to the E from the average V_s are approximately 0.9 and 0.8 for Unit E and Unit C, respectively, which shows good agreement. The E calculated from average V_s and laboratory tests are greater than the upper bound E using the Hoek-Brown criterion.

Information from Table 2.5.4-226 and Table 2.5.4-229 was used as inputs for the finite element analysis. The settlement analysis for the Seismic Category I structures was performed in stages. The initial stage was used to define the initial states of stress in the ground. The second stage simulated the rebound associated with load removal when excavation was performed to appropriate foundation elevations or to top of bedrock in the power block area. The remaining stages were simulated to estimate settlement after loadings were applied. Only elastic settlements are considered in the analysis and there is no long term (post-construction) settlement anticipated at the Fermi 3 site.

Figure 2.5.4-228 and Figure 2.5.4-229 show the graphical results from finite element analysis for excavation rebound at the completion of excavation, and for total settlements caused by structure and fill loads, respectively. The settlement analysis results are summarized in Table 2.5.4-230 and Table 2.5.4-231, respectively, for excavation rebound, and total (settlement from the rebounded position) foundation settlements. Only settlements under Seismic Category I structures are shown in these tables. The calculated total and differential settlements in Table 2.5.4-232 are within the acceptance criteria required in the Referenced DCD.

2.5.4.10.3 Lateral Earth Pressures

Static and seismic lateral earth pressures are addressed for Fermi 3 below-ground walls. From the Referenced DCD, the lateral soil pressure at rest is applied to external walls for R/FB and CB. Therefore, the R/FB and CB walls are assumed to not yield due to the lateral earth pressure applied to them. The at-rest pressure is the appropriate earth pressure to use for design of the walls per the Referenced DCD. For the Firewater Service Complex, the lateral soil pressure is not considered since it has no below-grade walls.

For a conservative analysis, the engineered granular backfill was assumed to be resting on the R/FB and CB walls from finish grade to bottom of foundation with concrete plug as per the Referenced DCD requirements. Therefore, properties of engineered granular backfill were used for calculating lateral earth pressure from plant grade to the bottom of foundation. It is expected that the ϕ' of the engineered granular backfill is a minimum of 30° ; therefore $\phi' = 30^\circ$ was used for lateral pressure analysis. The saturated and unsaturated unit weights of 21.2

35

35

The shear wave velocity of soil column is taken as the average measured $V_s = 725$ fps of the existing fill using SASW method as shown on Figure 2.5.4-225.

2.5.4.10.3.3 Results of Lateral Earth Pressure Analyses

The results of the static soil lateral earth pressure and seismic soil lateral earth pressure for the R/FB and CB are shown on Figure 2.5.4-230 and Figure 2.5.4-231, respectively.

2.5.4.11 Design Criteria

DCD Table 2.0-1 shows the envelope of ESBWR standard site parameters. Subsection 2.5.4 addresses specifically the following parameters listed in DCD Table 2.0-1:

- Minimum Static Bearing Capacity.
- Minimum Dynamic Bearing Capacity.
- Minimum Shear Wave Velocity.
- Liquefaction Potential.
- Angle of Internal Friction.
- Maximum Settlement Values for Seismic Category I Structures.

The design criteria required for minimum static and dynamic bearing capacity is addressed in Subsection 2.5.4.10.1. The factor of safety for static bearing capacity is at least 3 while for the dynamic bearing capacity is at least 2.25. The selection of shear strength parameters used in the bearing capacity evaluation is discussed in Subsection 2.5.4.2.1.

The minimum shear wave velocity of the supporting foundation material associated with seismic strains for lower bound soil properties at minus one sigma from the mean is greater than 1,000 fps as discussed in Section 2.5.4.7.2.

Results of the geophysical surveys for shear wave velocity are presented in Subsection 2.5.4.4.1 and shear wave velocity profiles are summarized in Subsection 2.5.4.7.2. Equivalent shear wave velocities (V_{eq}) under each Seismic Category I structure were calculated and presented in Subsection 2.5.4.7.2. The minimum V_{eq} is 1,219 m/s (4,000 fps) in the Control Building area which higher than 305 m/s (1,000 fps).

The static stability analyses are presented in Subsection 2.5.4.10. The design criteria for static stability analyses are identified in Subsection 2.5.4.10 and are compared to site parameters in Table 2.0-201. Discussion of the assumptions and methods of analyses for the static stability analyses are provided in Subsection 2.5.4.10.

Subsection 2.5.4.8 discusses the liquefaction potential of soils encountered and fill at the site. It is concluded that there are no liquefiable soils under and adjacent to all Seismic Category I structures.

DCD Table 2.0-1 requires that that $\phi' \geq 30^\circ$. Seismic Category I structures are founded on bedrock or lean concrete extending to bedrock. The angle of internal friction of bedrock is greater than 30 degree based on laboratory direct shear tests performed on samples with discontinuities from the Bass Islands Group and empirical correlations using Hoek-Brown criterion. Engineered granular backfill is used to backfill adjacent to all Seismic Category I structures and based on compaction requirements the angle of internal friction of engineered granular backfill should be greater than 30 degrees.

The design criteria required for the foundation settlement for Seismic Category I structures are addressed in Subsection 2.5.4.10.2. The calculated foundation settlements of all Seismic Category I structures were demonstrated to be less than the maximum settlement values specified in the Referenced DCD.

The computer program used in the settlement analysis (Subsection 2.5.4.10.2) was validated by comparing the results obtained from computer program to solutions obtained from theoretical equations.

2.5.4.12 Techniques to Improve Subsurface Conditions

The R/FB and CB are founded on bedrock. Based on the stability analysis presented on Subsection 2.5.4.10, no subsurface improvement is needed. The exposed foundation bedrock is sluiced with high-pressure water jets and carefully examined by a qualified geologist to ensure that no excessive natural fracturing or blasting back-break exists that might be unsuitable for foundation support. Any areas with open fractures are filled with concrete backfill.

For the FWSC, all soils are removed below the foundation to the top of bedrock and replaced with lean concrete fill to improve subsurface conditions. Since the Turbine Building is a large structure and in close proximity to the Reactor Building, glacial till below the Turbine Building is removed and replaced with lean concrete backfill.

Insert 1

To consider variation and uncertainties in dynamic soil properties, a suite of 60 randomized soil profiles were generated for soil amplification analyses as discussed in Section 2.5.2.5.1.3. Soil amplification analyses were performed for the R/FB, CB and FWSC soil profiles and the response motions at the foundation level were obtained for the 10^{-4} and 10^{-5} input ground motions. At each of the loading levels for the input ground motions used in the SHAKE analyses, the iterated shear wave velocities for each layer of the 60 randomized profiles were sorted into rank order (from the lowest to highest value), and the 16th, 50th and 84th percentiles shear wave velocity profiles at seismic strains were determined. The 16th percentiles of the randomized shear wave velocities at seismic strains represent mean minus one standard deviation (the lower bound soil properties) specified by the Reference DCD. The 16th percentiles of the randomized shear wave velocities at seismic strains for foundation materials below the R/FB, CB and FWSC are greater than 1,000 fps, as required by the Reference DCD.

Table 2.5.4-227 Results of Bearing Capacity Analysis

Maximum Static and Dynamic Bearing Demand

[EF3 COL 2.0-29-A]

Structure	Terzaghi Approach		Uniform Building Code	Required Minimum Bearing Capacity from Referenced DCD		
	Bearing Capacity		Allowable Loading Condition ⁽³⁾	Static Loading Condition ⁽⁴⁾	Dynamic Loading Condition ⁽⁵⁾	
	Ultimate (ksf)	Allowable Under Static Loading Condition ⁽¹⁾ (ksf)				Allowable Under Dynamic Loading Condition ⁽²⁾ (ksf)
Reactor/Fuel Building	281	94	125	259	14.6	112.8 23
Control Building	879	293	391	374	6.1	50.2 8.8
Firewater Service Complex	96	32	43	43	3.45	14.0 25.1

Notes:

1. Allowable static bearing capacity using factor of safety of 3.
2. Allowable dynamic bearing capacity using factor of safety of 2.25.
3. Method 2 only allowed determination of allowable bearing capacity under static loading condition.
4. Criterion from Referenced DCD; (1) and (3) were used to check against (4); (1) and (3) are greater than (4), therefore satisfy the Referenced DCD criterion.
5. Criterion from Referenced DCD; (2) was used to check against (5); (2) is greater than (5), therefore satisfies the Referenced DCD criterion.

ksf = kips per square foot

Subject ⁽¹⁶⁾	DCD Site Parameter Value ⁽¹⁾⁽¹⁶⁾	Fermi 3 Site Characteristic	Evaluation
Soil Properties			
Minimum Static Bearing Capacity ⁽⁷⁾	699 kPa (14,600 lbf/ft²)	Maximum Static Bearing Demand	The DCD site parameter of minimum static bearing capacity underlying the reactor building/fuel building foundation is determined by the minimum static bearing capacity for any layer of material under this foundation.
Reactor/Fuel Building	699 kPa (14,600 lbf/ft ²)	4,500 kPa (94,000 lbf/ft ²)	The site characteristic value for minimum bearing capacity is defined as the allowable load-bearing capacity of this layer for supporting plant structures. This value is 4,500 kPa (94,000 lbf/ft ²) and falls within (is greater than) the DCD site parameter value.
Control Building	292 kPa (6,100 lbf/ft ²)	14,029 kPa (293,000 lbf/ft ²)	The DCD site parameter of minimum static bearing capacity underlying the control building foundation is determined by the minimum static bearing capacity for any layer of material under this foundation. The Fermi 3 site characteristic value of 14,029 kPa (293,000 lbf/ft ²) is provided in Table 2.5.4-227 and falls within (is greater than) the DCD site parameter value.
Firewater Service Complex	165 kPa (3450 lbf/ft ²)	1,532 kPa (32,000 lbf/ft ²)	The DCD site parameter of minimum static bearing capacity underlying the firewater service complex (FWSC) foundation is determined by the minimum static bearing capacity for any layer of material under this foundation. The Fermi 3 site characteristic value for minimum bearing capacity of 1,532 kPa (32,000 lbf/ft ²) is described in Table 2.5.4-227. The Fermi 3 site characteristic value falls within (is greater than) the DCD site parameter value.

The Fermi 3 site characteristic value for allowable bearing capacity from Table 2.5.4-227 for the R/FB

The Fermi 3 site characteristic value for allowable bearing capacity from Table 2.5.4-227 for the CB

The Fermi 3 site characteristic value for allowable bearing capacity from Table 2.5.4-227 for the FWSC

Table 2.0-201 Evaluation of Site/Design Parameters and Characteristics (Sheet 8 of 28)

[EF3 COL 2.0-1-A]

Subject (16)	DCD Site Parameter Value ⁽¹⁾⁽¹⁶⁾	Fermi 3 Site Characteristic	Evaluation
Soil Properties (continued)			
Minimum Dynamic Bearing Capacity (continued)		Maximum Dynamic Bearing Demand	
Reactor/Fuel Building			allowable
Soft	1,100 → 2700 kPa 23,000 → (56,400 lbf/ft ²)	5,980 kPa (125,000 lbf/ft ²)	The Fermi 3 site characteristic value for minimum dynamic bearing capacity for the RB/FB structure is from Table 2.5.4-227 and falls within (is greater than) the DCD site parameter minimum value for any type of soil: hard, medium, or soft. Based on the equivalent uniform shear wave velocity identified below, the materials beneath the RB/FB structure are classified as hard in accordance with Note (7).
Medium	2,700 → 7300 kPa 56,400 → (152,500 lbf/ft ²)		
Hard	1,100 → 5400 kPa 23,000 → (442,800 lbf/ft ²)		
Control Building			allowable
Soft	500 → 2800 kPa 10,500 → (58,500 lbf/ft ²)	18,700 kPa (391,000 lbf/ft ²)	The Fermi 3 site characteristic value for minimum dynamic bearing capacity for the CB structure is from Table 2.5.4-227 and falls within (is greater than) the DCD site parameter minimum value for any type of soil: hard, medium, or soft. Based on the equivalent uniform shear wave velocity identified below, the materials beneath the CB structure are classified as hard in accordance with Note (7).
Medium	2,200 → 2500 kPa 46,000 → (52,300 lbf/ft ²)		
Hard	420 → 2400 kPa 8,800 → (50,200 lbf/ft ²)		
Firewater Service Complex (FWSC)			allowable
Soft	460 → 440 kPa 9,600 → (9200 lbf/ft ²)	2100 kPa (43,000 lbf/ft ²)	The Fermi 3 site characteristic value for minimum dynamic bearing capacity for the FWSC structure is from Table 2.5.4-227 and falls within (is greater than) the DCD site parameter minimum value for any type of soil: hard, medium, or soft. Based on the equivalent uniform shear wave velocity identified below, the materials beneath the FWSC structure are classified as hard in accordance with Note (7).
Medium	690 → 540 kPa 14,400 → (11,300 lbf/ft ²)		
Hard	1,200 → 670 kPa 25,100 → (44,000 lbf/ft ²)		

Table 2.0-201 Evaluation of Site/Design Parameters and Characteristics (Sheet 9 of 28)

[EF3 COL 2.0-1-A]

Subject ⁽¹⁶⁾	DCD Site Parameter Value ⁽¹⁾⁽¹⁶⁾	Fermi 3 Site Characteristic	Evaluation
Soil Properties (continued)			
Minimum Dynamic Bearing Capacity (continued)			
Minimum Shear Wave Velocity ⁽⁸⁾	300 m/s (1000 ft/s)	Value for each Seismic Category I structure: greater than 1,000 ft/sec → 1,768 m/s (5,800 ft/sec) for the reactor building/fuel building greater than 1,000 ft/sec → 1,219 m/s (4,000 ft/sec) for the control building greater than 1,000 ft/sec → 1,524 m/s (5,000 ft/sec) for the FWSC	The Fermi 3 site characteristic value for each Seismic Category I structure is based on the equivalent uniform shear wave velocity over the entire soil column calculated using the formula in Note (8). The value for each structure falls within (is greater than) the DCD site parameter minimum value. As shown in Figure 2.5.4-220 through Figure 2.5.4-225, the FB/RB, CB, and FWSC foundations are founded on uniform material. Therefore, the ratio of the largest to the smallest shear wave velocity over each mat foundation level does not exceed 1.7.
Liquefaction Potential			
Seismic Category I structures	None under footprint of Seismic Category I structures resulting from site-specific SSE	None at site-specific SSE under Seismic Category I structures	The Fermi 3 Category I structures are founded on bedrock or lean concrete and there is no potential for liquefaction under Fermi 3 Seismic Category I structures at the site-specific SSE ground motion.
Other than Seismic Category I structures	See Note (14)	See Evaluation column	Note (14) in DCD Table 2.0-1 identifies a requirement to address liquefaction potential under other than Seismic Category I structures. Subsection 2.5.4.8 provides the results of the analysis for the glacial till at the Fermi 3 site and addresses potential liquefaction under other than Seismic Category I structures. Based on the analysis provided, the glacial till is not susceptible to liquefaction.
Angle of Internal Friction	≥30 degrees ↑ 35	≥30 degrees ↑ 35	The Fermi 3 site characteristic value for angle of internal friction is provided in Subsection 2.5.4.10 and falls within (is the same as) the DCD site parameter value.

the shear wave velocity of the supporting foundation material associated with seismic strains for lower bound soil properties at minus one sigma from the mean

Figure 2.5.4-215 and Figure 2.5.4-216

**Attachment 6
NRC3-10-0012**

**Response to RAI Letter No. 17
(eRAI Tracking No. 4008)**

RAI Question No. 02.05.4-28

02.05.04-28

FSAR Section 2.5.4.10.3.2 indicates that the Ostadan method is used to compute seismic soil pressure on building walls. FSAR figures 2.5.4-230 and 2.5.4-231 present "smooth" seismic earth pressure distributions for the entire height of the embedded portions of the R/FB and CB walls. A comparison of the aforementioned figures with Figure 2.5.4-202 indicates that the lower portions of both the reactor building and control building would be surrounded by lean concrete/bedrock rather than engineered granular backfill.

- a) Please provide enough details on each step of the Ostadan method as applied to arrive at the seismic lateral earth pressures presented on FSAR figures 2.5.4-230 and 2.5.4-231. If the Ostadan method was simplified or modified in developing the seismic lateral earth pressures, please provide reasons for the changes.*
- b) Please provide an explanation on why the dynamic lateral earth pressures presented in FSAR figures 2.5.4-230 and 2.5.4-231 are appropriate for the R/FB and CB walls given the heterogeneous materials (granular fills, lean concrete, rock) surrounding those walls.*

Response

- a.) Please provide enough details on each step of the Ostadan method as applied to arrive at the seismic lateral earth pressures presented on FSAR figures 2.5.4-230 and 2.5.4-231. If the Ostadan method was simplified or modified in developing the seismic lateral earth pressures, please provide reasons for the changes.*

Ostadan (FSAR Reference 2.5.4-247) developed a method to compute seismic soil pressure that focused on building walls rather than soil retaining walls. The calculation steps are summarized as follows:

1. "Perform free-field soil column analysis and obtain the ground response motion at the depth corresponding to the base of the wall in the free-field. The response motion in terms of acceleration response spectrum at 30 percent damping should be obtained. The free-field soil column analysis may be performed using the computer Program SHAKE (Schnabel et al., 1972) with input motion specified either at the ground surface or at the depth of the foundation basemat. The choice for location of control motion is an important decision that needs to be made consistent with the development of the design motion. The location of input motion may significantly affect the dynamic responses of the building and the seismic soil pressure amplitudes." (FSAR Reference 2.5.4-247)

Fermi 3 FSAR, Revision 1, Section 2.5.2.5.1, states:

"In addition to the GMRS, foundation input response spectra (FIRS) are needed at the base of the Reactor/Fuel Building (R/FB), the Control Building (CB), and the

Fire Water Service Complex (FWSC). Foundation elevation for these structures are approximately 160 m (524 ft.), 164 m (540 ft.), and 177 m (582 ft.) NAVD 88, respectively (Table 2.5.4-224). The R/FB and CB are founded within the Bass Islands Group and the FIRS analyses profiles for these facilities are constructed by removing material above the foundation elevation from the GMRS profile shown on Figure 2.5.2-255.....”

Fermi 3 FSAR, Revision 1, Section 2.5.2.6.4, states:

“The process described in Subsection 2.5.2.4 was used to develop FIRS for the three foundation elevations. These are shown on Figure 2.5.2-289, Figure 2.5.2-290, and Figure 2.5.2-291 for the R/FB, CB, and FWSC FIRS, respectively. These spectra are listed in Table 2.5.2-224, Table 2.5.2-225, and Table 2.5.2-226. Also shown on the three figures are the ESBWR Certified Seismic Design Response Spectra (CSDRS) (Reference 2.5.2-291). The FIRS are enveloped by the ESBWR CSDRS in all cases.”

The FIRS for R/FB and CB are presented in FSAR Figures 2.5.2-289 and 2.5.2-290, respectively. The FIRS for R/FB and CB are considered as ground response motions at the depth corresponding to the base of the R/FB and CB walls, respectively, in the free-field.

2. Use Equation $m = 0.5 \times \rho \times H^2 \times \psi_v$ to compute the total mass, m , for a representative single degree-of-freedom (SDOF) system using the Poisson’s ratio, ν , and mass density of the soil, where ρ is the mass density of the soil, H is the height of the wall, and ψ_v is the factor to account for the Poisson’s ratio, ν . ψ_v is defined in the following Equation:

$$\psi_v = \frac{2}{\sqrt{(1-\nu)(2-\nu)}}$$

- i. Computation of total mass, m , for Reactor Building:

$$\psi_v = \frac{2}{\sqrt{(1-\nu)(2-\nu)}} = \frac{2}{\sqrt{(1-0.3)(2-0.3)}} = 1.83339 \approx 1.833$$

$$\begin{aligned} \text{Total mass, } m &= 0.5 \times \rho \times H^2 \times \psi_v = 0.5 \times \gamma / g \times H^2 \times \psi_v \\ &= 0.5 * (135 \text{ pcf} / g) * (65.6 \text{ ft})^2 * 1.83339 \\ &\approx \underline{(532557 / g) \text{ lb/ft}} \end{aligned}$$

- ii. Computation of total mass, m , for Control Building:

$$\psi_v = \frac{2}{\sqrt{(1-\nu)(2-\nu)}} = \frac{2}{\sqrt{(1-0.3)(2-0.3)}} = 1.83339 \approx 1.833$$

$$\begin{aligned}\text{Total mass, } m &= 0.5 \times \rho \times H^2 \times \psi_v = 0.5 \times \gamma / g \times H^2 \times \psi_v \\ &= 0.5 * (135 \text{ pcf} / g) * (48.9 \text{ ft})^2 * 1.83339 \\ &\approx (295921 / g) \text{ lb/ft}\end{aligned}$$

3. Obtain the lateral seismic force from the product of the total mass obtained in Step 2 and the spectral acceleration value of the free-field response at the soil column frequency obtained at the depth of the bottom of the wall (Step 1).

- i. Computation of lateral seismic force for Reactor Building:

$$\begin{aligned}\text{Lateral seismic force} &= m \cdot a_{\max} \\ &= (532557 / g) \text{ lb/ft} * (0.50 g) \approx 266280 \text{ lb/ft}\end{aligned}$$

The basis for the value of a_{\max} is provided in Part (b) of this response.

- ii. Computation of lateral seismic force for Control Building:

$$\begin{aligned}\text{Lateral seismic force} &= m \cdot a_{\max} \\ &= (295921 / g) \text{ lb/ft} * (0.50 g) \approx 147960 \text{ lb/ft}\end{aligned}$$

4. Obtain the maximum lateral seismic soil pressure at the ground surface level by dividing the lateral force obtained in Step 3 by the area under the normalized seismic soil pressure, 0.744 H.

- i. Computation of maximum lateral seismic soil pressure, $P_{\text{seismic,max}}$, at the ground surface level for Reactor Building:

$$\begin{aligned}P_{\text{seismic,max}} &= 266280 \text{ lb/ft} / (0.744 * 65.6 \text{ ft}) \\ &\approx 5456 \text{ lb/ft}^2 = 5.456 \text{ ksf}\end{aligned}$$

- ii. Computation of maximum lateral seismic soil pressure, $P_{\text{seismic,max}}$, at the ground surface level for Control Building:

$$\begin{aligned}P_{\text{seismic,max}} &= 147960 \text{ lb/ft} / (0.744 * 48.9 \text{ ft}) \\ &\approx 4067 \text{ lb/ft}^2 = 4.067 \text{ ksf}\end{aligned}$$

5. Obtain the pressure profile by multiplying the peak pressure with the pressure distribution relationship shown in Equation below:

$$p(y) = -0.0015 + 5.05y - 15.84y^2 + 28.25y^3 - 24.59y^4 + 8.14y^5$$

where, y is normalized height, $y = Y/H$ (Y is the distance from the base of the wall, and H is the height of the wall)

Table 1
 Seismic Lateral Earth Pressure Profile for the R/FB

Depth from Ground Surface (ft)	Height from Base of Wall, Y (ft)	Normalized Height, $y = Y/H$	Pressure distribution, $p(y)$ ⁽¹⁾	Maximum Lateral Seismic Soil Pressure at Ground Surface Level, $P_{\text{seismic,max}}$ (ksf) ⁽³⁾	Lateral Seismic Soil Pressure (ksf) ⁽⁴⁾
0.0	65.6	1.00	1.009	5.456	5.50
2.0	63.6	0.97	0.997	5.456	5.44
5.0	60.6	0.92	0.985	5.456	5.37
10.0	55.6	0.85	0.971	5.456	5.30
15.0	50.6	0.77	0.952	5.456	5.19
20.0	45.6	0.70	0.924	5.456	5.04
25.0	40.6	0.62	0.885	5.456	4.83
30.0	35.6	0.54	0.839	5.456	4.58
35.0	30.6	0.47	0.790	5.456	4.31
40.0	25.6	0.39	0.739	5.456	4.03
45.0	20.6	0.31	0.683	5.456	3.73
50.0	15.6	0.24	0.611	5.456	3.33
55.0	10.6	0.16	0.504	5.456	2.75
60.0	5.6	0.09	0.330	5.456	1.80
65.6	0.0	0.00	0.000 ⁽²⁾	5.456	0.00

Notes:

- $p(y) = -0.0015 + 5.05y - 15.84y^2 + 28.25y^3 - 24.59y^4 + 8.14y^5$
- Rounded to zero; actual value is -0.0015.
- See step 4 part i.
- Lateral Seismic Soil Pressure = $p(y) * P_{\text{seismic,max}}$

Table 2
 Seismic Lateral Earth Pressure Profile for the CB

Depth from Ground Surface (ft)	Height from Base of Wall, Y (ft)	Normalized Height, $y = Y/H$	Pressure distribution, $p(y)$ ⁽¹⁾	Maximum Lateral Seismic Soil Pressure at Ground Surface Level, $P_{\text{seismic,max}}$ (ksf) ⁽³⁾	Lateral Seismic Soil Pressure (ksf) ⁽⁴⁾
0.0	48.9	1.00	1.009	4.067	4.10
2.0	46.9	0.96	0.994	4.067	4.04
5.0	43.9	0.90	0.980	4.067	3.99
10.0	38.9	0.80	0.959	4.067	3.90
15.0	33.9	0.69	0.923	4.067	3.75
20.0	28.9	0.59	0.869	4.067	3.53
25.0	23.9	0.49	0.805	4.067	3.27
30.0	18.9	0.39	0.737	4.067	3.00
35.0	13.9	0.28	0.658	4.067	2.67
40.0	8.9	0.18	0.538	4.067	2.19
45.0	3.9	0.08	0.314	4.067	1.28
48.9	0.0	0.00	0.000 ⁽²⁾	4.067	0.00

Notes:

- $p(y) = -0.0015 + 5.05y - 15.84y^2 + 28.25y^3 - 24.59y^4 + 8.14y^5$
- Rounded to zero; actual value is -0.0015.
- See step 4 part ii.
- Lateral Seismic Soil Pressure = $p(y) * P_{\text{seismic,max}}$

Two modifications to the method described in FSAR Reference 2.5.4-247 associated with the free-field ground response motions were applied as follows:

- The truncated soil column with 5 percent spectral damping (FIRS), rather than the full soil column with 30 percent spectral damping was used to obtain the free-field ground response motions at the elevations of the foundations (base of the walls). As discussed in FSAR Section 2.5.2.5.1, material above the foundation elevation was removed from the GMRS profile to obtain the ground response motions at the base of the walls. The full soil column for the method in FSAR Reference 2.5.4-247 adds to the truncated soil column the materials extending from the base of the walls to the final grade.
- The maximum spectral acceleration values based on the FIRS were used to estimate the seismic lateral earth pressure on the walls (See Part (b) of this response.), rather than the spectral acceleration value of the free-field response at the soil column frequency obtained at the depth of the bottom of the wall (FSAR Reference 2.5.4-247). This provides a bounding analysis.

Sensitivity analyses were performed to investigate the effects of these modifications to the free-field ground response motions at the base of the R/FB and CB walls. The analyses were performed to ensure the appropriateness of using the spectral acceleration from the FIRS for R/FB and CB to estimate the seismic lateral earth pressure. The objective of the sensitivity analyses was to compare the mean ground motion response for the truncated soil column at 5 percent spectral damping to the mean ground motion response at the base of the R/FB and CB walls for the full soil column at 30 percent spectral damping (see item 1 of FSAR Reference 2.5.4-247 procedure listed above). If the mean ground motion response at the base of the R/FB and CB walls for the truncated soil column at 5 percent spectral damping is greater than for the full soil column at 30 percent spectral damping at frequencies of interest, then use of the ground motion response for the truncated soil column at 5 percent spectral damping is considered a bounding analysis.

The analyses are summarized in Table 3, and briefly discussed as follows:

- Two soil columns were considered – truncated versus full soil columns.
- For the truncated soil column, the truncated soil profiles including the shear wave velocities and unit weights of bedrock units below the foundation base for the R/FB and CB are shown in FSAR Tables 2.5.2-220 (sheet 2 of 4) and 2.5.2-220 (sheet 3 of 4), respectively. The damping ratios of bedrock units based on the 2 percent damping below the foundation base are shown on column 6 in FSAR Table 2.5.2-221. The dynamic properties of bedrock units below the foundation base remained constant for all analyses. Only the best estimate profile was used.
- The full soil column consists of the truncated soil column plus the soil column above the foundation base representing the engineered granular backfill. The full soil profiles for the R/FB consists of the truncated soil column shown in FSAR Tables 2.5.2-220 (sheet 2 of 4) plus the soil column above the foundation base as shown on attached Figure 1. The full soil profiles for the CB consists of the truncated soil column shown in FSAR Tables 2.5.2-220 (sheet 3 of 4) plus the soil column above the foundation base as shown on attached Figure 2.
- Two shear wave velocity profiles (high and low) as shown on Figures 1 and 2 are estimated for the soil column above the foundation base for the sensitivity analyses. The high and low shear wave velocities are used to investigate the effects of shear wave velocity of the backfill on the ground response motion.
- The shear modulus and damping curves for granular backfill are chosen from published correlations (EPRI, 1993, FSAR Reference 2.5.4-229). From 0 to 20 feet, 20 to 50 feet and 50 to 65.6 feet, the corresponding EPRI shear modulus and damping curves, EPRI 0-20 ft (sand), EPRI 20-50 ft (sand), and EPRI 50-100 ft (sand), respectively, were selected for engineered granular backfill as shown on FSAR Figure 2.5.4-227.
- Two sets of the deaggregation earthquake (DE) time histories were used for each shear wave velocity profile (Refer to FSAR Section 2.5.2.4.4.2 for more discussions about the deaggregation earthquakes). These sets of time histories are

for the deaggregation earthquakes that have the largest contribution to the hazard at the Fermi 3 site (as shown in FSAR Table 2.5.2 -222):

- High frequency with low-magnitude deaggregation earthquake (HF, DEL)
- Low frequency with high-magnitude deaggregation earthquake (LF, DEH)
- Thirty time histories were used for each deaggregation earthquake at each 10^{-4} and 10^{-5} ground motion level (Refer to FSAR Section 2.5.2.5.2 for more discussions of the development of time histories). The 10^{-4} and 10^{-5} input ground motion levels were applied at the top of the hard rock layer (Salina Group Unit B) which is at elevation 156 feet (NAVD 88) for the Fermi 3 site (FSAR Section 2.5.2.5.1).

Table 3 Number of Combinations for the Sensitivity Analyses at R/FB and CB Locations				
No. of Combination	Soil Column	Vs profile for Backfill Surrounding Embedded Walls	Deaggregation Earthquake ⁽³⁾	Ground Motion Level based on Annual Exceedance Frequency ⁽⁴⁾
1	Truncated Soil Column	Not Applicable ⁽¹⁾	HF, DEL	10^{-4}
2		Not Applicable ⁽¹⁾	LF, DEH	
3		Not Applicable ⁽¹⁾	HF, DEL	10^{-5}
4		Not Applicable ⁽¹⁾	LF, DEH	
5	Full Soil Column	High ⁽²⁾	HF, DEL	10^{-4}
6		High ⁽²⁾	LF, DEH	
7		Low ⁽²⁾	HF, DEL	
8		Low ⁽²⁾	LF, DEH	
9		High ⁽²⁾	HF, DEL	10^{-5}
10		High ⁽²⁾	LF, DEH	
11		Low ⁽²⁾	HF, DEL	
12		Low ⁽²⁾	LF, DEH	

Notes:

1. For the truncated soil column, the material above the foundation base was removed.
2. See attached Figures 1 and 2.
3. HF = high frequency; LF = Low frequency; DEL = low-magnitude deaggregation earthquake; DEH = high-magnitude deaggregation earthquake.
4. 30 time histories were used as input ground motions for each deaggregation earthquake.

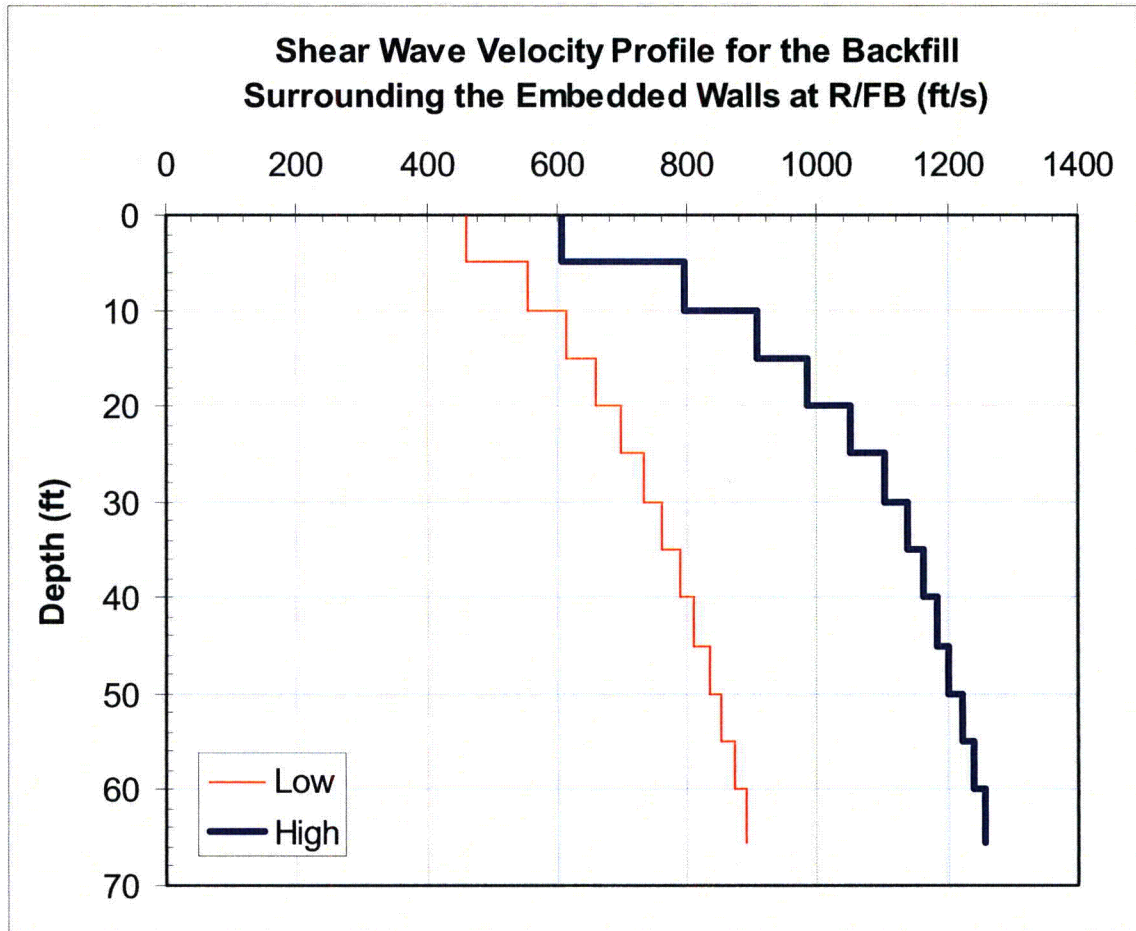


Figure 1 – Estimated Shear Wave Velocity Profiles Used for the Backfill Surrounding the Embedded Walls at R/FB Location for the Sensitivity Analyses.

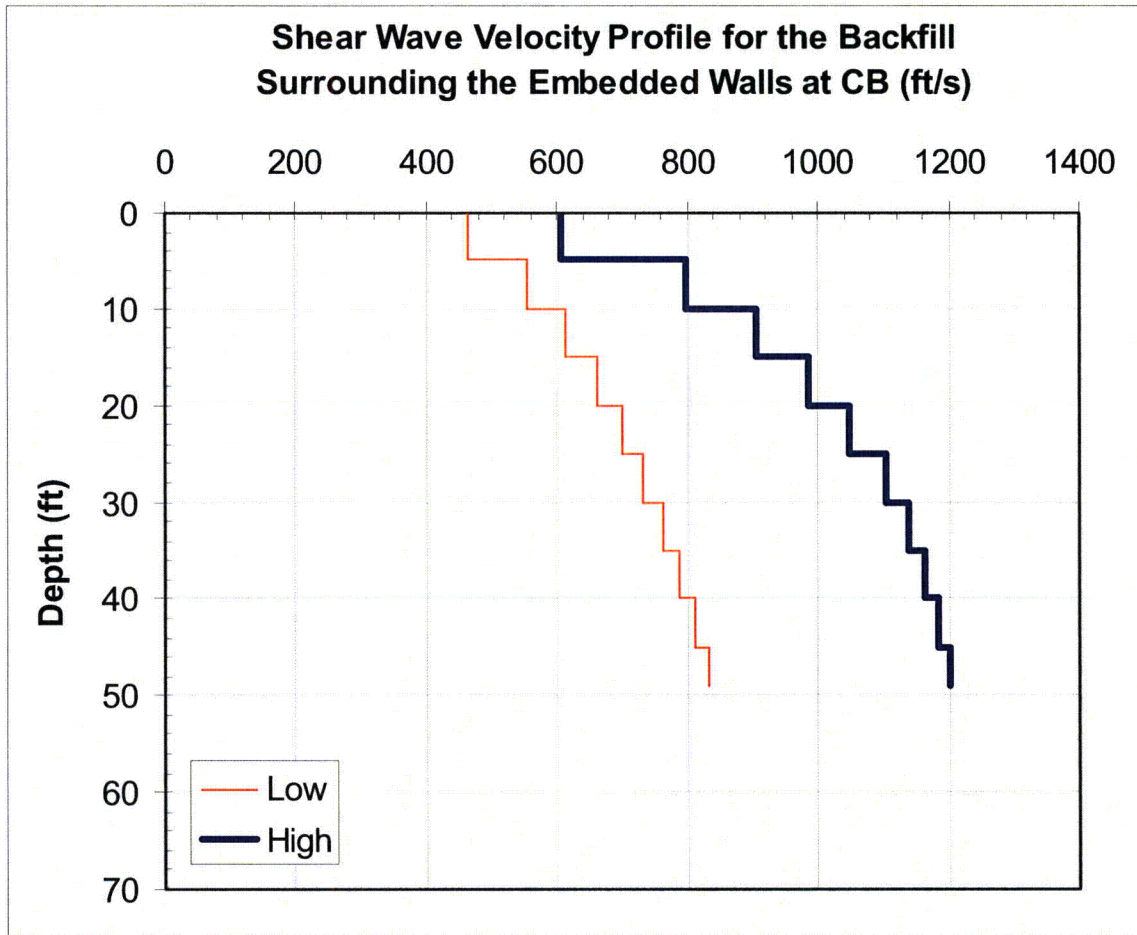


Figure 2 – Estimated Shear Wave Velocity Profiles Used for the Backfill Surrounding the Embedded Walls at CB Location for the Sensitivity Analyses.

Figure 3 shows example plots from two of the calculations. The top plot compares the response spectra for motions computed using a single 10^{-4} high frequency, low magnitude deaggregation earthquake time history and the bottom plot compares the response spectra for motions computed using a single 10^{-4} low frequency, high magnitude deaggregation earthquake time history. The black dashed lines in Figure 3 show the response at the top of the truncated soil column (base of the R/FB wall), and the red lines show the response at the same elevation from the full soil column analysis, both at 5 percent spectral damping. For the two plots shown in Figure 3, the 5 percent damped response spectra for the full and truncated soil column response analyses are similar, with the full soil column response being lower than the truncated soil column response at frequencies above about 2 Hz.

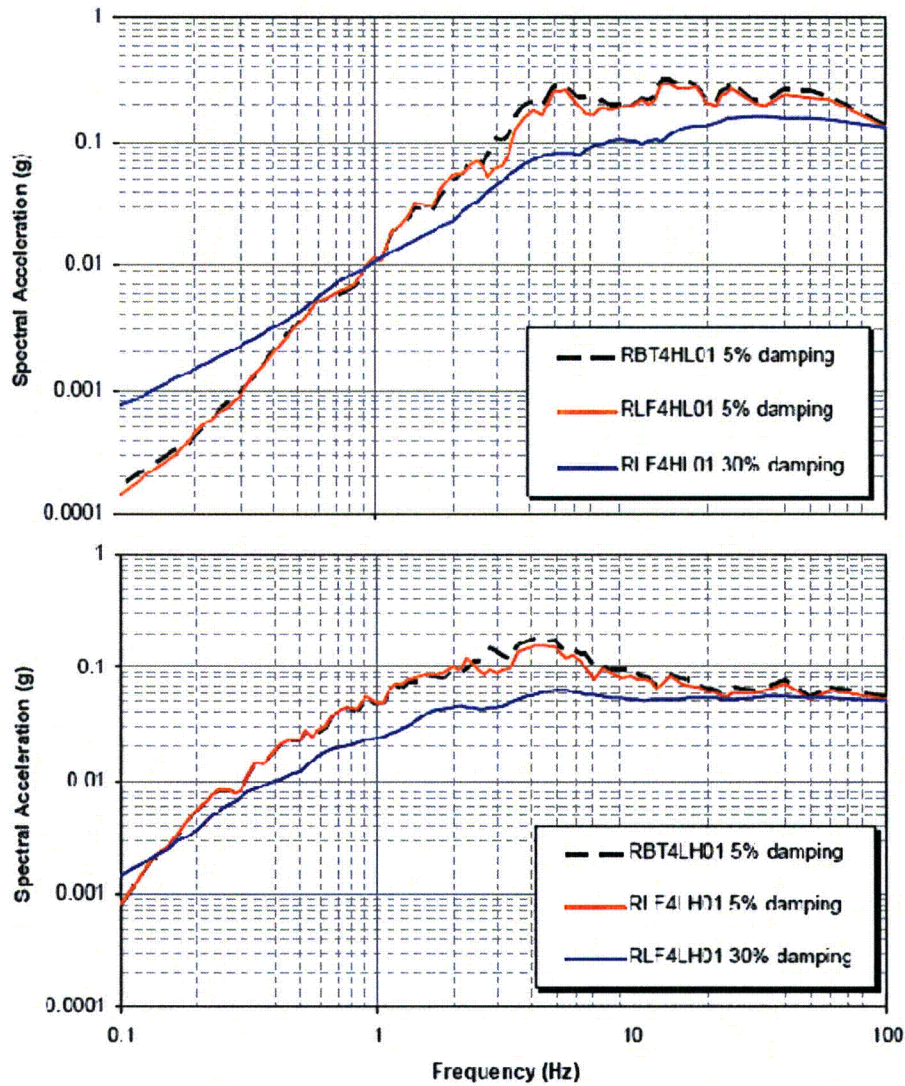


Figure 3 – Example Sensitivity Calculation Plot.

Figure 3 Notes:

1. Top plot is for a high frequency, low magnitude 10^{-4} deaggregation earthquake time history (designated by the code 4HL).
2. Bottom plot is for a low frequency, high magnitude 10^{-4} deaggregation earthquake time history (designated by the code 4LH).
3. Black dashed lines show the 5 percent damped responses for the R/FB truncated soil column (designated by the code RBT) at the base of the R/FB wall.
4. Red and blue lines show the response at the base of the R/FB wall for the full soil column at the low backfill shear wave velocity (designated by the code RLF) for 5 and 30 percent spectral damping.

The blue curves on the plots in Figure 3 show the response at the base of the R/FB wall using 30 percent spectral damping. Over the frequency range of energetic motion in the input time histories, the 30 percent damped response spectra are lower than the 5 percent damped response spectra. However, at low frequencies where there is little energy in the input time histories, the 30 percent damped response becomes higher than the 5 percent damped response because of the much broader frequency range of the 30 percent damped oscillator's transfer function. The effect is more pronounced for the high frequency, low magnitude deaggregation earthquake time history because it has much less low frequency energy. However, the higher response at low frequencies for 30 percent spectral damping is not significant for the following reasons:

- The higher response at 30 percent spectral damping is much less pronounced for the low frequency (LF) input motions, which control the development of the low frequency portion (2.5 Hz and less) of the design response spectra, as described in FSAR Section 2.5.2.6.
- Second, the higher low frequency response for 30 percent spectral damping occurs at frequencies where the spectral accelerations are well below the peak response that is used as the input to the seismic lateral earth pressure analysis.

The analysis used to develop the plots shown on Figure 3 was repeated for the sets of time histories listed in Table 3. Then, for each time history, the ratio of the response with 30 percent spectral damping for the full soil column to the response with 5 percent spectral damping for the truncated soil column was computed. The ratios for the 30 time histories were then averaged and a smooth envelope of the ratios for the high and low backfill shear wave velocity cases was constructed. The response computed for the two backfill velocities was generally similar. Consistent with the development of the FIRS presented in Section 2.5.2.6 of the Fermi 3 FSAR, composite average spectral ratios at the base of the R/FB and CB walls shown on Figure 4 were developed using the following approach:

- Composite average spectral ratios were developed using the low frequency results for spectral frequencies of 2.5 Hz and less.
- Composite average spectral ratios were developed using the high frequency results for spectral frequencies of 5 Hz and greater.
- Between frequencies of 2.5 and 5 Hz smooth interpolation was used to develop the average spectral ratios.

At all frequencies greater than 0.25 Hz, the ratio of the spectral accelerations are less than 1, indicating that the 5 percent damped spectral acceleration for the truncated soil column R/FB and CB FIRS is greater than that estimated using full soil column at 30 percent spectral damping. Therefore, using the maximum spectral acceleration estimated from the FIRS results in a bounding high estimate of the seismic lateral earth pressure for the R/FB and CB.

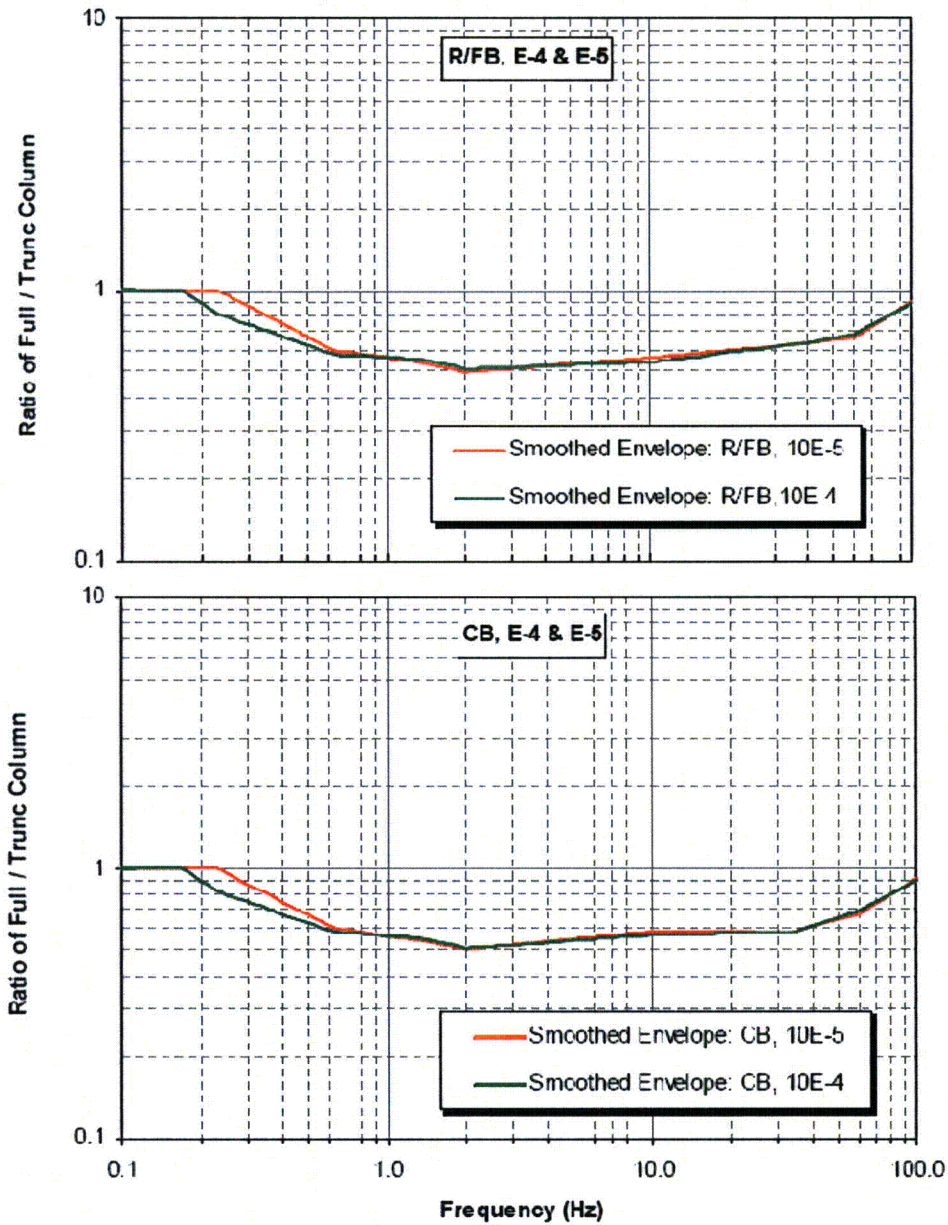


Figure 4 – Average Ratio of Spectral Acceleration of Full Soil Column Response at 30 percent Spectral Damping to Spectral Acceleration of Truncated Soil Column Response at 5 percent Spectral Damping at the base of the R/FB and CB walls .

b.) Please provide an explanation on why the dynamic lateral earth pressures presented in FSAR figures 2.5.4-230 and 2.5.4-231 are appropriate for the R/FB and CB walls given the heterogeneous materials (granular fills, lean concrete, rock) surrounding those walls.

Concrete backfill between the foundation mat of R/FB and CB and bedrock was eliminated from the ESBWR DCD, Revision 6. FSAR text and Figures 2.5.4-202 through 2.5.4-204 were revised and provided in the response to RAI 02.05.04-16. Therefore, the engineered granular backfill is the only type of backfill material adjacent to the R/FB and CB walls.

The bounding seismic lateral earth pressure analysis was performed in the response to RAI 02.05.04-1 by using the peak response horizontal ground acceleration from the R/FB and CB foundation input response spectra (FIRS). The dynamic lateral earth pressures presented are appropriate for the R/FB and CB walls as discussed in the response to RAI 02.05.04-1 which is repeated herein:

“The soil column frequency, and the resulting response horizontal ground acceleration change due to changes in the shear wave velocity of the engineered granular backfill. If the peak response horizontal ground acceleration is selected from the FIRS, then the seismic soil lateral earth pressures on the R/FB and CB walls will represent the maximum bounding pressures that can develop. The peak response horizontal ground acceleration from the FIRS on attached FSAR Figures 2.5.2-289 and 2.5.2-290 for the R/FB and CB is approximately 0.50 g. The results of the revised static soil lateral earth pressure and seismic soil lateral earth pressure on the R/FB and CB walls are shown on attached Figures 2.5.4-230 and 2.5.4-231, respectively. For both the static and seismic evaluations, the soil pressures are less than the lateral earth pressures required in the ESBWR DCD, Revision 6.”

Proposed COLA Revision

None.